Differential metabolic alterations in cortical cell types by feeding a ketogenic diet

Dissertation
for the award of the degree
"Doctor rerum naturalium" (Dr.rer.nat)
of the Georg-August University Göttingen

within the doctoral program *Molecular Physiology of the Brain*
of the Georg-August University School of Science (GAUSS)

submitted by
Tim Düking
from Schmallenberg-Dorlar, Germany

Göttingen, 2019

Thesis committee

Dr. Gesine Saher (Reviewer)
Department of Neurogenetics
Max-Planck-Institute of Experimental Medicine

Prof. Dr. Michael Müller (2nd Reviewer)
Department of Neuro- and Sensory physiology
University Medical Center Göttingen

Prof. Dr. Tiago Outeiro
Department of Experimental Neurodegeneration
University Medical Center Göttingen

Extended thesis committee

Prof. Dr. Swen Hülsmann
Department of Experimental Neuroanesthesiology
University Medical Center Göttingen

Prof. Dr. Ralf Heinrich
Department of Cellular Neurobiology
Schwann-Schleiden Research Center
Georg-August University Göttingen

Prof. Dr. Martin Göpfert
Department of Cellular Neurobiology
Schwann-Schleiden Research Center
Georg-August University Göttingen

Date of oral examination: 25.06.2019

Declaration

I hereby declare that the Ph.D. thesis entitled, “Differential metabolic alterations in cortical cell types by feeding a ketogenic diet”, was written independently and with no other sources and aids than quoted.

Göttingen, 25.04.2019

Tim Düking

-For my Family-

Acknowledgments

First of all, I want to thank my supervisor Dr. Gesine Saher for the opportunity to work on this project that really captured my interest. Furthermore, I want to thank her for continuous scientific support and fruitful discussions during my PhD that contributed to the success of my work.

I also thank Prof. Klaus-Armin Nave PhD, who gave me the opportunity to work in his department. It was a great pleasure to work in a multidisciplinary environment with a supportive atmosphere, in which I could freely discuss thoughts and ideas.

I thank the members of my thesis committee Prof. Dr. Michael Müller and Prof. Dr. Tiago Outeiro for helpful discussion and advices during the time of my graduation. I would like to thank the members of my examination board, Prof. Dr. Swen Hülsmann, Prof. Dr. Ralf Heinrich and Prof. Dr. Martin Göpfert for their interest in this project and the participation of my thesis defense.

Since this was a multidisciplinary project I want to thank my collaborators especially Dr. Olaf Jahn and Lars Piepkorn, who put a lot of effort in performing proteomic and statistic analysis, respectively. I further want to thank Dr. Till Ischebeck for his collaboration regarding metabolomics and for his introduction to the software VANTED. I also thank Dr. Livia de Hoz for her help and collaboration with audiobox experiments. Furthermore, I want to thank Prof. Dr. Moritz Rossner and Nirmal Kannaiyan for their collaboration regarding transcriptomics.

Many thanks also to

…Ramona Jung, Dr. Kathrin Kusch, Ulli Bode, Annette Fahrenholz, Torben Ruhwedel and Boguslawa Sadowski for their constant and very valuable support over the years.

…Torben Ruhwedel and Dr. Wiebke Moebius for introducing me into electron microscopy.

…Stefan Berghoff and Lena Spieth for assistance during cell type isolation.

…Ting Sun for her help regarding statistics of metabolomics data.

…Michaela Schmalstieg and Gabriele Endo for helping me with administrative issues.

…Hajo Horn, Rolf Merker and Lothar Demel for IT support.

…Ines Malade, Ute Bornmann, Kathrin Willig, Tanja Pawelz, Cornelia Casper and Nadja Hoffmeister for taking care of my mice and for maintaining an excellent animal facility.

…Heiko Roehse and Miso Mitkovski for introducing me to confocal microscopy and their technical support.

…the whole Neurogenetics department for creating a friendly working atmosphere, that I really enjoyed during my graduation.

My deepest gratitude goes also to the whole Saher group, Stefan Berghoff, Lena Spieth, Jan Winchenbach, Sina Stumpf, Nina Gerndt, Caro Böhler and Silvia Thüne for their scientific, technical and personal support over the years during my PhD. I am really thankful for such amazing teamwork and help during daily life in the lab.

During the years of my PhD I had the luck to work with colleagues that became friends, which I don't want to miss anymore. Therefore I want to thank

…Ramona Jung and Nina Gerndt for funny discussions during relaxing coffee breaks that I will always remember.

…Martin Meschkat for lively discussion and support in all topics of life during and besides work that I really appreciated.

…Maria Eichel and Stefan Berghoff for "cigarette" breaks (I'm non-smoker), their friendly discussions and help regarding general questions.

…Lena Spieth, Tobias Buscham and Sophie Siems for protecting me from starvation by regularly organizing dinner events.

…all of them for making life so much easier. Thanks guys!

At last I want to thank my family for their constant support and motivation during my whole education. I am especially grateful for the support of Evi Tsiakourma, who motivated me at all times with her trust and believe in me.

Table of Contents

List of figures

Abbreviations

µg	Microgram
µl	Microliter
µm	Micrometer
A1Rs	adenosine A1 receptor
AACS	Acetoacetyl-CoA synthetase
ABC	Ammonium bicarbonate
AcAc	Acetoacetate
AcAc-CoA	Acetoacetyl-CoA
ACAT1	Acetyl-CoA acetyltransferase 1
ACC	Acetyl-CoA carboxylase, Acetyl-CoA carboxylase
ACSAII	Astrocyte cell surface antigen II
ACSL	Long-chain fatty ayl-CoA synthetases
AGC1	Aspartate-glutamate carrier 1
ALB	Albumin
ALDH1L1	Aldehyde dehydrogenase 1 family member l1
APO	Apolipoprotein
ATP	Adenosine triphosphate
ATPase	Adenosine triphosphatase
BBB	Blood-brain barrier
BDH1	ß-hydroxybutyrate dehydrogenase 1
BDNF	Brain derived neurotrophic factor
BSA	Bovines serum albumin
BSG	Basigin
C	Celsius
CAPS1	Calcium-activator protein for secretion 1
cDNA	Complementary DNA
cm	Centimeter
CNP	2',3'-Cyclic Nucleotide 3' Phosphodiesterase
CNS	Central nervous system
CoA	coenzyme A
CPT	Carnitine palmitoyltransferase
CT	Cycle threshold
DAPI	'4',6-diamidino-2-phenylindole
ddH2O	Double distilled water
DDSA	Dodecenyl succinic anhydride

DNA	Desoxyribonucleic acid
dNTP	Deoxyribonucleotide triphosphate
DPBS	Dubelco's PBS
DTT	Dithiothreitol
EDTA	ethylenediaminetetraacetic acid
EGFP	Enhanced green fluorescent protein
EM	Electron microscopy
FABPs	Fatty acid binding proteins
FASN	Fatty acid synthase
FASP	Filter-aided sample preparation filter-aided sample preparation
FAT/CD36	Fatty acid translocase/cluster of differentiation 36
FATPs	Fatty acid transport proteins
FDR	False discovery rate
FWHM	Full width at half maximum
g	Standard gravity, Gram
G	Gauge
G6P	Glucose-6-phosphate
G6PD	Glucose-6-phosphate dehydrogenase
GABA	γ-ammino butyric acid
GC/MS	Gas chromatography/mass spectrometry
GLAST	Glutamate aspartate transporter
GLUT	Glucose transporter
GTPases	Guanosine triphosphatases
GYS1	Glycogen synthase 1
h	Hour
HK	Hexokinase
HMG	Hydroxymethylglutaryl
HMGCL	Hydroxymethylglutaryl-CoA lysase
HMGCR	HMG-CoA reductase
HMGCS2	3-hydroxymethylglutaryl-CoA synthase
ICAM2	intercellular adhesion molecule 2
IGF1	Insulin like growth factor 1
K	Kelvin
KB	Ketone bodies
kcal	Kilocalories
KD	Ketogenic diet
kDa	KiloDalton

kHz	kiloHertz
Kir4.1	Inwardly rectifying potassium channel 4.1
LC-MS	Liquid chromatography coupled to electrospray mass spectrometry
LDS	Lithium dodecylsulfate
M	Molar
m/z	Mass to charge ratio
MACS	Magnetic associated cell separation
MBP	Myelin basic protein
MCD	Malonyl-coA decarboxylase
MCT	Monocarboxylate transporter
MEOX	Methoxyimino
mg	Miligram
min	Minute
ml	Mililiter
mm	Milimeter
mM	Millimolar
MNA	Methyl nadic anhydride
MOG	Myelin-oligodendrocyte glycoprotein
mRNA	Messenger ribonucleic acid
MSTFA	N-methyl-N-trimethylsilyltriflu-oroacetamide
MTBE MeOH	2-Methoxy-2-methylpropan methanol
MYOF	Myoferlin
NADPH	Nicotinamide adenine dinucleotide phosphate
NeuN	Neuronal nuclei
ng	Nanogram
nl	Nanoliter
nm	Nanometer
OxPhos	Oxidative phosphorylation
P	Postnatal day
PBS	Phosphate buffered saline
PFA	Paraformaldehyde
PGLS	6-phosphogluconolactonase
PLP1	Proteolipid protein 1
pM	Picomolar
ppm	Parts per million
PPP	Pentose-phosphate pathway
PTPRB	Receptor-type tyrosine-protein phosphatase beta

PVDF	Polyvinylidene difluoride
qRT-PCR	Quantitative real time-polymerase chain reaction
Rab	Ras-associated binding
Ras	Rat sarcoma
ROS	Reactive oxygen species
Rplp0	60s acidic ribosomal protein P
rpm	Revelations per minute
Rps13	Ribosomal protein s13
RT	Room temperature
SCOT	Succinyl-CoA:3-oxoacid-CoA transferase
SD	Standard diet
SDS	Sodium deoxycholate
sec	Second
ßOHB	ß-hydroxybutyrate
SYNJ1	Synaptojanin 1
SYNPR	Synaptoporin
SYT1	Synaptotagmin 1
TBST	4.4.4 Tris buffered saline with Tween20
TCA	Tricarboxylic acid cycle
TEMED	Tetramethylethylenediamine
TFA	Trifluoroacetic acid
TIC	Total ion count
TMS	Trimethylsilyl
U	Units
UPLC	Ultra performance liquid chromatography
V	Volt
VAMP2	Vesicle-associated membrane protein 2
VGLUT1	Vesicular glutamate transporter 1
W	Watt

Abstract

The suckling period of rodents is accompanied by marked ketosis as a result of the high fat content of maternal milk. During this time, ketone bodies are the major source of energy for the brain. After weaning when the diet is mainly composed of carbohydrates, glucose becomes the major fuel for the brain. Here we could show that rearing mice on a ketogenic diet (KD) prolongs the metabolic state of ketosis in the brain seen during suckling. Reduced blood glucose concentration and increased ß-hydroxybutyrate levels are characteristic for KD fed animals, thereby reflecting the metabolic situation of the neonatal period. Inducing altered substrate availability by KD resulted in increased expression of monocarboxylate transporter 1 (MCT1) in cortical tissue as well as increased abundance of the key ketolytic enzyme Succinyl-CoA:3-oxoacid-CoA transferase (SCOT). However, detailed mechanistical insight *in vivo* is lacking and studies did not take into account cell type specific adaptations. We therefore established a refined protocol of MACS-technology, enabling isolation of highly pure cell fractions from individual cortices of adult animals. By using proteomic or transcriptomic analysis of astrocytes, oligodendrocytes, endothelial cells and neurons, cell type specific metabolic adaptations in response to KD feeding were analyzed. Surprisingly, our data indicate that endothelial cells under ketosis support brain metabolism through transport of ketone bodies while they rely on glycolysis. In contrast, astrocytes shifted their metabolism from glucose utilization to ketolysis and ß-oxidation thereby probably sparing glucose for neurons. Of note, oligodendrocytes largely remain metabolically unaltered and seem to support neuronal activity enhanced potassium buffering and potentially transport of ketone bodies. Interestingly, in addition to increased ketolysis neurons upregulated glycolytic enzymes. We speculate that increased utilization of KB and glucose leads to enhanced mitochondrial respiration. In turn, we hypothesize that enhanced mitochondrial respiration might support increased synaptic transmission in neurons and motor activity observed in KD fed mice. Taken together, our data highlight the compartmentalization of brain metabolism in different cell types under ketogenic conditions. Furthermore, these findings might build the basis to understand therapeutical effects of the KD on cellular level *in vivo* and underscore the need for future cell specific investigations.

1 Introduction

1.1 Central nervous system

The central nervous system (CNS), comprised of the brain and spinal cord, represent the control center of all vertebrates. Through its interconnection with peripheral organs, the CNS enables the organism to receive signals from the periphery, to process information and to trigger actions accordingly. It recognizes stimuli from the extremities (e.g. temperature, scents, feelings), manages body movements and inevitably sustains functionality of the body. In higher mammals the CNS constitutes the basis of superordinated functions like emotion, cognition, rational thinking and other more complex brain functions (Purves et al., 2004). To accomplish such a complex task, the brain is comprised of different specialized cells. Neurons, with their processes and especially their elongated axons, are well equipped for fast impulse propagation and information processing. To support neuronal functioning and to increase the speed of signal transduction, glial cells comprised of oligodendrocytes, astrocytes and microglia, evolved over time. It has been shown, that these glial cells, first considered as simple “glue” that holds neurons together (Virchow, 1854) are indispensable for proper brain function. Oligodendrocytes form myelin sheaths that enwrap axons, an event that is called myelination, to form internodes that restrict action potentials to the nodes of Ranvier. The lipid-rich myelin insulates axons and leads to increased trans-fiber resistance thereby creating the basis for fast saltatory nerve conduction (Baumann & Pham-Dinh, 2001; Kettenmann & Ransom, 2005). In addition to insulating axons, oligodendrocytes also control ion homeostasis due to their close contact with axons (Kamasawa et al., 2005; Larson et al., 2018) and support them with metabolites (e.g. lactate) (Funfschilling et al., 2012). However, especially for astrocytes it is known that these cells supply energy for neurons. These stellate cells are ideally positioned to distribute nutrients within the brain, due to their near complete coverage of blood vessels in the CNS (Cancilla et al., 1972; Kacem et al., 1998) and forming contacts with oligodendrocytes and especially neurons. It has been shown that glycolytic astrocytes support axons and synapses with nutrients like lactate during phases of increased activity (Pellerin & Magistretti, 1994; Supplie et al., 2017). Additionally, they are also essentially involved in transmitter clearing from the synaptic cleft thereby modulating synaptic transmission (Araque et al., 1998). Furthermore, astrocytes contribute to the formation of the blood-brain barrier (BBB), a unique structure of the brain mainly formed by endothelial cells to control the flux of metabolites from the blood stream to brain parenchyma and prevent the entry of unintended substances or pathogens. A hallmark of the BBB is the formation of tight junctions between endothelial cells that restrict

uncontrolled transport of substances (Abbott et al., 2010). However, if a pathogen nonetheless enters the CNS, microglia as immune cells of the brain are activated to remove these pathogens by their phagocytic functions (Kettenmann & Ransom, 2005; Ransohoff & Cardona, 2010). The tight interplay between all brain cells enables the CNS to carry out all its important functions. To sustain constant functionality of the system an immense amount of metabolites is required to provide energy for the cellular machinery.

1.2 Brain metabolism

Despite the fact, that the human brain only accounts for approximately 2% of the body weight, 20% of the energy produced within the body is consumed by cells of the CNS (Erbslöh et al., 1958). Among these cells, neurons are believed to have the highest energy demand, due to synaptic transmission and maintenance of ion gradients needed for production of action potentials (Howarth et al., 2012). Glucose is assumed as the major energetic source for the adult brain to fuel energy consumption by its oxidative metabolism (Sokoloff et al., 1977).

1.2.1 Glucose metabolism

Within the CNS, energy requirements are mainly accomplished by utilization of glucose that is also used for generation of neurotransmitters and sustaining cellular homeostasis (Mergenthaler et al., 2013). To facilitate constant supply of glucose from the blood stream, glucose transporters (GLUTs) are expressed by endothelial and brain cells. GLUT1 (encoded by *Solute carrier family 2 member 1; Slc2a1*) the major glucose transporter of the brain, predominantly expressed in brain endothelial cells, mediates the entry of glucose into the extracellular fluid and the subsequent uptake into astrocytes, oligodendrocytes and microglia (Vannucci, 1994). GLUT3 (encoded by *Slc2a3*) is specifically expressed in neurons and ensures sufficient supply of glucose for neurons even under low glucose conditions due to its higher affinity and transport capacity compared to GLUT1 (Simpson et al., 2008). In general, it is suggested that glucose is mainly taken up by astrocytes and is shuttled to neurons directly or after conversion to lactate to support neuronal activity (Pellerin & Magistretti, 1994; Rouach et al., 2008). In addition, it was shown that oligodendrocytes like astrocytes are capable of producing lactate to support axons (Funfschilling et al., 2012). The so called “lactate shuttle”, first described by Pellerin and Magistretti in 1994 (Fig. 1), couples the transport of astroglial derived lactate to neuronal activity. However, experiments predict also simple diffusion to neurons bypassing the intracellular astrocytic transport (Simpson et al., 2007). Once in the cell, glucose is phosphorylated by hexokinases (HK) to produce glucose-6-

phosphate (G6P) thereby trapping the molecule in the cell. G6P is metabolized via glycolysis to form pyruvate and lactate, which is then in turn transported into mitochondria to be used for ATP generation. Additionally, in astrocytes G6P is used to form glycogen (Cataldo & Broadwell, 1986), the only energy reservoir of the brain. G6P is also used by brain cells as substrate for the pentose-phosphate pathway (PPP) generating the reducing equivalent NADPH to control oxidative stress and to produce precursors for nucleic acid synthesis (Stincone et al., 2015). Within mitochondria, pyruvate is converted to acetyl-CoA by the pyruvate dehydrogenase complex. Acetyl-

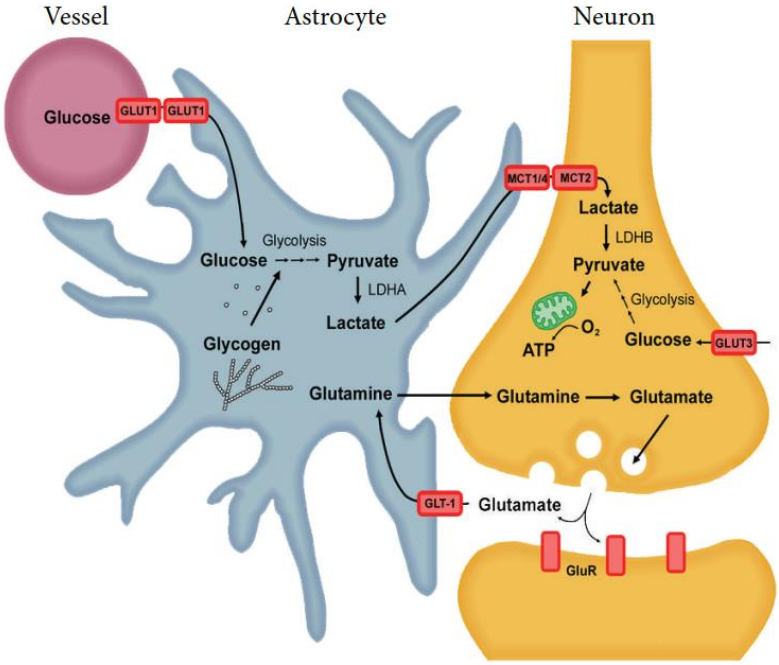

Fig. 1: The astrocyte-neuron lactate shuttle hypothesis

Glucose is taken up by astrocytic endfeed via glucose transporter 1 (GLUT1) and utilized to produce pyruvate and lactate, respectively by lactate dehydrogenase isoenzyme A (LDHA). Upon stimulation of astrocytes via glutamate uptake by glutamate transporters (GLT1) lactate can be shuttled to neurons via monocarboxylate transporters 1, 2 and 4 (MCT1/2/4). Reconversion of lactate into pyruvate via LDHB fuels oxidative phosphorylation within mitochondria. In addition, glucose can also enter neurons via GLUT3. Taken from (Newington et al., 2013).

CoA is then inserted into the tricarboxylic acid cycle (TCA) that is coupled to oxidative phosphorylation (OxPhos) to produce energy in form of ATP.

The transport of neurotransmitter from blood to brain is highly restricted due to action of the BBB. Therefore, neuromodulators have to be produced endogenously from intermediates derived during glycolysis or PPP. In this regard, glucose is required as carbon donor for the biosynthesis of complex carbohydrates incorporated into glycoproteins and glycolipids, the construction of amino acids and monosaccharides, which are essential for functional neurotransmission (Dienel, 2012; Mergenthaler et al.,

2013). To summarize, glucose is essential to maintain brain function, either as substrate for biosynthetic processes or as energy supplier.

1.2.2 Fatty acids as alternative fuel for the brain

Undoubtedly, glucose is the preferred energy source for the brain, but also other metabolites contribute in smaller proportions to brain metabolism. Studies using isotopic labeled fatty acids revealed that ß-oxidation can account for approximately 20% of total brain energy production in rats (Ebert et al., 2003). Back in 1969 it could already be shown that fatty acids are transported into the brain (Dhopeshwarkar & Mead, 1969), but mechanisms facilitating the uptake of fatty acids are still a matter of debate.

Currently two possible hypotheses exist that can act in concert by which fatty acids could enter the brain. On the one hand, fatty acids could cross the endothelial membrane by simple diffusion, independent of transport proteins, using a so called “flip-flop” mechanism (J. A. Hamilton, 2007). On the other hand, selective transport of fatty acids could be facilitated by specific transport proteins present at the cell membrane as well as intracellularly (Schwenk et al., 2010; Storch & Corsico, 2008) (Fig. 2). The most important members of fatty acid transport proteins are comprised of fatty acid transport proteins (FATPs), fatty acid translocase/CD36 (FAT/CD36), intracellular fatty acid binding proteins (FABPs) and long-chain fatty acyl-CoA synthetases (ACSL) (Doege & Stahl, 2006; Glatz & van der Vusse, 1996; Schaffer, 2002; Schaffer & Lodish, 1994; Stremmel et al., 1985). Among these, FATP-1 and FATP-4 seem to be the predominant fatty acid transporters expressed at the BBB of mice (Hirsch et al., 1998; Mitchell & Hatch, 2011), as well as FABP5 (Mitchell et al., 2011) and FAT/CD36 that has been shown to be involved in oleate transport (Mitchell et al., 2009). Knockdown of these transporters significantly reduced the transport of different fatty acids across human brain microvessel endothelial cells, indicating active transport of various fatty acids (Mitchell et al., 2011). In contrast, docosahexaenoic and eicosapentaenoic acid likely cross the BBB via diffusion (Ouellet et al., 2009). This is further supported by studies using CD36(- /-) mice. Experiments showed that incorporation of monounsaturated acids into phospholipids was decreased in CD36(-/-) mice, but polyunsaturated fatty acids like arachidonic and docosahexaenoic acid were incorporated into brain phospholipids at normal levels (Song et al., 2010). Since fatty acids are variable in chain length and their degree of saturation, it is very likely that different mechanisms are in place to mediate the transport and uptake into the brain dependent on the individual properties of a given fatty acid.

Following transport, fatty acids are metabolized via ß-oxidation to produce energy. Astrocytes are thought to be the major cell type in the brain capable of metabolizing fatty acids (Edmond et al., 1987; Romano et al., 2017). Prior to their degradation, fatty acids need to be activated for transport into mitochondria. Fatty acyl-CoA synthetase converts long-chain fatty acids to acyl-CoA thioesters, which then can be transferred to carnitine.

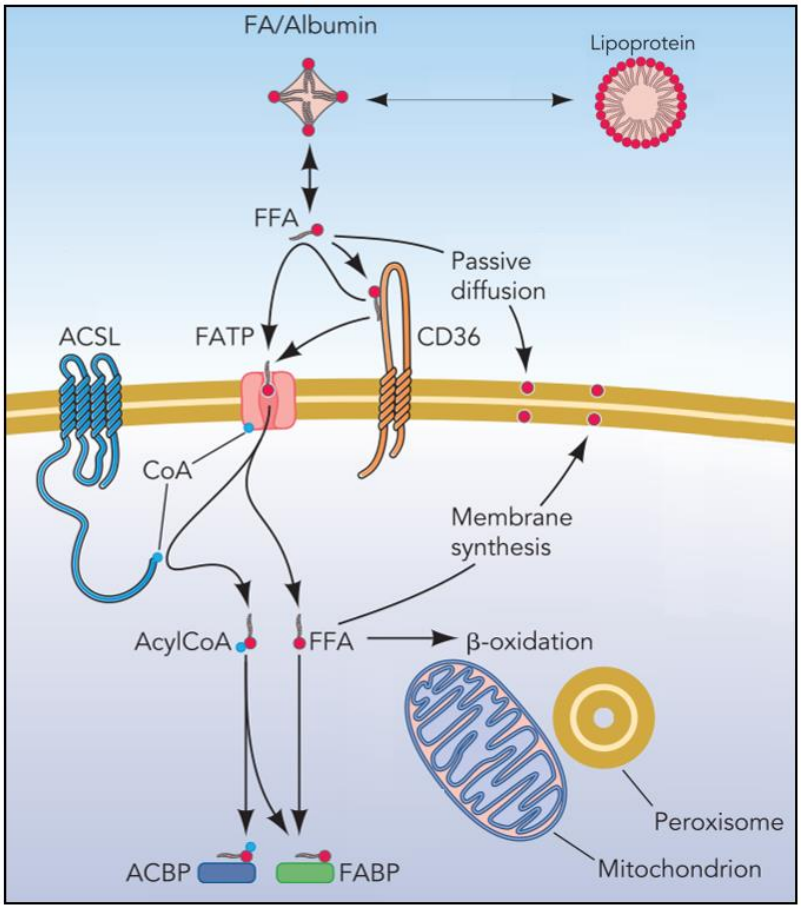

Fig. 2: Free fatty acid uptake

Free fatty acids (FFA) generated from lipoproteins within serum are mainly bound to albumin. Transport across the plasma membrane can occur via different transport proteins and mechanisms. FFA can directly interact with fatty acid transport proteins (FATP) facilitating the transport of FFA across the plasma membrane or by previous binding to fatty acid translocase (CD36). Long-chain fatty acyl-CoA synthetases (ACSLs) might facilitate activation of FFAs by its conversion to acyl-CoA after entering the cytosol. Fatty acid binding proteins (FABPs) or acyl-CoA binding proteins (ACBPs) further facilitate intracellular transport of FFAs. Passive diffusion by FFAs is also a possible mechanism by which FFAs can cross the cell membrane. Within the cell FFAs can be used for membrane synthesis or utilized via ß-oxidation. Adapted from (Doege & Stahl, 2006).

Since CoA is unable to cross the mitochondrial membrane carnitine needs to be added to the acyl-CoA thioester. Carnitine palmitoyltransferase 1 (CPT1) catalyzes the rate limiting step in ß-oxidation by conversion of long-chain acyl-CoA to long-chain acylcarnitine (Lopaschuk et al., 2010; Schulz, 2002), thereby enabling the transport of fatty acids into mitochondria. Oxidation of fatty acyl-CoA thioester is carried out within

mitochondria in a repeated sequence comprised of four steps. The successive action of the main ß-oxidizing enzymes leads to the formation of one acetyl-CoA per cycle, shortening the acyl-CoA molecule until complete oxidation (Schulz, 2002).

CPT1 can be allosterically inhibited by malonyl-CoA to prohibit vicious cycles between fatty acid synthesis and degradation (McGarry & Brown, 1997). Malonyl-CoA is produced from acetyl-CoA by the cytosolic enzyme acetyl-CoA carboxylase (ACC), which accomplishes the rate-limiting step in fatty acid synthesis (Awan & Saggerson, 1993). In turn, malonyl-CoA can be degraded by malonyl-CoA decarboxylase (MCD, encoded by *Mlycd*) (Dyck et al., 1998). Consequently, ß-oxidation is controlled by the precisely balanced synthesis and degradation of malonyl-CoA.

1.2.3 Ketone body synthesis and utilization

Besides their direct utilization within the brain, fatty acids can support brain metabolism indirectly via production of ketone bodies. Under specific physiological conditions, the liver is essentially involved in the production of ketone bodies (KB) by using fatty acid derived acetyl-CoA as substrate. No other metabolite class is able to replace glucose to the same extent as brain energy source as ketone bodies can.

The term KB summarize the three metabolites ß-hydroxybutyrate (ßOHB), acetoacetate (AcAc) and to a minor portion acetone, which is spontaneously formed from AcAc. KB can meet the energetic needs of the brain to nearly 70% under starvation in humans (Cahill, 2006; Owen, 2005) or during the suckling period in rats (Nehlig, 2004). Ketogenesis occurs mainly in the liver by using Acetyl-CoA as substrate when fatty acid availability is high such as during fasting/starvation, post-exercise, the neonatal period or by adhering to a ketogenic diet. ß-oxidation derived acetyl-CoA is condensed to acetoacetyl-CoA (AcAc-CoA) via a thiolase (Fig. 3). Mitochondrial 3-hydroxymethylglutaryl-CoA synthase (HMGCS2) catalyzes the rate-limiting step by condensation of AcAc-CoA and acetyl-CoA leading to the formation of hydroxymethylglutaryl (HMG)-CoA. HMG-CoA lyase (HMGCL) cleaves HMG-CoA to release AcAc, which is reduced to ßOHB by ßOHB dehydrogenase 1 (BDH1) (Grabacka et al., 2016; Puchalska & Crawford, 2017). AcAc and ßOHB are then released into the circulation and transported into extrahepatic tissues such as brain, heart or muscle for oxidation (Cotter et al., 2011). Monocarboxylate transporters (MCTs) facilitate the transport of KB from blood to brain (Grabacka et al., 2016).

Once within the brain, KB utilization takes place in mitochondria. BDH1 catalyzes the first reaction of ketolysis by oxidation of ßOHB to generate AcAc (Lehninger et al., 1960). Oxidation of AcAc to AcAc-CoA is facilitated by the rate-limiting enzyme Succinyl-CoA:3-oxoacid-CoA transferase (SCOT; encoded by *3-Oxoacid CoA-Transferase 1, Oxct1*) through exchange of CoA from succinyl-CoA to AcAc (Cotter et al., 2011). SCOT is not expressed in liver, avoiding futile cycling between synthesis and breakdown of KB (Orii et al., 2008). Breakdown of AcAc, which is mediated by acetyl-CoA acetyltransferase 1

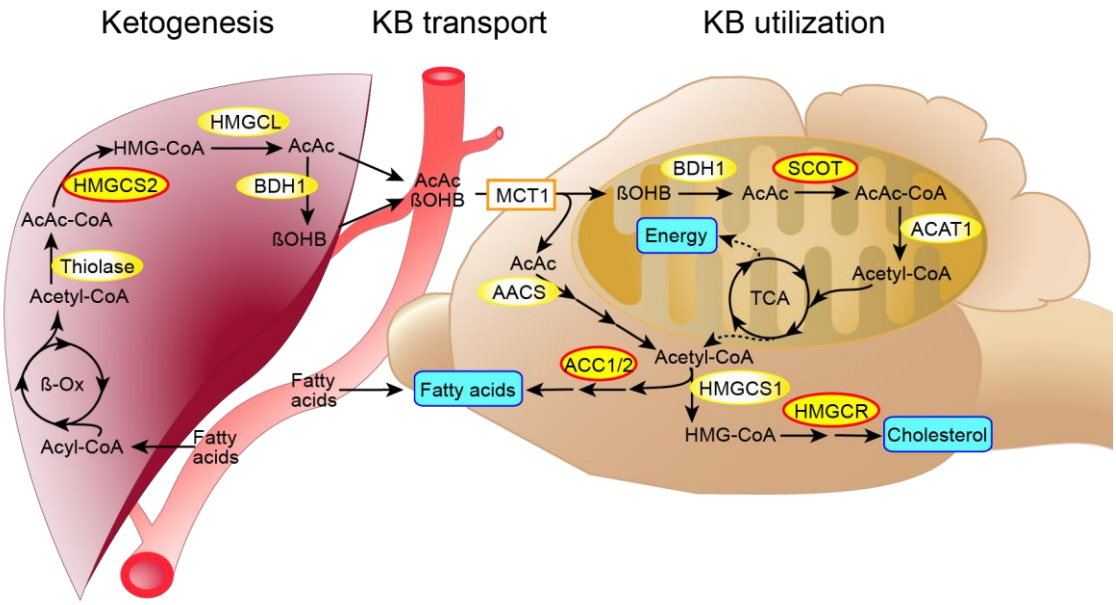

Fig. 3: Ketone body metabolism

When fatty acids are available in excess amounts in the circulation and glucose is in short supply, they undergo ß-oxidation in the liver resulting in the formation of acetyl-CoA that serves as substrate for ketogenesis. HMGCS2 catalyzes the rate-limiting step of ketogenesis leading to the production of AcAc and ßOHB. These KB are released into the circulation and can be taken up via MCT1 into the brain. Herein KB can undergo ketolysis in mitochondria to produce acetyl-CoA that is inserted into the TCA cycle to produce energy. SCOT facilitates the rate-limiting step of ketolysis by conversion of AcAc to AcAc-CoA. Within the cytosol, KB can also be used as precursor for cholesterol and fatty acid synthesis. AACS converts AcAc to AcAc-CoA that is further processed. Resulting Acetyl-CoA derived from AcAc can be used by HMGCS1 to direct it to sterol synthesis, which is controlled byHMGCR. In addition, cytosolic acetyl-CoA can also be directed to fatty acid synthesis by the rate-limiting enzymes ACC1/2. See main text for further information.

(ACAT1) produces two molecules acetyl-CoA, which are fueled into the TCA cycle for production of ATP (Fig. 3).

Next to the energy producing oxidation, KB can be used as precursors for anabolic pathways in the cytosol. Here, cytoplasmic acetoacetyl-CoA synthetase (AACS) facilitates the ATP-dependent conversion of AcAc to AcAc-CoA that in turn can be directed towards sterol biosynthesis. Cytosolic HMGCS1 catalyzes the first step of cholesterol synthesis to form cytosolic HMG-CoA from AcAc-CoA and acetyl-CoA.

Subsequently, HMG-CoA reductase (HMGCR) conducts the rate-limiting step of sterol synthesis by production of mevalonate. However, AcAc-CoA can also be cleaved to generate acetyl-CoA that is needed for synthesis of fatty acids by acetyl-CoA carboxylase 1 and 2 (ACC1/2, encoded by *Acaca* and *Acacb*) (Fig. 3). Especially during the neonatal period in rodents, the use of KB as energy source but also as precursor for lipidogenesis and cholesterogenesis is crucial for maintaining brain development (Bergstrom et al., 1984; Edmond, 1974; Webber & Edmond, 1979).

1.3 KB during suckling and the metabolic switch upon weaning

It has been known for decades, that the suckling period of rodents is accompanied by marked ketosis due to the high fat content of maternal milk (Czajka et al., 1964). During this time levels of KB range between 1 and 2 mM in the blood stream (E. Bailey & Lockwood, 1971; Hawkins et al., 1971). Interestingly, despite sufficient circulating amounts of glucose, the brain of suckling rodents might not be able to use glucose very efficiently as energy source since glycolytic enzymes are low expressed at this time (Booth et al., 1980; Gaitonde & Richter, 1966; Moore et al., 1971). In contrast, the immature brain is well equipped to utilize KB for energy production and biosynthesis of lipids and sterols. Sufficient cerebral KB metabolism dependents on three different aspects: (1) KB concentration within blood, (2) expression of transporters, (3) activity and expression of ketolytic enzymes. The uptake of KB by the brain directly relates to the circulating concentration of AcAc and ßOHB (Morris, 2005), but the brain of suckling rats is able to oxidize KB at higher rates than the mature brain at a given arterial concentration (Schroeder et al., 1991). Since KB level in blood of suckling rats is already high, the cerebral KB metabolism is further increased. In addition to KB concentrations in the circulation, KB metabolism in the brain is regulated by the abundance of MCTs within the BBB (Morris, 2005). MCT1 (encoded by *Solute carrier family 16 member 1; Slc16a1*) is mainly expressed by endothelial cells (Gerhart et al., 1997) while MCT2 (encoded by *Slc16a7*) has been related to neurons (Pellerin et al., 1998) and MCT4 (encoded by *Slc16a3*) might be astrocyte specific (Bergersen et al., 2001). In particular, the expression of MCT1 is significantly higher expressed in endothelial cells and astrocytes during suckling compared to adult conditions (Leino et al., 1999). Therefore, the transport capacity of ßOHB across the BBB is high during the suckling period, but declines drastically during adulthood (Cremer, 1982; Daniel et al., 1977) (Fig. 4). Following transport of KB into the brain, the ketolytic capacity therein is directly proportional to the activity and expression of SCOT (Orii et al., 2008) the rate-limiting enzyme of ketolysis. During the postnatal development, ketolytic enzymes are increased in expression compared to adulthood to serve brain energy requirements. Early studies

revealed that SCOT activity within the immature rat brain reaches maximal levels at approximately postnatal day 20 (P20), drastically declining afterwards to reach low adult levels (Krebs et al., 1971; Page et al., 1971) (Fig. 5A).

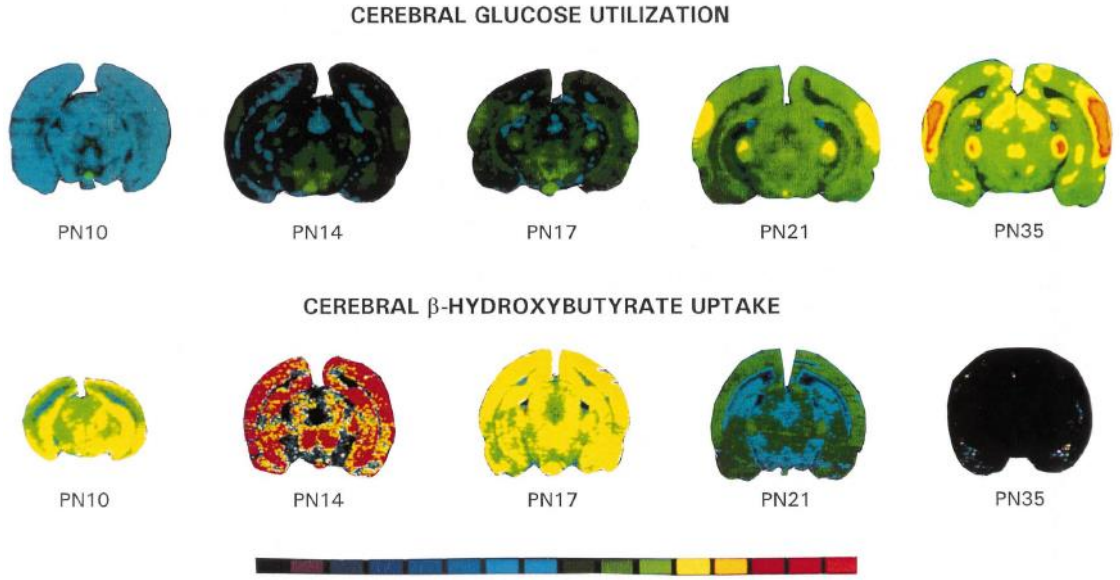

Fig. 4: Cerebral glucose and ßOHB utilization

Color-coded autoradiographic representation of the postnatal time course of glucose utilization and rates of cerebral ßOHB uptake in rat brain sections. The color scale at the bottom depicts quantitative rates of glucose utilization or ßOHB uptake. Black and blue indicate low rates, green medium rates and yellow to red high rates of utilization or uptake. Note that while glucose utilization is low during the first three weeks of postnatal development it starts to increase after weaning at PN21. In contrast, ßOHB uptake is highest during the suckling period and declines after weaning. PN= postnatal day. Taken from (Nehlig, 1999).

Similar results have been observed for BDH1 (Krebs et al., 1971; Leong & Clark, 1984). Only ACAT1 shows a somewhat different activity pattern during the postnatal period. Already maximal at birth, ACAT1 activity remains constantly high until P30 but decreases later on by 40% to reach adult levels (DeVivo et al., 1976; Krebs et al., 1971). ACAT1 might be used additionally in isoleucine breakdown (Su et al., 2017), which could explain the already high activity seen at birth. The developmental pattern of activity and expression of KB transporters and ketolytic enzymes seem to be well orchestrated by the increased KB availability in the circulation during suckling. When mice and rats are weaned at around P21 levels of ßOHB and AcAc decline to reach adult levels, which normally range between 0.2 and 0.5 mM in blood (E. Bailey & Lockwood, 1971). This might reflect the switch of suckling rodents from ingestion of maternal milk to carbohydrate rich chow. As a result, cerebral uptake of KB decreases with a concomitant increase in utilization of glucose (Nehlig & Pereira de Vasconcelos, 1993) (Fig. 4). In fact, development of brain glucose metabolism is contrasting cerebral KB metabolism. While expression of MCTs is highest during the first weeks of age, GLUT1 and GLUT3 reach their highest levels at around P30 (Vannucci, 1994). In addition, activity of the

major glycolytic enzymes reach maximal levels at weaning, when rodents start to ingest carbohydrate rich chow (Booth et al., 1980). This metabolic switch occurs during weaning and coincides with the peak of myelination, for which KB might serve as important substrates (Fig. 5B).

1.3.1 KB as precursor for lipid and sterol synthesis during myelination

In the brain, the amount of fatty acids and sterols increases about 4-fold during suckling until adulthood (Edmond et al., 1998; Nehlig, 2004). It has been shown that the increase in fatty acids and sterols is mainly attributable to *de novo* synthesis (Edmond et al., 1998). As consequence, the brain is dependent on precursors for fatty acid synthesis important

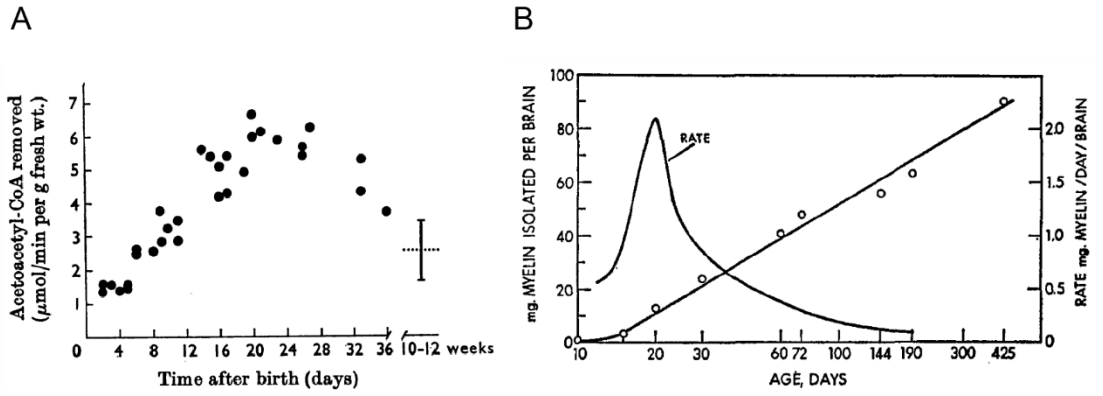

Fig. 5: Developmental course of SCOT activity and myelination

(A) Activity of SCOT in brain during postnatal development of the rat. Maximal activity is observed at around P20, after which it declines to adult levels (broken line with vertical bar). Taken from (Page et al., 1971). (B) Accumulation of myelin content within the brain during postnatal development in the rat (left ordinate, circles). Rate of myelin accumulation is plotted as smooth curve (right ordinate) with maximal rate occurring at P20. Taken from (Norton & Poduslo, 1973).

for myelination. ßOHB and AcAc have been shown to be suitable substrates for the synthesis of fatty acids and cholesterol (Edmond, 1974; Lopes-Cardozo & Klein, 1985) and are even preferentially used over glucose (Koper et al., 1981). AcAc seem to be the major substrate for lipid synthesis. The rate of fatty acid synthesis from AcAc increases until P5 declines rapidly during the residual suckling period, but still exceeds the rate of fatty acid synthesis of ßOHB (Yeh et al., 1977). However, others reported that ßOHB is the preferred substrate for lipid biosynthesis at later stages (i.e. P9-12 and P18) (Edmond, 1974; Webber & Edmond, 1979). Nonetheless, KB are important substrates for cholesterol synthesis to facilitate myelination and brain growth during the neonatal period. Indeed, during adulthood, KB are virtually not incorporated into lipids or proteins, but might exclusively be used for oxidation (Lopes-Cardozo & Klein, 1985). In rats, active

myelination is considered to start around P10 in rats (Edmond et al., 1998; Norton & Poduslo, 1973) and reaches its highest rate at P20 (Norton & Poduslo, 1973) (Fig. 5B). Despite the fact that at this age only 15% of the total adult myelin content is synthesized, the rate of myelin synthesis decreases sharply (Norton & Poduslo, 1973). These findings highlight the importance of KB as source for myelin cholesterol due to the fact that the rate of fatty acid and cholesterol synthesis decreases when glucose is used as energy source.

1.4 The ketogenic diet and its potential mechanisms for treating neurological disorders

Ketogenic diet (KD) is a high fat, low carbohydrate diet with a fat-to-carbohydrate plus protein ratio of 4:1, resulting in over 90% of metabolizable energy from fat with residual calorie intake from protein and carbohydrates (Gano et al., 2014; Kossoff & Rho, 2009). As hallmark of the KD, production of KB is observed with concurrent reduction in glucose availability (Gano et al., 2014) resembling the metabolic state seen during suckling. Discovered almost a century ago, anticonvulsive properties were linked to fasting (Lennox & Cobb, 1928) and feeding a KD replicated this metabolic effect but at the same time allows sufficient calorie intake and preserves endogenous lipid stores (Clanton et al., 2017; Wheless, 2008). The KD became the treatment of choice for epilepsy, but fell out of focus after the development of the first anti-seizure drugs in 1938 (Bailey et al., 2005). During the past 20 years interest returned after recognition that the KD was able to treat pharmacoresistant forms of epilepsy especially in children (Freeman & Vining, 1999; Neal et al., 2008). Additionally, extensive research indicated that the effectiveness of a KD is not restricted to treating epilepsy. The KD exhibits beneficial effects for treating models of neurological disorders such as brain cancer (Abdelwahab et al., 2012), Alzheimer, Parkinson and Huntington disease (Henderson, 2008; Lim et al., 2011; Vanitallie et al., 2005), amyotrophic lateral sclerosis (Zhao et al., 2006) and very recently in a mouse model of the hereditary leukodystrophy Pelizaeus-Merzbacher disease (Stumpf et al., 2019). The broad anticonvulsant spectrum of the KD might be attributable to the plethora of possible mechanisms by which the KD influences brain metabolism, neurotransmitter release/synthesis and mitochondrial biogenesis.

1.4.1 Proposed anticonvulsant effects of the ketogenic diet

Epilepsy describes states of spontaneously synchronized depolarization of neurons leading to situations of unawareness, unconsciousness and uncontrolled motor activity that occur paroxysmally (Koppel & Swerdlow, 2018).

Table 1: potential beneficial effects of the ketogenic diet

Dietary changes	Potential mechanism of action	Effects	Reference
Increased levels of AcAc	Inhibition of glutamate release from vesicular glutamate transporter	Reduced neuronal hyperexcitability	(Juge et al., 2010)
Enhanced TCA cylce	Increased synthesis of GABA	Shift towards inhibitory neurotransmission	(Gano et al., 2014; Yudkoff et al., 2005)
Increased ATP/Adenosine level	Activation of Adenosine A1 receptors on excitatory neurons	Inhibition of excitatory neurons	(Masino et al., 2011)
Increased KB level	Altered mitochondrial respiration	Circumvention of complex I decreases superoxide formation, stimulated ATP production by increased flux through complex II	(Ho et al., 2012; Tieu et al., 2003)
	Inhibiton of HDAC through ßOHB	Enhanced expression of antioxidative genes	(Shimazu et al., 2013)

Such seizures could be reduced in 75% of patients, who adhered to the KD over a three-months period (Neal et al., 2008). It is hypothesized that the KD induces anti-seizure effects by increasing KB level. AcAc has been found to reduce neuronal hyperexcitability by inhibition of glutamate release (Table 1) as it is the major excitatory neurotransmitter (Koppel & Swerdlow, 2018). Another possible mechanism by which the KD could influence neuronal excitability involves direct changes in levels of glutamate and its counterpart γ-ammino butyric acid (GABA). Through anaplerosis the KD increases the need of oxaloacetate to condense with acetyl-CoA, thereby reducing the production of aspartate from glutamate and favoring the synthesis of GABA through glutamate decarboxylase (Gano et al., 2014; Yudkoff et al., 2005). In turn, increased GABA levels could lead to enhanced inhibitory neurotransmission (Yudkoff et al., 2005). Indeed, changes in brain neurotransmitter levels were found to be altered upon KD ingestion, but obtained results are inconsistent. Nonetheless, a shift of the balance between these neurotransmitters by the KD has to be considered as potential mechanism.

Since application of the KD increases ATP levels (DeVivo et al., 1978; Kim et al., 2010) it was proposed that the KD ultimately leads to increased adenosine levels (Maalouf et al., 2009) (Table 1). Adenosine is thought to modulate antiseizure effects by activation of adenosine A_1 receptors (A_1Rs) leading to inhibition of excitatory neurons (Masino et al., 2012; Rogawski et al., 2016).

One hallmark of the KD is a reduction of blood glucose levels through reduction of carbohydrates by the diet. Since KB level does not necessarily correlate with levels of seizure control, it was hypothesized that decreased glucose metabolism may be important for seizure prevention (Lutas & Yellen, 2013). Best evidence supporting this

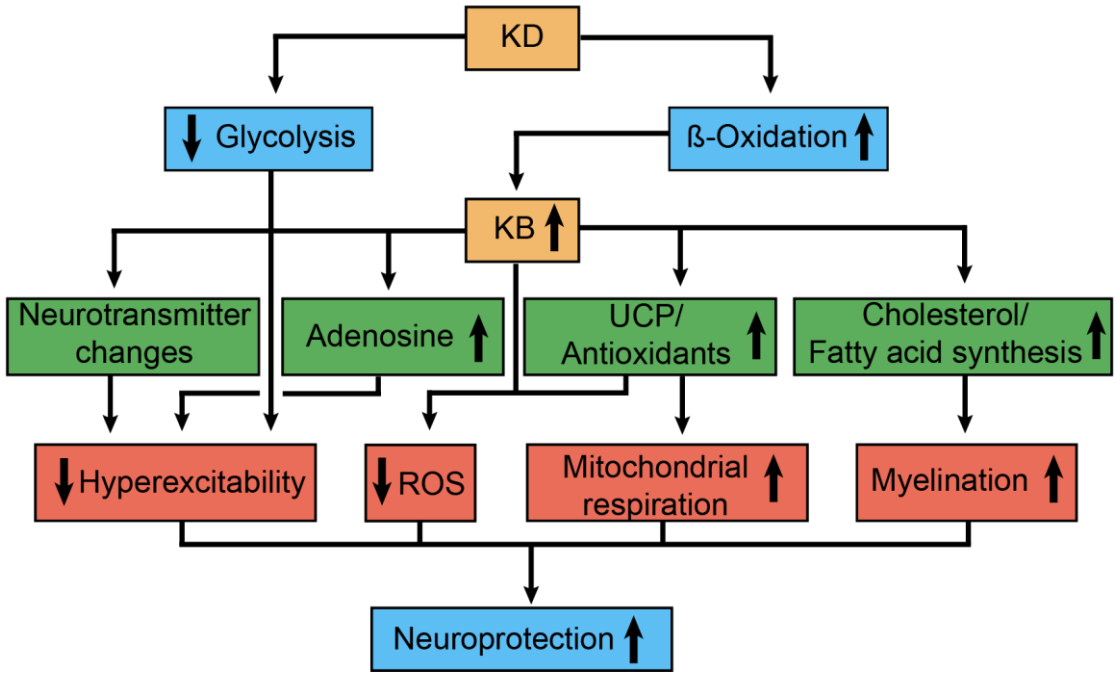

Fig. 6: Possible mechanism of the ketogenic diet leading to neuroprotection

The KD leads to metabolic changes (blue) enhancing KB level. KB might influence factors and mechanisms (green) resulting in anticonvulsant effects and metabolic improvements. As consequence, harmful processes are reduced whereas positive mechanism are enhanced (red) to provide neuroprotection. See text for further details.

assumption is the observation that seizure control can be rapidly reversed after ingestion of carbohydrates (Huttenlocher, 1976). However, mechanisms by which glucose reduction leads to decreased hyperexcitability remain unknown. In regard of glucose reduction, the KD gained interest in treating brain cancer. As cancer cells are mainly dependent on glycolysis and lactate production without relying on oxidative phosphorylation, a process known as “Warburg effect”, the KD is a suitable tool to withdraw these cells their metabolic basis. Indeed, the KD has been shown to be an effective alternative therapy for treating malignant glioma (Abdelwahab et al., 2012; Zhou et al., 2007).

Oxidative stress has been linked to the progression of multiple neurodegenerative diseases (Barnham et al., 2004). Several studies indicated that the KD might be able to decrease oxidative stress by enhancing antioxidant mechanisms (Table 1). Direct effects of the KD might be displayed by the scavenging potential of KB. ßOHB and AcAc have been shown to reduce numerous reactive oxygen species (ROS) *in vitro*, but only under unphysiological conditions (Haces et al., 2008). Another possibility by which the KD could decrease mitochondrial ROS production is the stimulation of ATP production through increased complex II flux of the electron transport chain (Ho et al., 2012). In turn, superoxide formation by complex I is potentially diminished. Thereby, the KD could be able to improve mitochondrial respiration and enhance energy production.
In conclusion, the KD might exhibit multiple beneficial effects that could act in concert to modulate synaptic transmission and alter brain metabolism thereby ameliorating different symptoms of neurological disorders (Fig. 6).

1.4.2 The KD's potential in supporting myelination in neurodegenerative diseases

In mice, developmental myelination is primarily ongoing between P10 and P60 in most brain regions (Baumann & Pham-Dinh, 2001). Myelination is carried out by oligodendrocytes to enable fast saltatory nerve conduction and axonal integrity (Nave & Werner, 2014). This process requires extensive formation of oligodendrocytic plasma membrane mostly comprised of lipids and sterols to enwrap and insulate axons. KB are the preferred substrate for cholesterol and lipid synthesis for myelination during development (Edmond, 1974; Yeh et al., 1977), raising the question of the KD's potential to support remyelination in neurodegenerative diseases. However, direct evidence that the KD supports remyelination is scarce and only a few case studies support this hypothesis. Aspartate-glutamate carrier 1 (AGC1) is involved in the malate-aspartate shuttle (Falk et al., 2014), that facilitates neuronal export of glial aspartate important for proper myelination (Clanton et al., 2017). Deficiency of AGC1 causes infantile epilepsy and hypomyelination (Falk et al., 2014). Recently, in a patient with AGC1 deficiency, the KD improved psychomotor development and myelination measured by magnetic resonance spectroscopy (Dahlin et al., 2015) indicating potential effects in treating myelination defects. Similar improvements of myelination could be observed in a patient with GLUT1 deficiency adhering to the KD (Klepper et al., 2007) (Fig. 6). Very recently, a study using proteolipid protein 1 (PLP1) transgenic mice to model Pelizaeus-Merzbacher disease, showed enhanced myelination when mice were treated with the KD (Stumpf et al., 2019). In addition to reducing endoplasmatic reticulum stress, the

authors speculated that the KD might enhance remyelination by supporting local cholesterol synthesis and enhances oligodendrocyte precursor cell proliferation.
However, given the immense amount of possible mechanisms by which the KD modulate anticonvulsant effects, reduce oxidative stress and improve mitochondrial respiration, comparatively little is known of potential mechanisms affecting remyelination.

1.5 Aim of the study

The KD is widely used to treat certain forms of epilepsy and is extensively studied for its potential to ameliorate neurodegenerative diseases such as Alzheimer or Parkinson disease. Studies investigating the KD's beneficial effects revealed a plethora of potential mechanisms. However, evidence supporting the positive effects of the KD originate from experiments using cell culture, *ex vivo* slice experiments or global assessment of tissue changes. All of these have certain disadvantages with respect to analyzing the KD's mechanism. *In vitro* or *ex vivo* studies use unphysiological concentrations of KB or artificial serum conditions not observed *in vivo*. Additionally, the contribution of the BBB and the adaptation of the brain to the peripheral metabolism cannot be attributed. On the other hand, *in vivo* studies draw their conclusion from global tissue changes lacking the cell type specific resolution needed to assess cell type specific adaptation. Furthermore, the influence of the KD on brain metabolism was often investigated under disease conditions that themselves can influence brain metabolism. Hence, cell type specific metabolic changes *in vivo* in response to feeding a KD under non disease conditions have not yet been studied to unravel actions of the KD on brain cell metabolism.

Here, we aimed at testing the cell type specific metabolic changes of brain cells under physiological conditions in mice fed a KD. To address the question whether the metabolic switch seen upon weaning in the brain is due to endogenous signals or caused by dietary changes, mice were fed a KD for up to six weeks of age. Investigation of global metabolic changes within the brain by using immunoblot, fluorescent immunohistochemistry and ultrastructural analysis was used to select the age of mice where adaptation to ketosis is maximal.

In depth analysis was performed at the time point with maximal effects to address the following questions: Which metabolic pathways will be altered in brain cells? Will they switch to KB utilization under low glucose conditions or rely on residual glucose? Furthermore, is it possible to draw conclusions in which way substrates are distributed among cell types under ketogenic conditions?

Therefore, cell type specific isolation from adult mouse brain coupled to subsequent proteomic and transcriptomic analysis was performed to investigate cell type specific metabolic changes. This enabled comparison between cell types and helped to understand changes in overall brain metabolism.

2 Results

2.1 Experimental design

During weaning the brain metabolism undergoes a rapid change that switches substrate preferences from ketone bodies (KB) to glucose (Nehlig, 2004). To test, if this metabolic switch of the brain can be prevented and to investigate the time course of metabolic events within the brain, mice were reared by a ketogenic diet (KD). To achieve a smooth transition from ingestion of mother's milk to adhering to the KD, food was applied from two weeks of age onward, when pups still ingest milk. Application of the KD to the dam

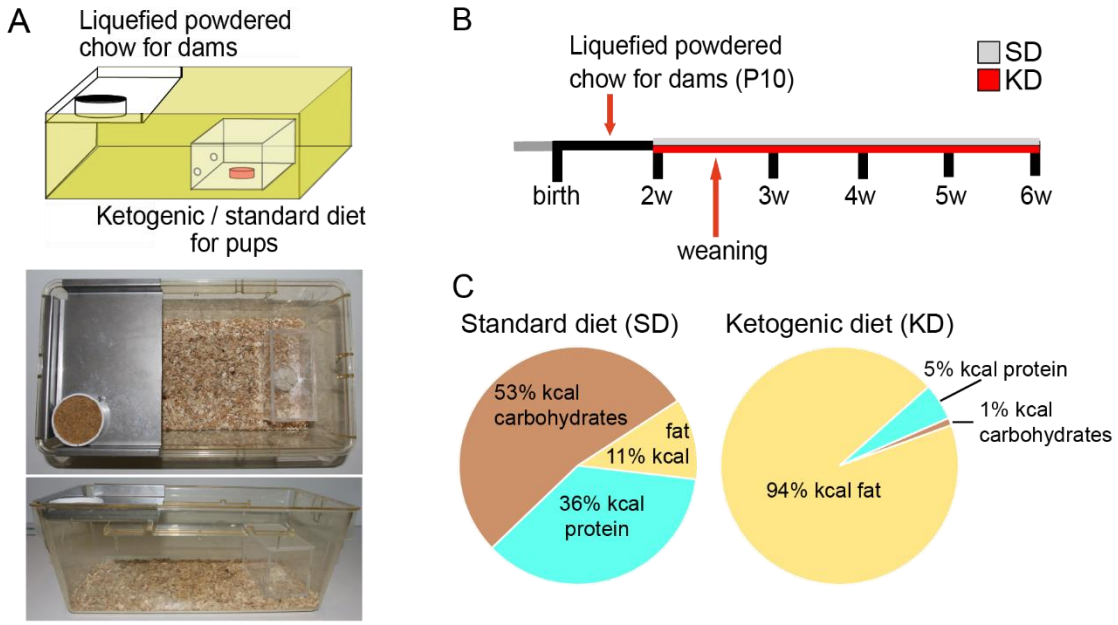

Fig. 7: Rearing device, investigation strategy and diet composition.

(A) Rearing devices to achieve food separation between dams and pups. (B) Investigation strategy with indicated time points for food change for dams and weaning. Standard diet (SD) or ketogenic diet (KD) were applied from two weeks onward for pups. (C) Composition of standard and ketogenic diet.

can cause severe ketoacidosis and prevent lactation (Sussman et al., 2013). To circumvent this issue, special rearing devices were developed to achieve food separation between mother and pups (Fig. 7A). Liquefied powdered chow was applied to the mother on a shelf that is not accessible for the pups. However, pups could reach the KD applied in a small box with holes, which were too small for the mother. Food for the mother was applied at P10 of the pups, whereas the food for the pups (either KD or standard diet) was applied at two weeks of age (Fig. 7B). Mice were weaned at P17 and fed the KD or standard diet (SD) for up to six weeks. The high fat content of the KD results in altered proportion of gained kcal from fat, protein and carbohydrates (Fig. 7C). We speculated

that resulting ketosis will prolong the metabolism of mice seen during the suckling period due to reflections of mother's milk.

2.2 Blood level of mice react to rearing on a KD

Due to the high fat content, the KD leads to hepatic production of KB that are released into the circulation increasing the concentration of ßOHB as major KB. In turn, glucose concentration decreases (Gano et al., 2014; Kossoff & Rho, 2009). Therefore,

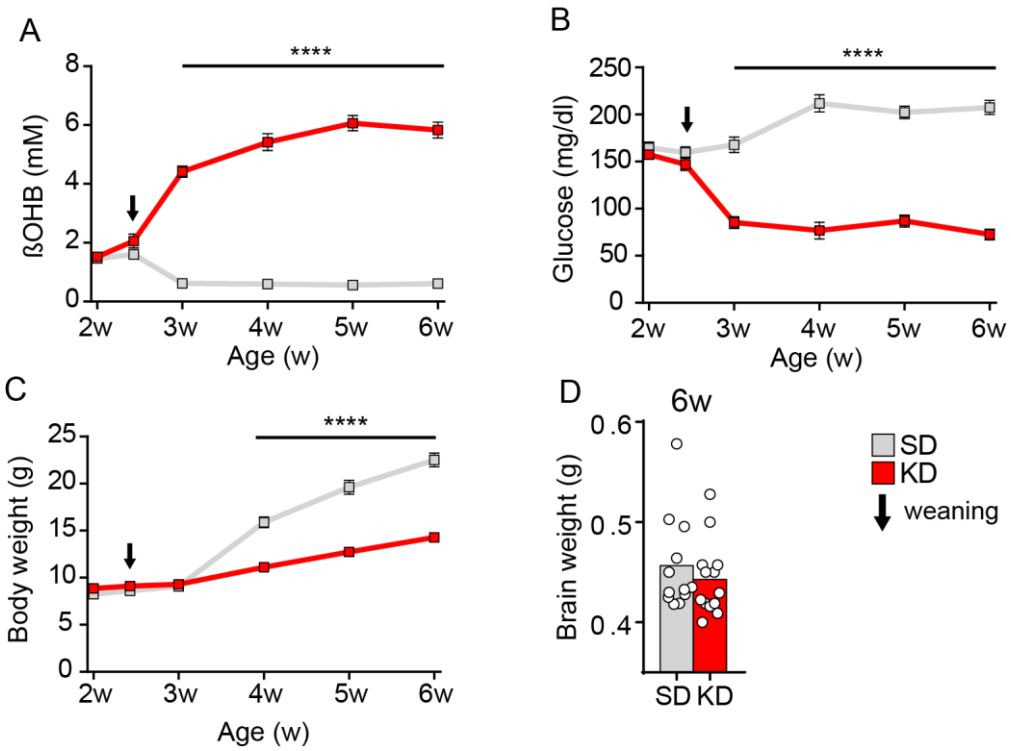

Fig. 8: Induction of ketosis upon feeding a ketogenic diet.

Blood level of ßOHB (A) increase over time while Glucose (B) decreases when mice are fed a ketogenic diet. (C) Body weight in mice fed a ketogenic diet increase slower than mice fed a standard diet. Graphs represent mean values ± SEM of n=20 animals. Asterisks depict significant differences with *p<0.05, **p<0.005, ***p<0.001, ****p<0.0001 (two-way ANOVA with Sidak's post test). (D) Brain weight of mice at six weeks of age is unaffected. Bars represent mean values with individual data points (n=12-13). Student's t-test. SD= standard diet; KD= ketogenic diet.

investigation of blood levels of ßOHB and glucose served to determine successful induction of ketosis through feeding a KD. After weaning, concentration of ßOHB increased significantly in mice fed the KD to reach maximal values at five weeks of age (Fig. 8A). In SD fed mice, concentration of ßOHB declined after weaning to reach adult levels in accordance with previous studies (E. Bailey & Lockwood, 1971; Hawkins et al., 1971) and remained constant after three weeks of age. Glucose concentration inversely correlated with ßOHB levels in blood and decreased significantly in mice fed a KD compared after weaning. In contrast, SD fed mice showed increased glucose

concentrations after starting to ingest the SD (Fig. 8B). Concentration of ßOHB and glucose seemed to stabilize at a certain level after four to five weeks of age in both groups.

Ingestion of a KD is known to reduce body weight (Bergqvist, 2012; Thio et al., 2006). Therefore, gain of body weight of mice fed SD or KD was analyzed. KD mice steadily increased body weight over time but at a significantly slower rate than mice fed the SD (Fig. 8C). However, brain weight of KD fed mice was unaltered at six weeks of age (Fig. 8D) suggesting normal brain growth. This finding is in line with previous results reporting stable brain volume of mice after three weeks of age (Hammelrath et al., 2016). Taken together, these results indicate successful induction of ketosis in KD mice after weaning. Furthermore, despite slower increase in body weight, brain growth is facilitated at normal levels in mice fed KD.

2.3 Brain maturation of mice reared with a ketogenic diet

Since mice reared on the KD exhibit reduced body growth, analysis of brain maturation was performed to investigate possible effects of the KD on brain development. Brain derived neurotrophic factor (BDNF) is considered as general maturation marker, as expression increases with brain maturation (Maisonpierre et al., 1990). Expression analysis of *Bdnf* in cortex of mice revealed no differences between dietary groups, suggesting normal brain maturation (Fig. 9A). In addition, expression of *Myelin basic protein* (*Mbp*), a mature myelin marker (Winters et al., 2011) showed no changes in expression at any investigated time point (Fig. 9B). However, expression of *Myelin-oligodendrocyte glycoprotein* (*Mog*), a marker for oligodendrocyte maturation (Scolding et al., 1989), was slightly reduced at six weeks of age in cortex of KD mice indicating alterations of oligodendrocyte maturation (Fig. 9C). Nonetheless, these results indicate an overall normal brain growth and maturation in mice fed the KD.

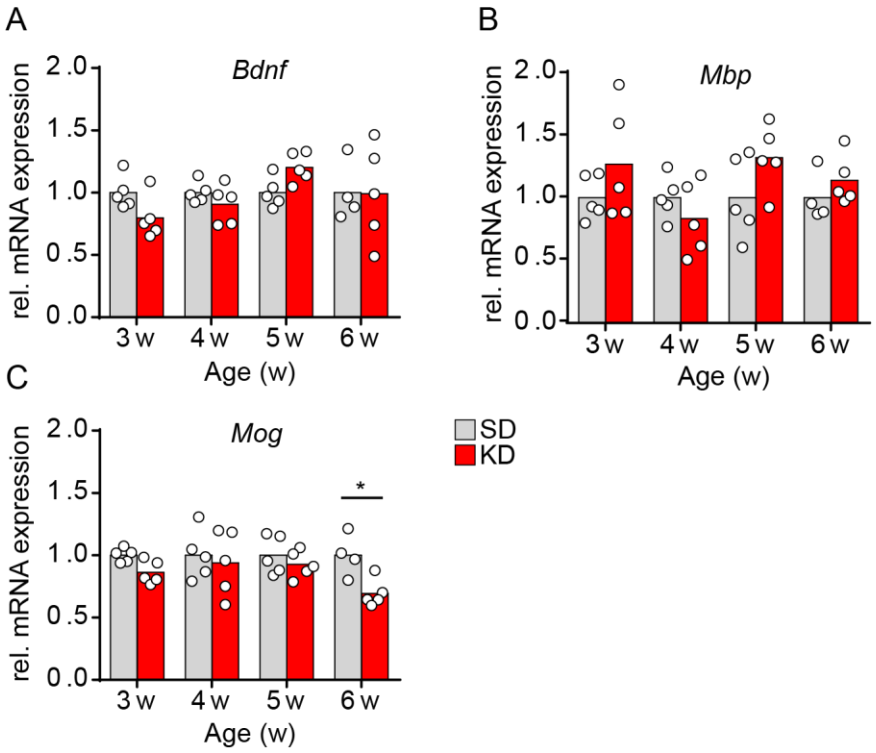

Fig. 9: Expression analysis of brain maturation marker

(A-C) qRT-PCR analysis in cortex of mice fed KD or SD at indicated time points show no changes for the brain maturation marker *Bdnf* (A) and the mature myelin marker *Mbp* (B) but slight reduction of the oligodendrocyte maturation marker *Mog* at six weeks of age (C). Bars represent mean expression normalized to SD fed animals with individual data points (n=4-5). Asterisks depict significant differences with *p<0.05, (two-way ANOVA with Sidak's post test). SD= standard diet; KD= ketogenic diet.

2.4 Myelination is unaltered in mice reared with a ketogenic diet

KB have been shown to be suitable substrates for the synthesis of fatty acids and cholesterol (Edmond, 1974; Lopes-Cardozo & Klein, 1985), thereby facilitating myelination. Since mRNA expression does not necessarily reflect protein abundances, myelination was analyzed on morphological level in response to the KD. Therefore, cortices of mice were investigated using electron microscopic analysis at six weeks of age. Fluorescent immunolabeling of MBP in sagittal sections of mice did not show alterations regarding MBP abundance in cortex of KD fed animals (Fig. 10A). MBP positive signal, reflecting myelinated fibers traversing throughout the cortex, was comparably present in mice of both dietary groups. This finding supported results from expression analysis suggesting no alterations in *Mbp* expression (compare Fig. 9B). However, ultrastructural differences of myelin or axon thickness still could be present. To address this issue, number of myelinated fibers and myelin thickness was assessed on electron micrographs in cortex of mice at six weeks of age. Electron micrographs

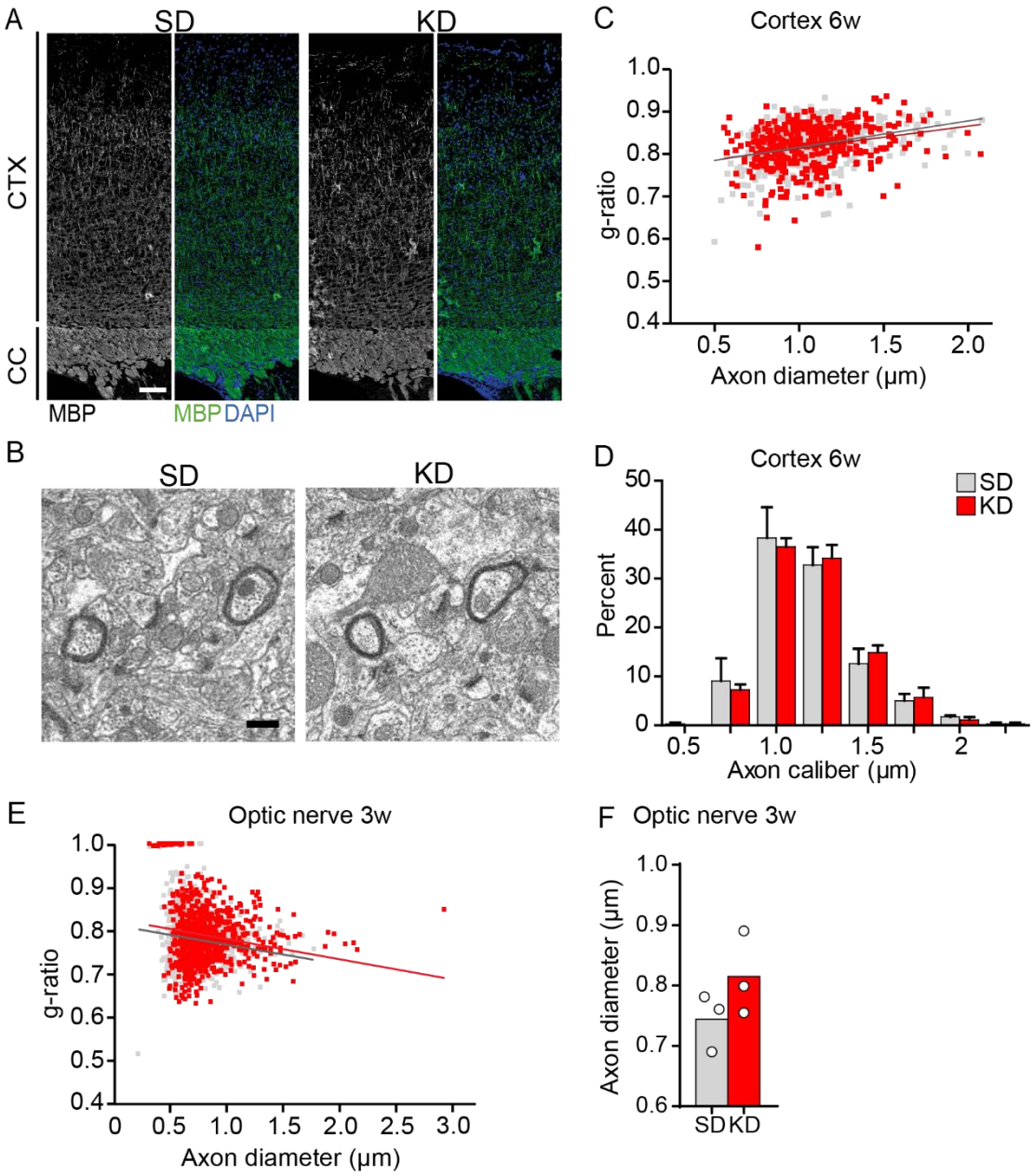

Fig. 10: Myelination remains unchanged when mice fed a ketogenic diet

(A) Fluorescent staining of MBP in sagittal sections of mice fed SD or KD at six weeks of age reveals no obvious differences. Scale, 100µm. (B) Representative electron microscopic image in cortex of mice fed SD (left) or KD (right) at six weeks of age. Scale, 500nm. (C) G-ratio analysis of cortical axons and axon caliber distribution (D) shows no difference at six weeks of age (n=3). (E) G-ratio analysis of axons in optic nerve at three weeks of age. (F) Mean axon diameter in optic nerve at three weeks of age (n=3). One-way ANOVA with Sidak's post test. SD= standard diet; KD= ketogenic diet.

revealed normal appearance of myelinated fibers in cortex of KD fed mice (Fig. 10B). The g-ratio is a measurement to assess myelin thickness and hence sufficient insulation for proper conduction velocity (Waxman, 1980). It is calculated by division of axon diameter through the diameter of fiber plus surrounding myelin (Saher et al., 2012). Assessment of g-ratio revealed normal ratios between mice either fed the SD or KD (Fig.

10C), suggesting no alterations in myelin thickness. In addition, distribution of analyzed fibers did not differ between groups (SD: 107.67 ±8.37 SEM; KD: 121.67 ±6.90 SEM; p=0.389; two-sided Student's t-test), further supporting normal myelination of axons within the cortex of KD fed mice. The diameter of axons is an important structural characteristic of the CNS and correlates with conduction velocity. In addition, it can be affected by neurological disorders (Sepehrband et al., 2016). Changes in the distribution of axon calibers could therefore indicate altered conduction velocity of axons. However, frequency distribution of axon calibers within the cortex of mice fed the KD did not show any signs of changed axon calibers (Fig. 10D). In summary, the current findings indicate normal myelination at six weeks of age within the cortex of ketogenic reared mice. Myelination was unaffected at six weeks of age in cortex of mice on KD. However, the KD could exhibit transient effects at earlier time points. To test this idea, myelination was assessed at three weeks of age within the optic nerve where rate of myelination is maximal (Dangata et al., 1996). Since myelin formation occurs in an eye-to-chiasm direction (Colello et al., 1995) g-ratio measurements were performed at the chiasmatic end of the nerve where possible effects would be most pronounced. However, g-ratio analysis did not reveal significant differences in myelin thickness in regard to axon diameter suggesting unaltered myelination at three weeks of age in KD fed mice (Fig. 10E). Additionally, mean axon caliber in optic never showed no significant alterations in response to KD feeding (Fig. 10F) suggesting normal axon growth. Taken together, these results indicate that rearing mice on a KD does not alter myelination during highest rate of myelin formation. However, it has to be considered that the time of application of the KD might be too short to have influence on myelin formation.

2.5 KD support normal development of cognition and learning in mice

To analyze if the KD in mice could lead to altered cognition or learning ability we performed a sound discrimination experiment in collaboration with Dr. Livia de Hoz from the neurogenetics department of the Max-Plank Institute of Experimental Medicine. Mice at five weeks of age were placed into cages connected to an audiobox, a setup suitable to measure cognition and learning ability in mice (de Hoz et al., 2018; de Hoz & Nelken, 2014). Mice can freely move within their home cage with access to food. Water is provided within the audiobox behind openable doors (Fig. 11A). To get access to water, mice need to perform nose poke to open the doors in front of the water bottles. Always when a mouse visits the audiobox, a specific sound is played. To test the ability of cognition and learning a sound discrimination paradigm was designed (Fig. 11B). During

the habituation phase, mice always hear the “safe” sound (6.67 kHz) when entering the audiobox without consequences after nose poking. From day six of the experiment (training phase) at a certain percentage the “conditioned” sound (13.34 kHz) is played after a visit. Nose poking during a conditioned visit resulted in an aversive air puff and no access to water. Therefore, mice need to discriminate between a “safe” and “conditioned” sound and need to learn to avoid nose poking after a conditioned visit. During the whole experiment mice reared on the KD or SD had comparable number of

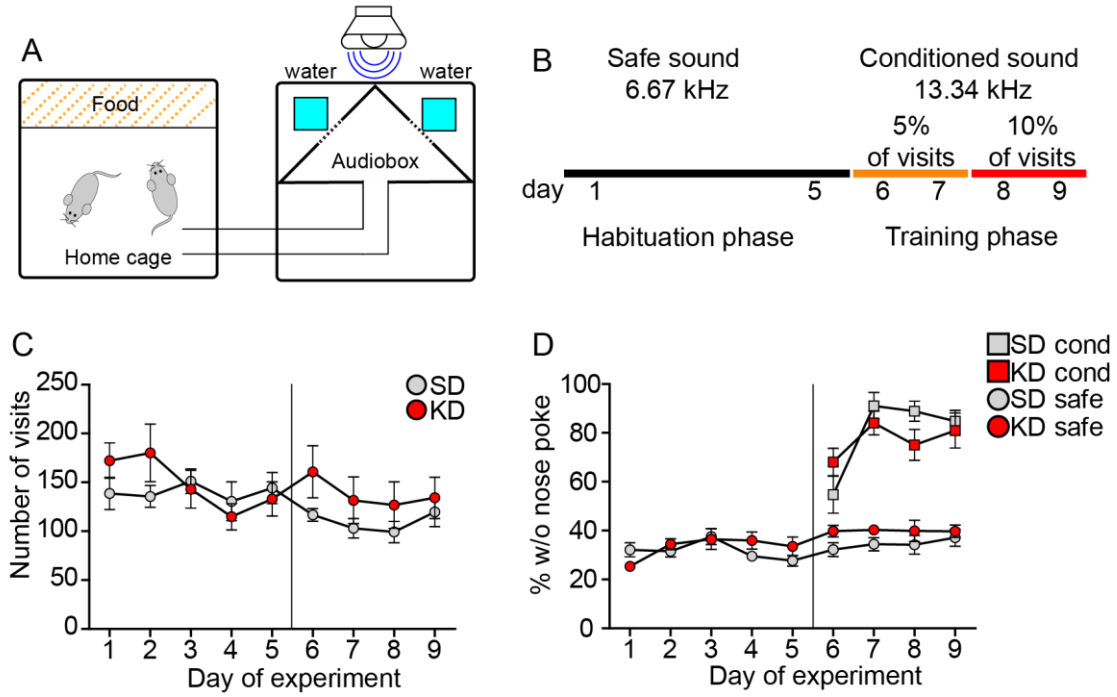

Fig. 11: Ketogenic diet feeding does not impair learning ability

(A) Schematic construction of the Audiobox. Mice can freely move within their home cage with access to food *ad libitum*. Mice need to nose poke to get access to water within the Audiobox while different sounds can be played. (B) Paradigm to test learning ability of mice. During the habituation phase mice hear the safe sound when entering the Audiobox and nose poking has no negative effect. At day 6-9 in indicated percentages a conditioned sound is played when mice visit the Audiobox. Nose poking after a conditioned visit leads to the application of an aversive air-puff and no access to water. Mice need to learn to avoid nose poking after hearing the conditioned sound. (C) Total number of visits between mice fed SD or KD during the experiment is not altered. (D) Percentage of visits without nose poke under safe and conditioned conditions for mice on KD or SD at five weeks of age reveal similar learning ability. Graphs represent mean values ± SEM, n=5. Two-way ANOVA

visits per mouse per day (Fig. 11C). This suggests, that KD fed mice did not show any signs of fatigue or lack of motivation. Furthermore, this result confirms, that both dietary groups had comparable amount of visits to learn to avoid the conditioned sound. Evaluation of visits without a nose poke revealed that mice on SD or KD, respectively avoided nose poking in approximately 30-40% of the visits during the whole experiment when a “safe” sound is played with no significant difference between groups (Fig. 11D).

At day 6 of the experiment, mice avoided nose poking after a conditioned sound in over 50% and 65% of the visits for SD and KD fed mice, respectively. This percentage further improved during the following days to approximately 75-90% of the cases for both groups. No significant differences were detected at any time point between SD and KD fed mice, indicating normal learning curves between SD and KD fed mice. Taken together, these results indicate that mice are able to discriminate between different sounds and quickly learn to avoid the “conditioned” sound within one day. Furthermore, it supports the previous findings, that the KD in mice facilitate normal brain growth and development. Hence, apart from reducing body growth, no signs for reduced development within the brain was found.

2.6 Glycolytic changes in cortex of mice fed KD

The observed reduction in blood glucose could influence glucose metabolism within the brain. To address the question whether the KD would alter glycolysis in cortex of mice, qRT-PCR were performed for *Glut1* and *Hk1.* Despite the observed reduction of glucose within the blood (compare Fig. 8B), expression of *Glut1,* the major glucose transporter within the brain (Vannucci, 1994), showed no significant decrease at six weeks of age upon feeding a KD (Fig. 12A). Expression of *Hk1,* the enzyme facilitating the first committed step of glycolysis, showed similar results (Fig. 12B). In previous studies results reported conflicting results for GLUT1 abundance upon feeding a KD ranging from decrease over no change to increased levels (Forero-Quintero et al., 2017; Hernandez et al., 2018; Leino et al., 2001). Therefore, we analyzed GLUT1 protein level in cortex of mice at six weeks of age, where blood levels of glucose appeared stable. Immunoblot showed the expected bands of GLUT1 at 45 and 55 kDa according to literature (Sivitz et al., 1989). Both bands were used for quantification, indicating no significant difference in GLUT1 abundance between SD and KD fed mice (Fig. 12D), confirming the results of the qRT-PCR analysis.

Despite unaltered expression of GLUT1, metabolite levels within the brain still could be different due to changes in circulation. To test this hypothesis, metabolite profiling using gas chromatography/mass spectrometry (GC/MS) was performed in collaboration with Dr. Till Ischebeck from the department of Plant Biochemistry at the University of Göttingen. Metabolites were extracted from cortex of mice at six weeks of age and following metabolomics results will refer to this analysis. Interestingly, glucose within the cortex of KD fed animals decreased to around 30% of normal level when compared to SD fed mice (Fig. 12E), indicating decreased influx of glucose into the cortex. Metabolite levels were not corrected for residual blood content of cortical tissue. However, this accounts for only 3% in brain (Hindfelt & Siesjo, 1970; Mark et al., 1968) and might

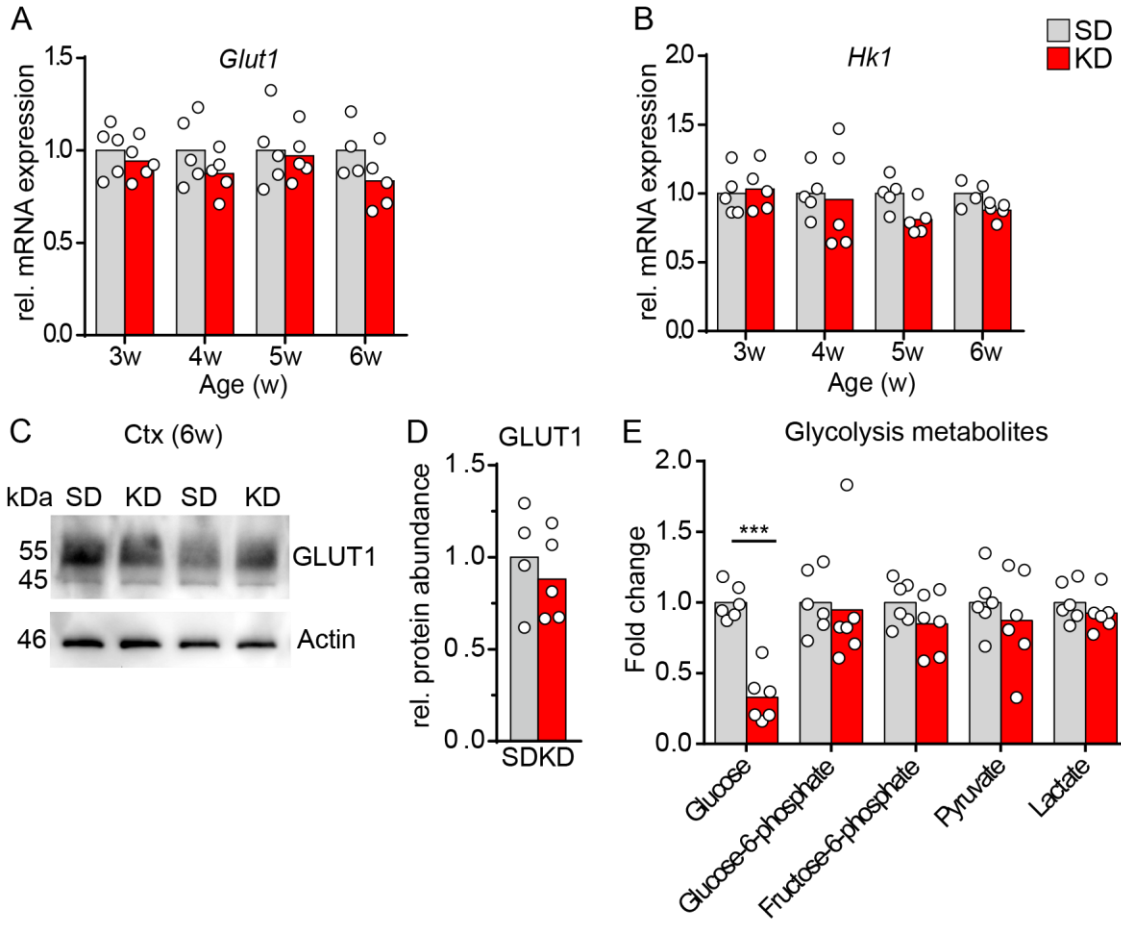

Fig. 12: Global glycolytic changes upon KD feeding

Expression analysis of *Glut1* (A) and *HK1* (B) at indicated time points in cortex of SD or KD fed mice are unaltered (n=4-5). Two-way ANOVA with Sidak's post test. (C) Representative immunoblot for GLUT1 at six weeks of age in cortex of mice fed SD or KD and its quantification (D) reveal no alterations. Actin served as loading control (n=4-5; two sided Student's t-test). (E) Glycolysis metabolites measured by GC/MS (all metabolites were measured in collaboration with Dr. Till Ischebeck) in cortex of mice at six weeks of age (n=6). Significance is indicated with *padj<0.05, **padj<0.005, ***padj<0.001 (Benjamini-Hochberg correction, DESeq2 R package) SD= standard diet; KD= ketogenic diet.

therefore be of minor importance. Interestingly, all identified glycolytic intermediates remained unchanged. This is in partial disagreement with previous results reporting increased glucose and glycolytic intermediates despite reduced blood glucose in rats fed a KD that was speculated to occur due to increased GLUT1 expression (DeVivo et al., 1978; Roy et al., 2015). However, other studies found decreased brain glucose uptake in ketogenic rats (Jiang et al., 2011; Zhang et al., 2013). One could speculate that our finding is due to slowed glycolytic rate leading to accumulation of the intermediates or that the absolute glucose concentration is still high enough to support glycolysis at normal levels. Further experiments need to be performed to address these possibilities. Taken together these results suggest that the overall glucose metabolism including

expression of transporter and enzymes in cortex is unaltered and glucose is reduced within cortical tissue due to reduction of glucose concentration within the blood.

2.7 ßOHB uptake is increased in cortex of mice on KD

The brain responds to the KD by increasing the expression of MCT1, the major KB transporter (Leino et al., 2001; Noh et al., 2004). MCT1 expression determined by qRT-PCR from cortex samples revealed no changes in *Mct1* mRNA level up to five weeks of age in KD fed mice (Fig. 13A). At six weeks of age the expression of *Mct1* almost doubled, suggesting adaptation to the KD. To test, whether MCT1 is also altered on protein level, immunoblot analysis of MCT1 at six weeks of age was performed (Fig. 13B). Indeed MCT1 protein level was significantly increased in KD fed mice (Fig. 13C), suggesting increased transport of KB.

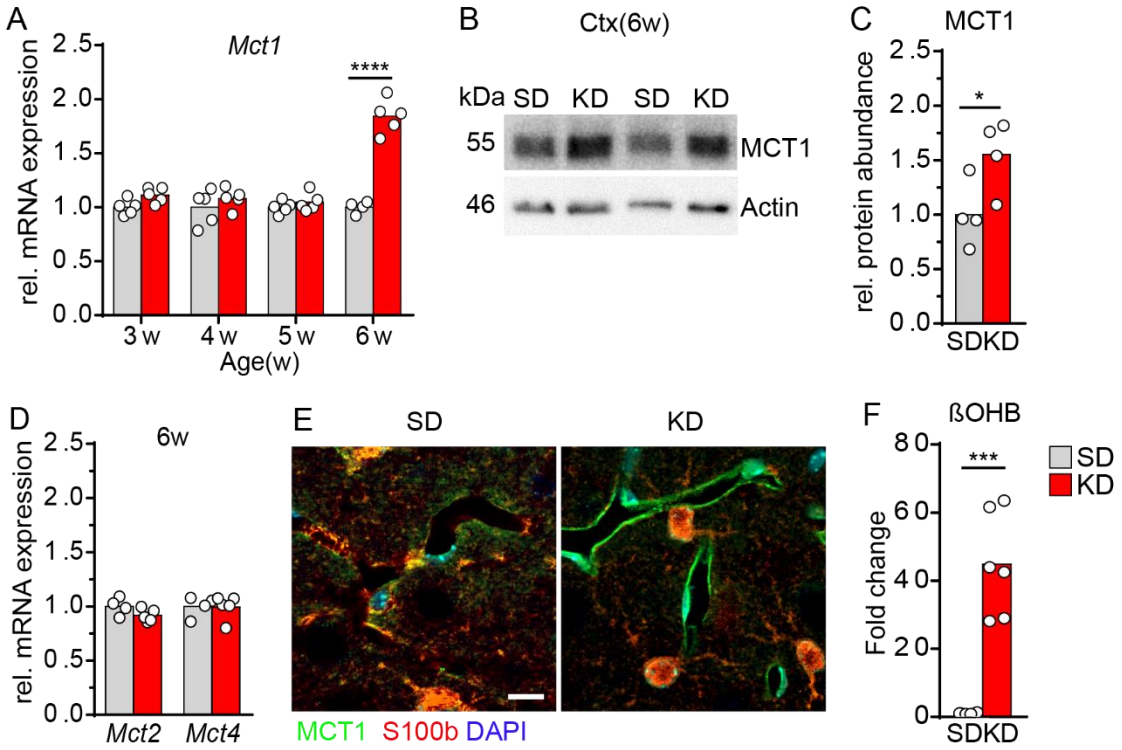

Fig. 13: Transport of ßOHB across BBB is increased in KD fed mice

(A) Expression of *Mct1* is increased in cortex at 6 weeks of age by ketogenic diet (n=4-5). Asterisks depict significant differences with *p<0.05, **p<0.005, ***p<0.001, ****p<0.0001 (two-way ANOVA with Sidak's post test). (B-C) Immunoblot for MCT1 in cortex of mice fed SD or KD at 6 weeks of age shows increased protein abundance. Actin served as loading control (n=4). Asterisks depict significant differences with *p<0.05 (two-sided Student's t-test). (D) Expression of *Mct2* and *Mct4* in cortex of SD or KD fed mice at 6 weeks of age is unaltered (n=4-5; Student's t-test). (E) Fluorescent immunolabeling of MCT1 (green), S100b (red, astrocytic staining) and DAPI (blue, nuclear staining) in cortex of SD (left) and KD (right) fed animals at 6 weeks of age reveal strong increase of MCT1 mainly restricted to blood vessels. Scale, 10 µm. (F) ßOHB level as measured by GC/MS are increased in KD fed mice at 6 weeks of age (n=6). Significance is indicated with *padj<0.05, **padj<0.005, ***padj<0.001 (Benjamini-Hochberg correction, DESeq2 R package) SD= standard diet; KD= ketogenic diet.

MCT2 and MCT4 are suggested to be mainly expressed on neurons and astrocytes, respectively (Bergersen et al., 2001; Pellerin et al., 1998). Regarding MCT2 expression it has been shown that this transporter does not react to the KD (Forero-Quintero et al., 2017). In line, expression analysis of *Mct2* and *Mct4* at six weeks of age where MCT1 was significantly increased, no expressional changes could be observed confirming the previous observations (Fig. 13D). To identify MCT1 expression on cellular level, double fluorescent immunolabeling of cortical sections of mice was performed. The majority of MCT1 signal was found on blood vessels in KD fed animals (Fig. 13E). Low signal intensity could be detected in mice fed the SD. Astrocytes stained with S100ß an astrocytic marker did not show visible co-labeling with MCT1 supporting that MCT1 is mainly expressed on endothelial cells (Gerhart et al., 1997).

Whether the observed increase in MCT1 protein abundance could lead to increased ßOHB uptake, relative concentration of ßOHB was determined within cortex of mice at six weeks of age using GC/MS. Quantification revealed a 44-fold increase in ßOHB concentration in animals on KD (Fig. 13F), indicating functional uptake of ßOHB most probably via MCT1 into the brain. Of note, increased brain ßOHB levels upon KD feeding is in line with previous observations (DeVivo et al., 1978).

Taken together, these results indicate that increased uptake of ßOHB is facilitated by MCT1 upregulation in response to feeding a KD. However, it just can be speculated how different brain cells take up KB since cell type specific MCTs were not responding to the KD and MCT1 signal was mainly found on endothelial cells.

2.8 Influence of KD feeding on ketolytic enzymes in cortex

Next, we asked whether ßOHB reaching the brain via MCT1 can be metabolized. To address this question, protein abundances of the ketolytic enzymes SCOT, BDH1 and ACAT1 in cortical samples were investigated using immunoblots. Fig. 1A shows representative immunoblots of cortex from six weeks old mice for all enzymes investigated. A stronger SCOT signal on the immunoblot was visible in samples of KD fed mice. In contrast, no obvious differences in protein expression could be observed for BDH1 and ACAT1. Quantification of protein levels of SCOT showed steady increase over time reaching statistical significance at five and six weeks of age in KD fed mice (Fig. 14B). In line with previous studies, this supports the notion that KD is able to induce upregulation of SCOT as it was previously shown in muscle of mice fed the KD (Schnyder et al., 2017). However, abundances of BDH1 and ACAT1 were unaltered at all investigated time points (Fig. 14C,D) despite minor increase at six weeks of age that were not statistically significant. To summarize, these results indicate that within cortical

tissue the rate-limiting enzyme SCOT increases likely to facilitate utilization of KB in KD fed mice. Based on the findings, that expression of MCT1 and SCOT was found to be highest at six weeks of age, further analyses were focused on this time point.

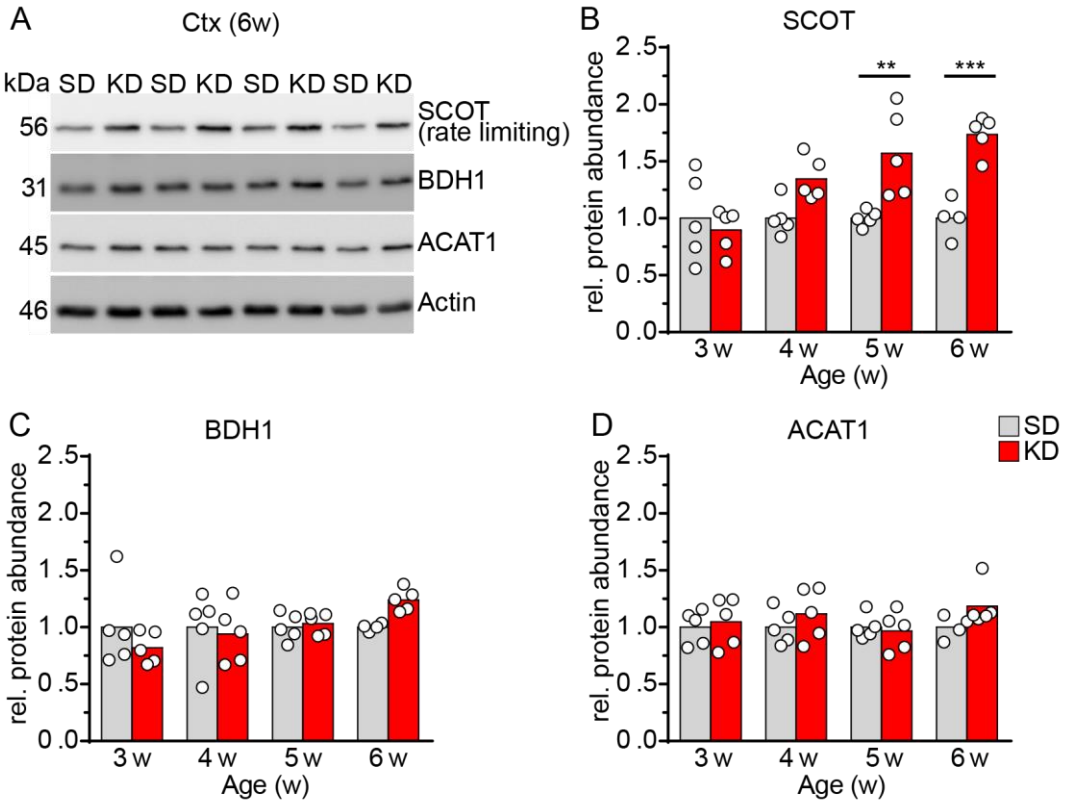

Fig. 14: Ketogenic diet increases SCOT protein abundance in cortex of mice

(A) Immunoblots of ketolytic enzymes SCOT, BDH1, ACAT1 and Actin (loading control) in cortex of mice fed SD or KD at six weeks of age. Quantification of protein abundance for SCOT (B), BDH1 (C) and ACAT1 (D) of mice on SD or KD reveals gradual increase of SCOT over time (n=4-5). Asterisks depict significant differences with *p<0.05, **p<0.005, ***p<0.001, ****p<0.0001 (two-way ANOVA with Sidak's post test). SD= standard diet; KD= ketogenic diet.

2.9 Cell type specific isolation of cortical brain cells

Our data indicate that the KD is able to increase MCT1 and SCOT expression within cortical tissue, probably due to increased ßOHB concentration in blood. To obtain cell type specific insights into changes induced by feeding a KD in mice, cell isolation from adult mouse cortices was performed. So far the most striking differences between SD and KD fed mice were found at six weeks of age which therefore served as time point for in depth analysis of isolated cell types. Cells were isolated using a refined protocol of the magnetic associated cell separation technique (MACS), based on tissue dissection, homogenization and labeling with magnetic antibodies enabling magnetic isolation of cell types (Fig. 15A). Proteomic analysis of cell fractions was performed. Astrocytes, oligodendrocytes, neurons and endothelial cells were isolated and subjected to mass

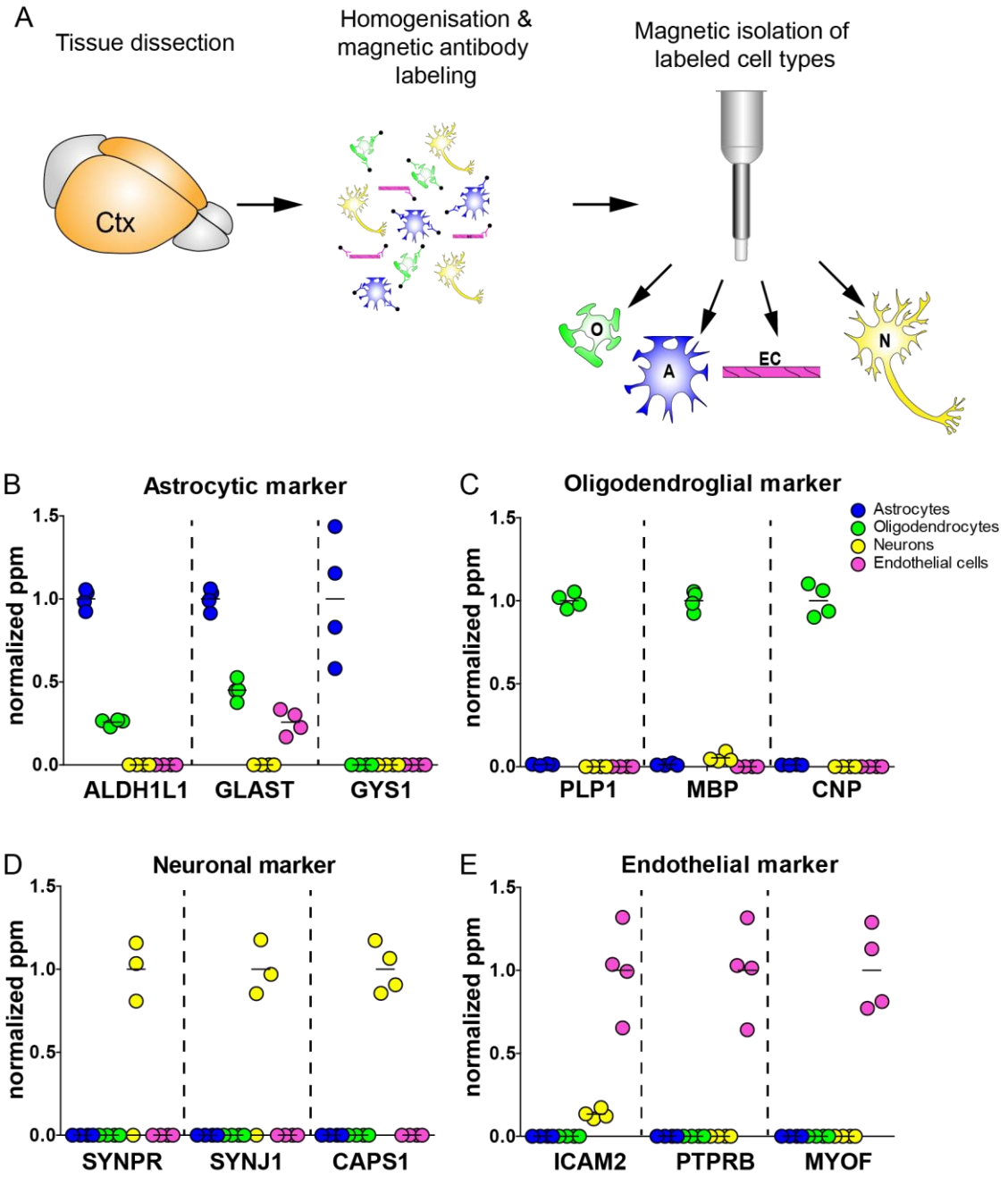

Fig. 15: Isolation of different cell types from cortex of adult mice

(A) Schematic representation of the Magnetic Associated Cell Sorting (MACS) based strategy to isolate different cell types from cortex of adult mice. O= Oligodendrocytes; A= Astrocytes; EC= Endothelial cells; N= Neurons. Proteome analysis of cell types reveal high purity and enrichment of specific marker proteins for astrocytes (B), oligodendrocytes (C), neurons (D) and endothelial cells (E) within the respective cell fraction. Graphs depict parts per million (ppm) of individual data points normalized to the mean ppm of the respective marker fraction (n=4). Protein mass spectrometry and statistical evaluation was performed in collaboration with Dr. Olaf Jahn and Lars Piepkorn. See appendix for full protein names.

spectrometric analysis. To check for purity of isolated cell fractions, specific cell markers were extracted from the proteome dataset for every cell type. For astrocytes the cell marker ALDH1L1 (aldehyde dehydrogenase 1 family member l1), GLAST (glutamate aspartate transporter) and GYS1 (glycogen synthase 1) were used (Brown & Ransom,

2007; Cahoy et al., 2008; Shibata et al., 1997) (Fig. 15B). ALDH1L1 as well as GLAST show maximal enrichment in astrocytes with minimal variance between biological replicates. These markers were only low abundant in oligodendrocytes and endothelial cells and could not be detected in neurons. Despite higher variability within astrocytes, GYS1 could only be detected in this cell fraction. For oligodendrocytes the myelin proteins PLP1 (proteolipid protein 1), MBP (myelin basic protein) and CNP (2',3'-Cyclic Nucleotide 3' Phosphodiesterase) (Lappe-Siefke et al., 2003; Verity & Campagnoni, 1988) were analyzed. All three markers exhibited their highest abundance in oligodendrocytes (Fig. 15B). Within other cell types, these markers could barely be detected. Neurons expressing the markers SYNPR (synaptoporin), SYNJ1 (Synaptojanin 1) and CAPS1 (calcium-activator protein for secretion 1) (Farina et al., 2015; Herrera et al., 2009; Jahn & Sudhof, 1994) (Fig. 15D) were investigated for accumulation within the neuronal fraction. All of these markers showed most abundance in neurons. In fractions of astrocytes, oligodendrocytes and endothelial cells these markers were not detected, indicating that these fractions are not contaminated with neurons. Endothelial cells were investigated for enrichment of the adhesion molecule ICAM2 (intercellular adhesion molecule 2), the endothelial PTPRB (receptor-type tyrosine-protein phosphatase beta) and MYOF (Myoferlin) needed for functional endocytosis within endothelial cells (Bernatchez et al., 2009; Fachinger et al., 1999; Renkonen et al., 1992). Expression of these markers appeared to be rather variable between biological replicates but clearly indicate enrichment of endothelial cells (Fig. 15E). In addition, none of these markers was found in other cell fractions.

Taken together these results show that our cell isolation protocol coupled to subsequent proteomic analysis yields highly enriched fractions of astrocytes, oligodendrocytes, neurons and endothelial cells. In addition, it underscores the purity of cell types by the nearly complete absence of markers not associated with the isolated fraction. This enables highly specific proteomic analysis of isolated cells from as less as just one single cortex.

2.10 Proteomic analysis of isolated astrocytes from cortex of KD fed mice

To investigate cellular adaptations to KD feeding in mice, astrocytes were analyzed using proteomics to address the question whether these cells alter their metabolism in response to feeding mice a KD. Astrocytes are ideally positioned to distribute metabolites within the brain and shuttle substrates to neurons (Cancilla et al., 1972; Kacem et al.,

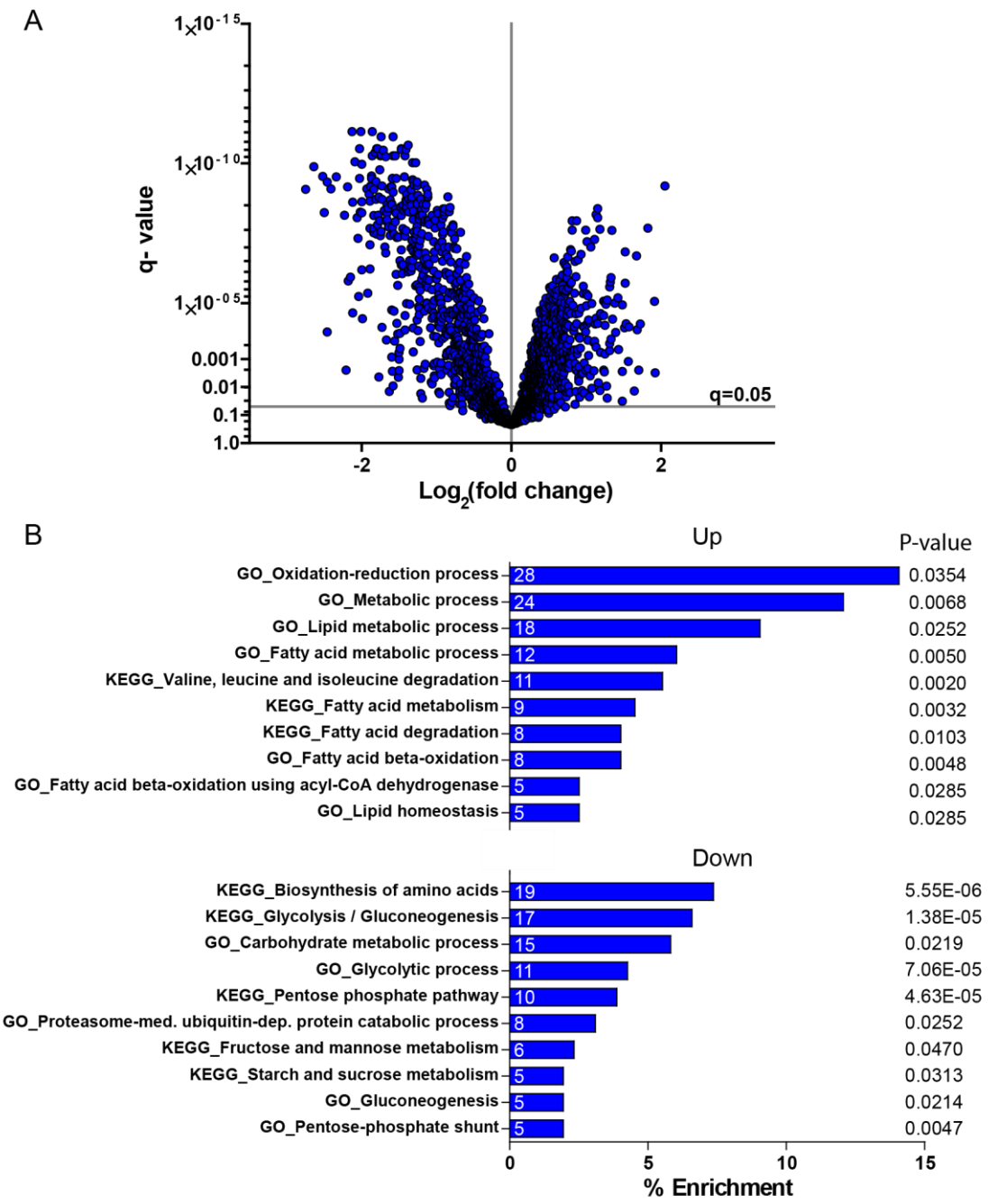

Fig. 16: Proteomic analysis of isolated astrocytes from cortex of KD fed mice

(A) Volcano plot of astrocytes isolated from cortex of mice depicting differentially regulated proteins upon feeding a KD (n=4). (B) Pathway analysis (Top10) of the most differentially regulated proteins of astrocytes suggest upregulation of lipid metabolic pathways and downregulation of carbohydrate metabolism. X-axis depict percentage of proteins found to be differentially regulated within the proteome belonging to the respective pathway. Number within bars represent amount of associated proteins.

1998; Pellerin & Magistretti, 1994). We speculated that astrocytes will change their metabolism to support neuronal function.

By using proteomics, over 2100 different proteins could be detected in both dietary groups. As expected, from the volcano plot depicting expressional changes of proteins in relation to its significance, it is clearly visible that the proteomic composition of

astrocytes from KD fed animals is strongly changed (Fig. 16A). To determine possible pathways that could be altered due to the KD, functional annotation analysis was performed using DAVID (Huang da et al., 2009a, 2009b) mainly focussing on distinct metabolic pathways of KEGG and GO_BP terms. The pathway analysis shows the Top10 ranking pathways with their respective p-values (Fig. 16B). Within astrocytes from KD fed mice there was a clear separation of proteins related to lipid or sugar metabolism as indicated by up and downregulated pathways. Metabolic pathways related to degradation of fatty acids and lipid synthesis were enriched in proteins with increased abundance, whereas sugar and carbohydrate metabolic pathways showed opposing changes. This finding indicates that astrocytes shift their carbohydrate-based metabolism to utilization of fatty acids.

2.10.1 Astrocytes utilize KB upon feeding mice a KD

Astrocytes derived from developing brain are thought to be able to utilize KB (Edmond et al., 1987). To address the question, whether astrocytes increase the necessary ketolytic enzymes when mice are fed a KD, proteins involved in ketolysis were investigated. Pathways were visualized using the software VANTED version 2.6.5 (Rohn et al., 2012) with $\log_2$ fold changes of individual mice depicted as heatmap (Fig. 17A). Astrocytes seem to import KB via MCT1 as indicated by significant higher abundance of this protein. In Addition, BSG (Basigin, also known as CD147) a glycoprotein necessary for the correct translocation of MCT1 to the plasma membrane (Kirk et al., 2000) was also increased to the same extent in astrocytes. MCT4 the proposed major astrocytic monocarboxylate transporter (Bergersen et al., 2001) was neither detected in the SD nor in the KD group. The ketolytic enzymes BDH1, SCOT and ACAT1 showed significant increase in protein expression in astrocytes with strongest increase in SCOT level suggesting increased rate of ketolysis of KB. Indeed, further evidence from immunohistochemistry of astrocytes point to enhanced utilization of KB. Astrocytes were visualized using ALDH1L1-EGFP mice, which express the green fluorescent protein (GFP) under the *Aldh1l1* promotor ubiquitously expressed in astrocytes (Heintz, 2004) (Fig. 17B). Colabeling of SCOT clearly indicated increased abundance in sagittal sections of cortical slices in animals fed the KD. Due to mitochondrial localization, SCOT labeling appeared as punctual staining. Interestingly, although staining of SCOT within the astrocytic soma was visible, increased labeling was especially localized to astrocytic processes (arrowheads). Therefore, results obtained by proteomic analysis might underestimate the increase in SCOT protein expression, since processes might partially be lost during the isolation process. These results support findings from immunoblot

analysis of ketolytic enzymes and indicate that astrocytes readily utilize KB in cortex of KD fed mice.

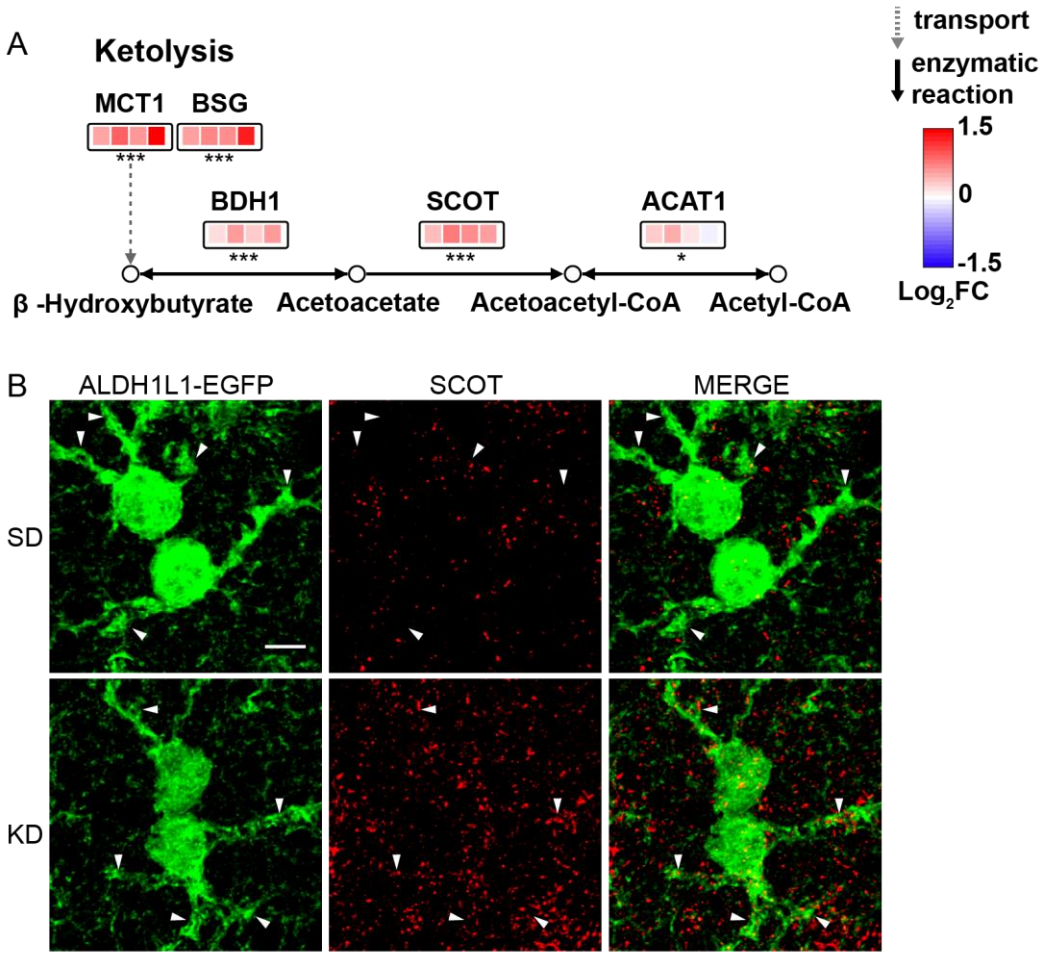

Fig. 17: Astrocytes readily utilize ketone bodies

(A) Proteins identified by proteome analysis involved in transport and utilization of KB where mapped to the ketolysis pathway with corresponding Log_2 fold changes of individual sample values (n=4). (B) Maximum intensity projection of sagittal brain sections of SCOT (red) labeling from animals receiving KD or SD. Astrocytes were visualized by using mice expressing EGFP (green) under the astrocytic promotor ALDH1L1. Arrowheads depict astrocytic processes and show increase in SCOT staining in mice on ketogenic diet. Scale, 5µm. SD= standard diet; KD= ketogenic diet. Significance is indicated with *q<0.05, **q<0.005, ***q<0.001, (moderated t-statistics with multiple comparison correction).

2.10.2 Glycolysis is decreased in cortical astrocytes of mice on KD

As indicated by pathway analysis, sugar and carbohydrate based metabolic pathways were downregulated in astrocytes of mice fed a KD. Since glycolysis and pentose-phosphate pathway (PPP) were identified with KEGG as well as in GO terms (see Fig. 16B) these pathways were assessed in detail. All proteins identified by proteome analysis related to glycolysis and PPP were depicted (Fig. 18), regardless of significance or log_2 fold change enabling better evaluation of pathway alterations. Nearly all identified

proteins were strongly decreased indicating reduced glycolytic rate and PPP metabolism within astrocytes. Interestingly, despite obvious downregulation of glycolysis, GLUT1 was slightly enhanced suggesting increased uptake of glucose. In addition, Hexokinase 2 was increased as well. This might trap glucose within the cell as it is converted to G6P (Mergenthaler et al., 2013). However, the question arises what is the fate of G6P within astrocytes if all downstream glycolytic enzymes are decreased? One explanation could be that it is rather directed towards PPP than utilized via glycolysis. The PPP can be divided in a first oxidative and a following non-oxidative part. Glucose-6-phosphate dehydrogenase (isoforms G6PD2, G6PDX) is considered as the first and rate-limiting enzyme of this pathway (Stincone et al., 2015).

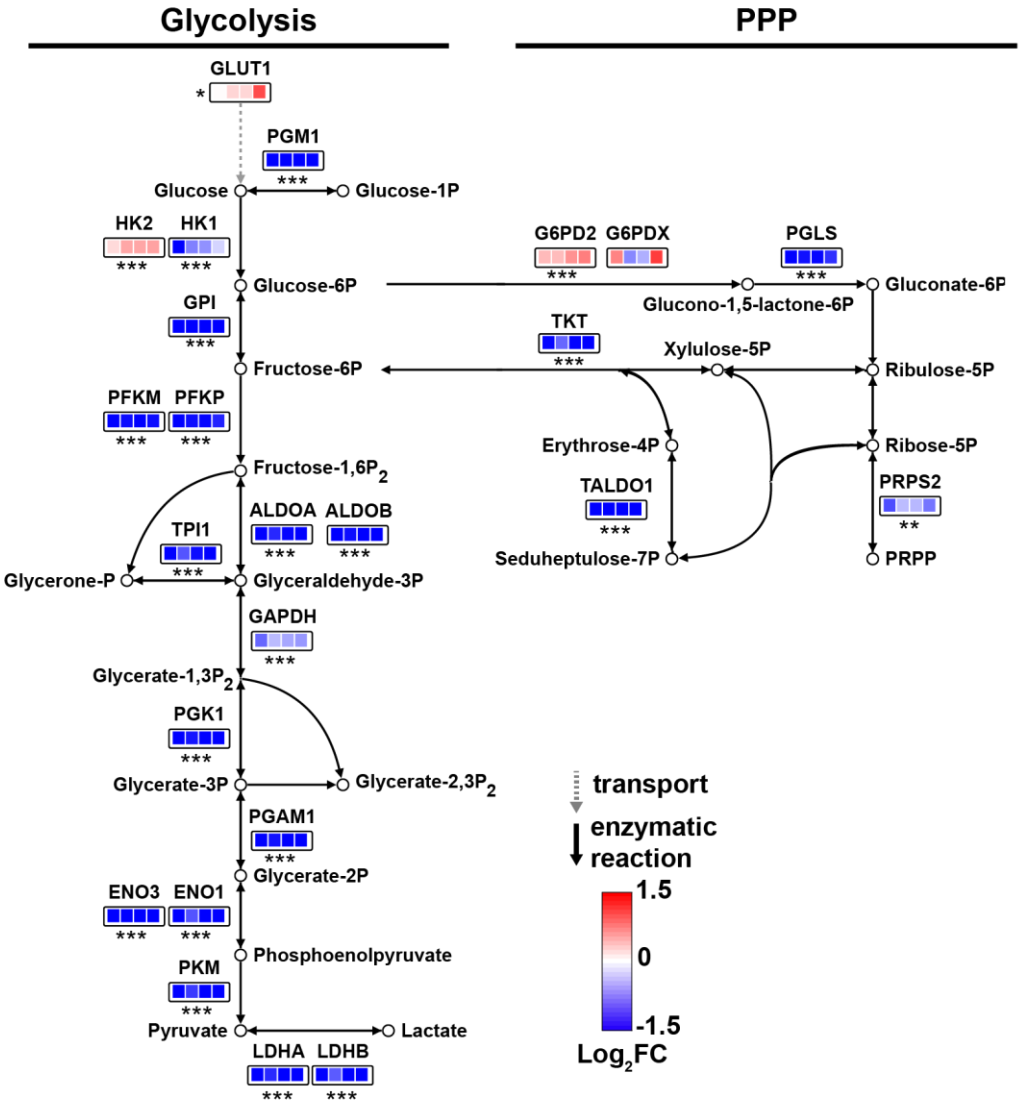

Fig. 18: Astrocytes decrease glycolysis and PPP in mice on ketogenic diet

Proteins identified by proteome analysis involved in glycolysis and pentose-phosphate pathway where mapped to their respective pathway with corresponding log_2 fold changes of individual sample values (n=4), indicating pathway downregulation. Significance is indicated with *q<0.05, **q<0.005, ***q<0.001, (moderated t-statistics with multiple comparison correction; "limma" Bioconductor package). See appendix for table of full protein names.

As the enzymatic step facilitated by G6PD is assumed to be unidirectional, the resulting product would unequivocally undergo utilization via this pathway. G6PDX was found to be slightly increased without reaching significance. However, G6PD2 was strongly increased in astrocytes of animals on KD (Fig. 18) suggesting that G6P is directed towards PPP metabolism. The oxidative part of PPP is necessary to produce reducing equivalents in form of NADPH and produces ribulose-5-phosphate necessary for RNA and DNA synthesis (Stincone et al., 2015) making it indispensable for normal cellular function. Interestingly, the second enzyme 6-phosphogluconolactonase (PGLS) of the oxidative PPP was downregulated (Fig. 18). However, PGLS is not necessarily needed since the formation of the product gluconate-6-phosphate can occur spontaneously and rapid (Miclet et al., 2001), thereby questions the necessity of an enzymatic facilitated step under conditions of reduced glucose availability. Enzymes related to the non-oxidative part showed consistent downregulation indicating reduced flux probably due to reduced glycolytic intermediates (Fig. 18).

Taken together, these data suggest that astrocytes in KD fed mice decrease glycolysis. However, the current results might also suggest direction of residual glucose into the PPP as GLUT1, HK2 and G6PD2 are upregulated that likely leads to trapping of glucose into the oxidative part of the PPP. In turn, this suggest that astrocytes spare glucose to produce reducing equivalents and precursors for nucleotide synthesis. To verify these findings experiments need to be performed to further shed light on this possibility.

2.10.3 Astrocytes enhance ß-oxidation under ketogenic conditions

Astrocytes are known to be the major cell type of the brain to be capable of metabolizing fatty acids via ß-oxidation (Edmond et al., 1987). Pathway analysis indicated upregulation of lipid and fatty acid related metabolism in astrocytes from animals fed the KD (compare Fig. 16B). To examine this possibility all identified proteins involved in ß-oxidation were assessed. Indeed, most of the identified enzymes were significantly upregulated, although the rate-limiting protein CPT1 was unaltered in abundance (Fig. 19A). These result suggest increased utilization of fatty acids within astrocytes of KD fed mice. However, further experiments need to be performed to see whether CPT1 enzyme activity is increased and thereby facilitates enhanced ß-oxidation.

Astrocytes are also known to produce lipids that are critical for synapse formation (van Deijk et al., 2017). Lipid synthesis is mainly facilitated by the rate-limiting enzyme ACC (Awan & Saggerson, 1993) and the multifunctional enzyme fatty acid synthase (FASN) (Witkowski et al., 1991).

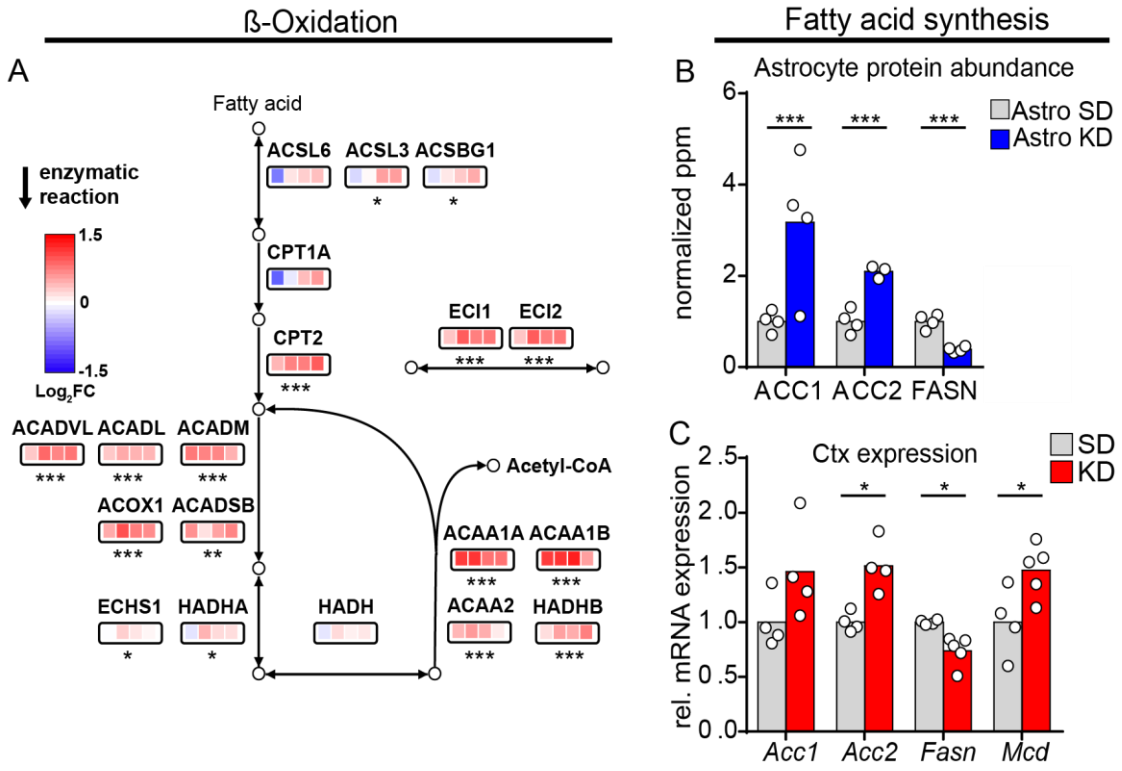

Fig. 19: Astrocytes alter fatty acid metabolism when mice fed a ketogenic diet

(A) Proteins identified by proteome analysis involved in ß-oxidation where mapped to their respective pathway with corresponding log_2 fold changes of individual sample values (n=4) indicating increased utilization of fatty acids. (B) Abundance of Proteins involved in synthesis of fatty acids from astrocytes isolated from mice on SD or KD show inconsistent changes. Bars represent parts per million (ppm) normalized to mean value of SD condition with individual data points (n=4). Significance is indicated with *q<0.05, **q<0.005, ***q<0.001, (moderated t-statistics with multiple comparison correction; "limma" Bioconductor package). (C) Expression analysis of genes involved in fatty acid synthesis from cortex of mice fed SD or KD reflect results of isolated astrocytes in regard of fatty acid synthesis (n=4-5). Asterisks depict significant differences with *p<0.05, (two sided Student's t-test). SD= standard diet; KD= ketogenic diet. See appendix for table of full protein names.

Investigation of lipid synthesis of astrocytes revealed conflicting result. Two isoforms of ACC exist (Phillips et al., 2010) that were found to be increased in astrocytes upon feeding mice a KD (Fig. 19B). In contrast, FASN was significantly decreased. Since FASN utilize malonyl-CoA produced by ACC1/2 this finding would indicate accumulation of this metabolite within astrocytes. This is of particular interest, since malonyl-CoA is a known inhibitor of ß-oxidation (McGarry & Brown, 1997). Malonyl-CoA can also be reconverted to acetyl-CoA via malonyl-CoA decarboxylase (MCD) (Dyck et al., 1998), but this enzyme could not be detected within astrocytes. To further address this issue, expression analysis via qRT-PCR in cortical tissue was performed and revealed an increase in *Acc1* and *Acc2* expression, the latter of them significantly, which supports proteomic data (Fig. 19C). In addition, *Fasn* was decreased, reflecting the reduction of protein abundance in astrocytes. Since findings obtained from cortical tissue seemed to

reflect changes within astrocytes, expression of *Mcd* was examined. *Mcd* was enhanced to the same extent as *Acc1* and *Acc2* (Fig. 19C). These findings suggest that astrocytes in KD fed animals increase the rate of malonyl-CoA synthesis and also indicates that ß-oxidation in astrocytes is facilitated despite increased malonyl-CoA production by ACC1/2.

2.11 Analysis of isolated oligodendrocytes from cortex of KD fed mice

Oligodendrocytes are crucial for maintaining proper conduction velocity by insulating axons (Baumann & Pham-Dinh, 2001; Kettenmann & Ransom, 2005). In addition, it was shown that oligodendrocytes support axons metabolically by providing lactate (Funfschilling et al., 2012), indicating that oligodendrocytes support axons in a similar way to astrocytes (Pellerin & Magistretti, 1994). Therefore, it could be possible that upon feeding a KD in mice oligodendrocytes react in a similar manner as astrocytes. To test this hypothesis, isolated oligodendrocytes, derived from the same animals as astrocytes, were investigated by proteomic analysis. Almost 1800 proteins were detected in both dietary groups. Surprisingly, only minor differences between treatment groups could be detected (Fig. 20A), implying that oligodendrocytes seem to be mostly unchanged under ketotic conditions. Indeed, pathway analysis revealed only few upregulated pathways mostly related to ion and protein transport processes (Fig. 20B). No downregulated pathway passed the filter settings.

Due to these little alterations we asked whether oligodendrocytes increase utilization of KB for energy production. Similar to astrocytes, oligodendrocytes seemed to enhance KB uptake by increasing MCT1 and BSG (Fig. 20C). Surprisingly this was not the case for ketolytic enzymes. Protein abundance of BDH1, SCOT and ACAT1 was not significantly increased in oligodendrocytes of KD fed animals, suggesting no increased ketolysis. Fluorescent co-labeling of oligodendrocytes stained for CNP revealed similar appearance in cortex of SD and KD fed mice (Fig. 20D). Although SCOT were obviously increased in tissue of ketogenic animals, SCOT labeling was obviously not increased in oligodendrocytes (arrowheads), further supporting that SCOT protein expression in oligodendrocytes might not be changed.

Taken together these results imply that oligodendrocytes react differently to a KD compared to astrocytes. This is particularly important since oligodendrocytes were obtained from cortex of the same animals as astrocytes, enabling direct comparison of cell types within the same mouse. Furthermore, the findings suggest that oligodendrocytes do not prefer to utilize KB although increased MCT1 expression

suggest increased uptake. This raises the question of the fate of KB if they are taken up but not metabolized.

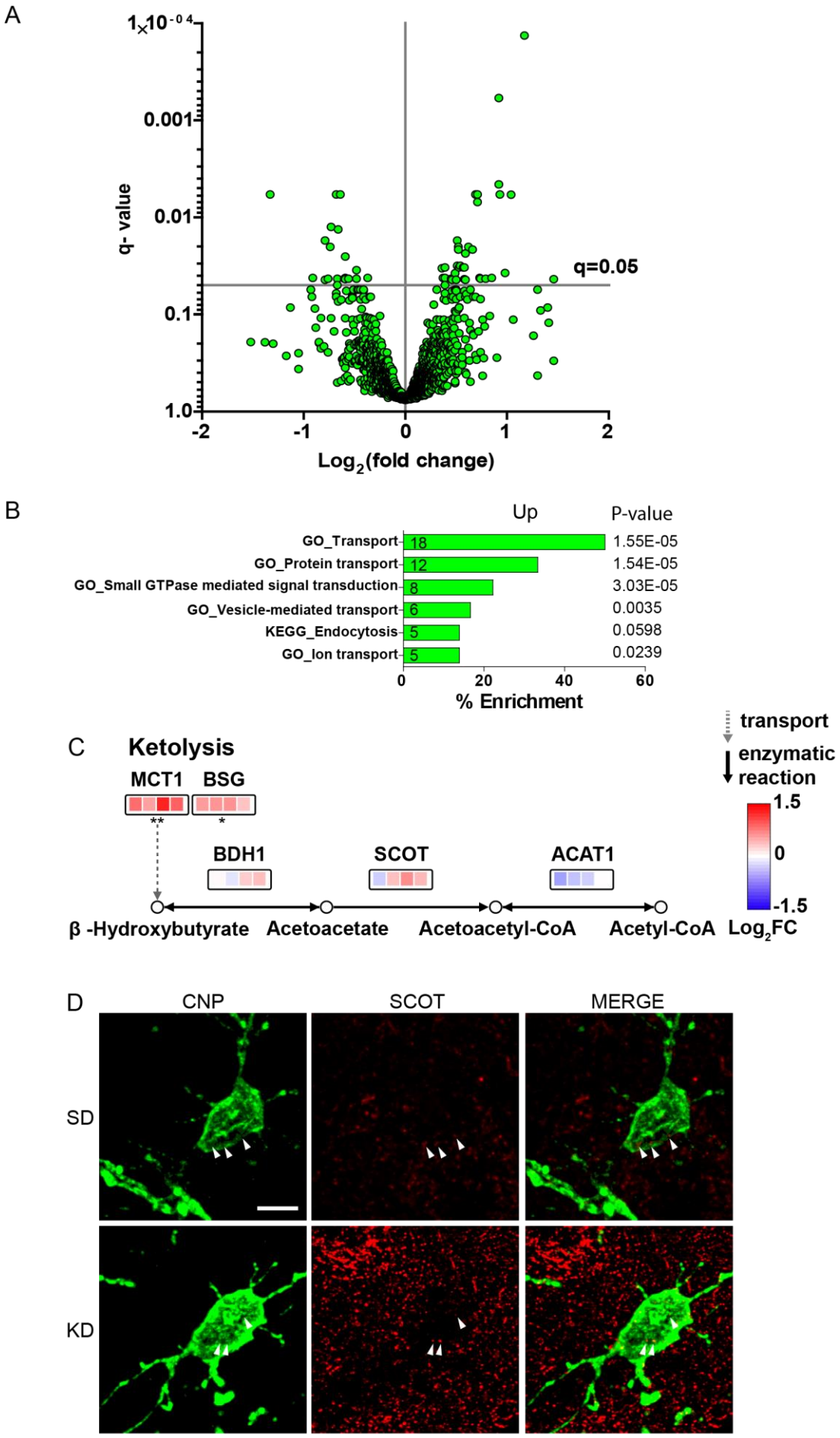
A
1x10-04
0.001
0.01
0.1
1.0
q- value
q=0.05
-2
-1
0
1
2
Log2(fold change)
B
Up
P-value
GO_Transport
18
1.55E-05
GO_Protein transport
12
1.54E-05
GO_Small GTPase mediated signal transduction
8
3.03E-05
GO_Vesicle-mediated transport
6
0.0035
KEGG_Endocytosis
5
0.0598
GO_Ion transport
5
0.0239
0
20
40
60
% Enrichment
C
Ketolysis
MCT1
BSG
**
*
BDH1
SCOT
ACAT1
β -Hydroxybutyrate
Acetoacetate
Acetoacetyl-CoA
Acetyl-CoA
transport
enzymatic reaction
1.5
0
-1.5
Log2FC
D
CNP
SCOT
MERGE
SD
KD

Fig. 20: Proteome analysis of oligodendrocytes from cortex of mice fed KD

(A) Volcano plot of oligodendrocytes isolated from cortex of mice depicting differentially regulated proteins upon feeding a KD (n=4). Note that only a small fraction of proteins exceed the significance threshold. (B) Pathway analysis of the most differentially regulated proteins reveal the top ranking up regulated pathways within oligodendrocytes with indicated p-values. No downregulated pathway passed the filter requirements. X-axis depict percentage of proteins found to be differentially regulated within the proteome belonging to the respective pathway. Number within Bars represent number of associated proteins. (C). Proteins identified by proteome analysis involved in transport and utilization of KB where mapped to the ketolysis pathway with corresponding log_2 fold changes of individual sample values (n=4). Significance is indicated with *q<0.05, **q<0.005, ***q<0.001, (moderated t-statistics with multiple comparison correction; "limma" Bioconductor package). (D) Maximum intensity projection of sagittal brain sections from animals receiving KD or SD indicate no increase in SCOT signal (red) within oligodendrocytes (stained for CNP, green). Arrowheads depict SCOT signal within Oligodendrocytes. Scale, 5µm. SD= standard diet; KD= ketogenic diet.

2.11.1 Oligodendrocytes might increase protein and ion transport

Pathway analysis suggested that oligodendrocytes seem to enhance transport processes. Therefore, proteins involved in protein transport as well as vesicle-mediated transport were further assessed. Both pathways showed certain overlap of involved proteins so that both pathways were analyzed together. Indeed, all proteins showed consistent increase (Fig. 21A). Especially proteins of the Rab family were significantly increased. Rab proteins belong to the Ras superfamily of small GTPases and are thought to maintain membrane trafficking (Hutagalung & Novick, 2011; Stenmark & Olkkonen, 2001). Rab proteins regulate release of exosomes (Blanc & Vidal, 2018) and oligodendrocytes have been shown to increase exosomal secretion upon treatment with the calcium-ionophore ionomycin *in vitro* (Kramer-Albers et al., 2007). Of note, Rab11b that is known to play a direct and significant role in exosome biogenesis (Blanc & Vidal, 2018) was found to be increased. This might imply that oligodendrocytes increase exosomal secretion probably to support other cells. However, no conclusion can be drawn from these results regarding the possible cargo of the exosomes. Therefore, further experiments have to be conducted to address this and to confirm the current results.

In addition to protein and vesicle-mediated transport, pathway analysis implicated enhanced ion transport within oligodendrocytes. A few proteins could be detected to be increased related to transport of ions (Fig. 21B). Oligodendrocytes are known to facilitate ion homeostasis (Kamasawa et al., 2005; Larson et al., 2018) that together with the current findings could suggest that oligodendrocytes might enhance ion buffering. Further experiments are needed to examine possible alterations of exosomal transfer and ion homeostasis in response to the KD in oligodendrocytes.

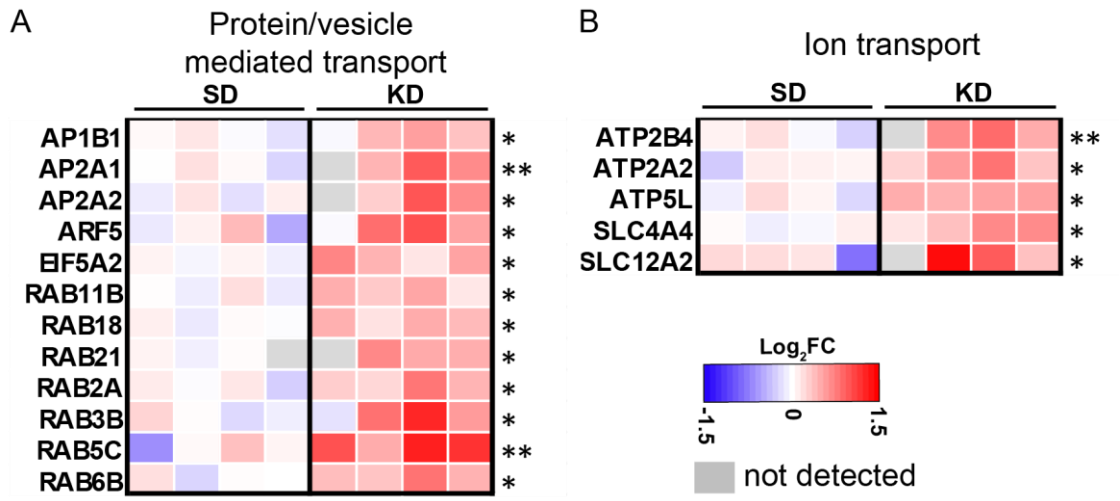

Fig. 21: Oligodendrocytes might increase transfer processes under ketogenic conditions

(A) Proteins involved in protein or vesicle mediated transport are significantly increased. (B) Ion transport might be increased in oligodendrocytes upon feeding a ketogenic diet. Log_2 fold changes of individual samples normalized to the mean of SD condition are shown (n=4). Significance is indicated with *q<0.05, **q<0.005, ***q<0.001, (moderated t-statistics with multiple comparison correction; "limma" Bioconductor package). SD= standard diet; KD= ketogenic diet. See appendix for table of full protein names.

2.11.2 Transcriptomic analysis of isolated cortical oligodendrocytes

To identify more subtle changes that might not be observed on protein level upon KD feeding in oligodendrocytes, these were again isolated and subjected to transcriptomic analysis. Transcriptomic analysis was performed in collaboration with Prof. Dr. Moritz Rossner and Nirmal Kannaiyan from the department of Psychiatry at the LMU Munich. In total nearly 14000 genes were identified with differentially regulated genes that reached the significance threshold (Fig. 22A). However, downregulated genes were not related to distinct metabolic pathways that were in the focus of this study (see Material and Methods) (Fig. 22). Interestingly, multiple pathways suggested to be enriched with upregulated genes associated to transport and ion transport processes reflecting results of the proteomic analysis (see Fig. 21A). This further strengthens the idea that oligodendrocytes might enhance transport processes and ion buffering in animals on KD. Hence, further analysis was focused on these pathways.

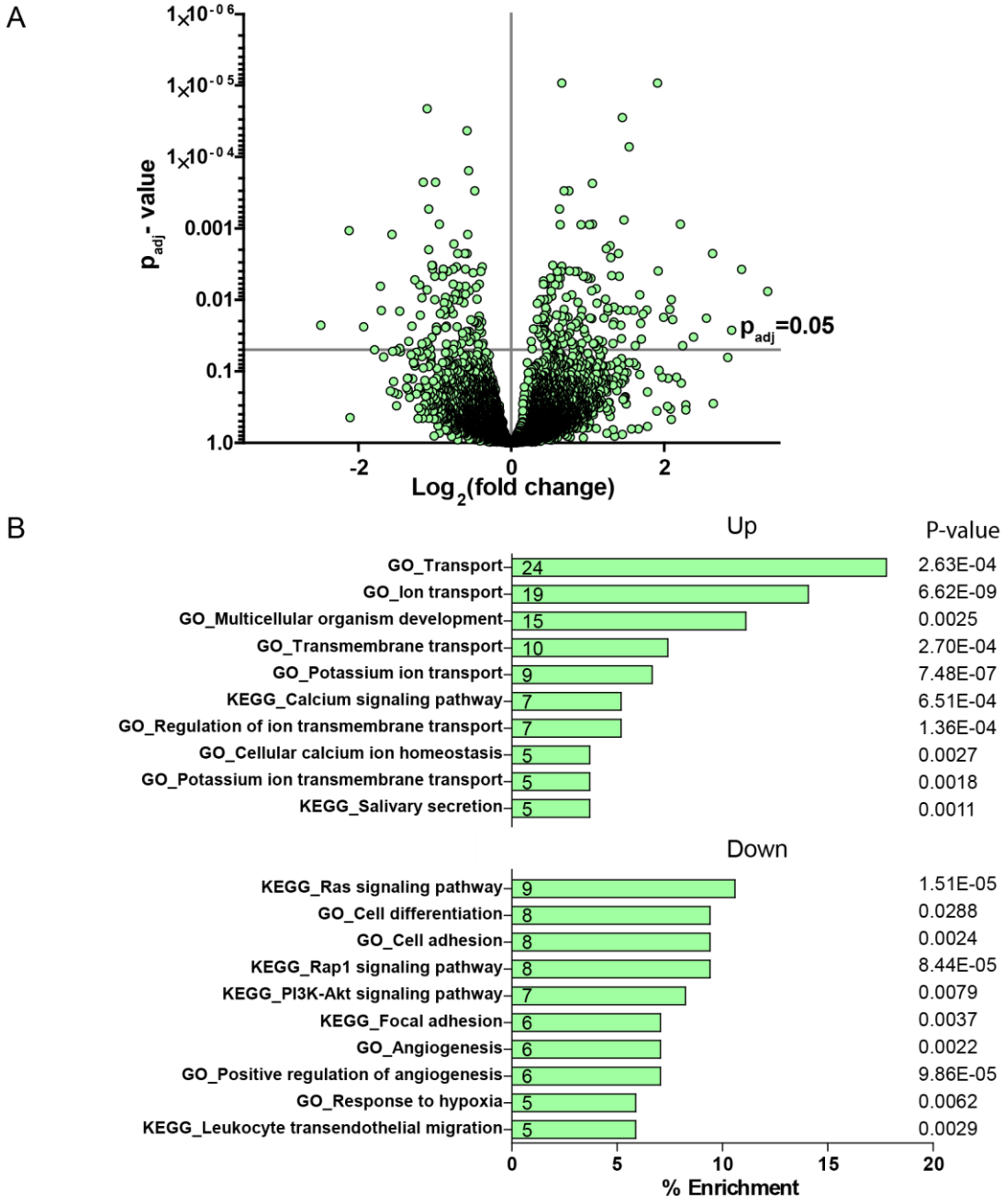

Fig. 22: Transcriptomic analysis of isolated oligodendrocytes of mice receiving KD

(A) Volcano plot of oligodendrocytes isolated from cortex of mice depicting differentially regulated genes upon feeding a KD (n=4-5). (B) Pathway analysis (Top10) of the most differentially regulated genes of oligodendrocytes partially reflect enhanced proteomic pathways. X-axis depict percentage of genes found to be differentially regulated within the transcriptome belonging to the respective pathway. Number within Bars represent number of associated genes.

2.11.3 Oligodendrocytes enhance ion transport processes in mice on KD

DAVID functional annotation analysis revealed multiple pathways related to ion transport processes. Obviously all of these pathways share similar upregulated genes as can be seen from the Venn diagram (http://bioinformatics.psb.ugent.be/webtools/Venn/) (Fig.

23A). Strongest overlap was identified between transport, ion transport and potassium ion transport. Involved proteins were therefore depicted together in Fig. 23B, revealing strong upregulation of these genes. However, no overlap between these genes and increased proteins of the proteomic analysis could be found (compare Fig. 21). Nevertheless, these results support the observations obtained from proteomic analysis since the transcriptomic investigation was independently performed leading to the same conclusion. The current data do not reveal the reason of increased ion transport in oligodendrocytes in response to KD feeding. However, these data together with proteomic results strengthen the hypothesis that KD feeding might enhance ion transport in oligodendrocytes.

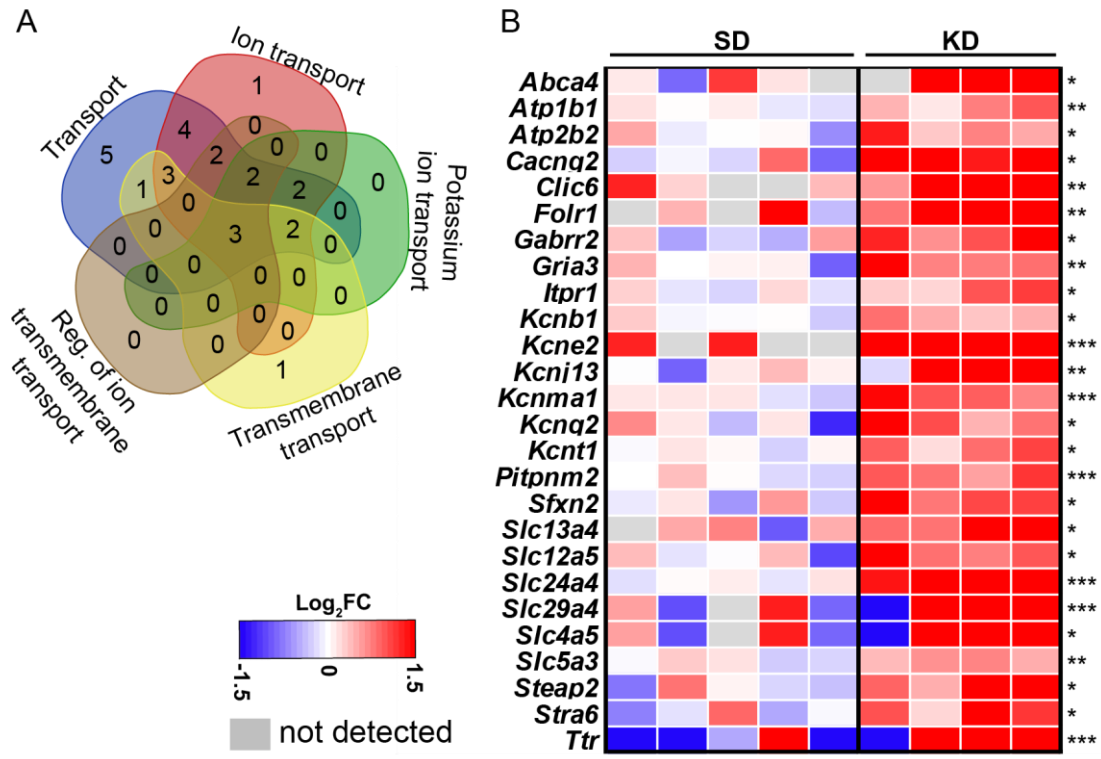

Fig. 23: Oligodendrocytes increase ion transport under ketogenic conditions

(A) Venn diagram of the top-ranking transcriptomic transport pathways upregulated in oligodendrocytes when mice fed a KD reveal strong overlap of pathways. (B) Heatmap of all involved genes from pathways depicted in (A) show significantly increased expression indicating enhanced ion transport. Log_2 fold changes of individual samples normalized to the mean of SD condition are shown (n=4-5). Significance is indicated with *padj<0.05, **padj<0.005, ***padj<0.001 (Benjamini-Hochberg correction, DESeq2 R package). See appendix for table of full protein names.

2.12 Proteomic analysis of isolated endothelial cells

Endothelial cells are known to regulate the flux of metabolites in and out of the brain (Abbott et al., 2010). It is therefore worth considering to what degree endothelial cells could adapt to the KD to deliver metabolites to brain cells. As MCT1 was shown to be

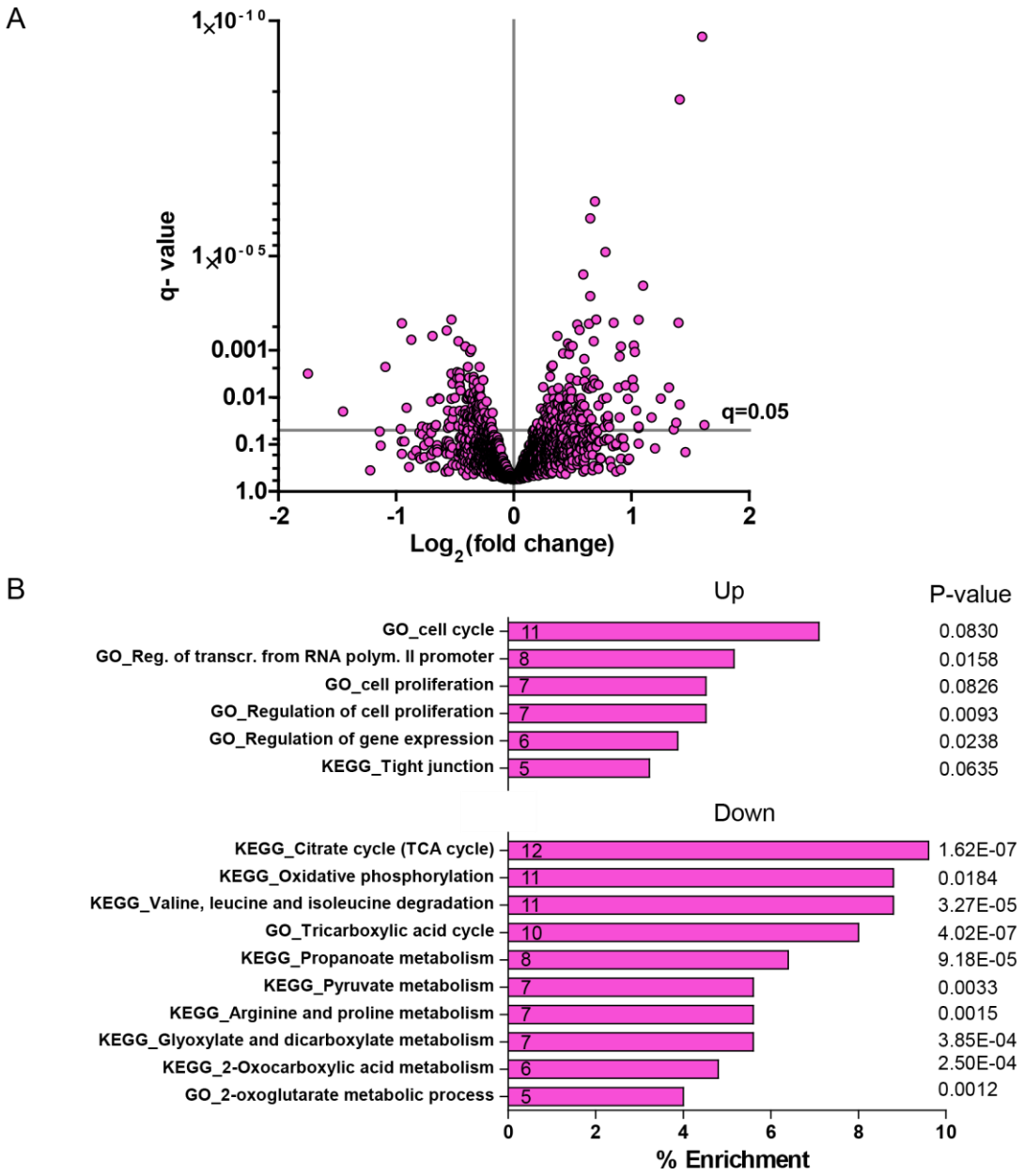

Fig. 24: Proteome analysis of endothelial cells from cortex of mice fed KD

(A) Volcano plot of endothelial cells isolated from cortex of mice depicting differentially regulated proteins upon feeding a KD (n=4). (B) Pathway analysis (Top10) of the most differentially regulated proteins of endothelial cells suggest that these cells downregulate most metabolic pathways when mice are fed a KD. X-axis depict percentage of proteins found to be differentially regulated within the proteome belonging to the respective pathway. Number within Bars represent number of associated proteins.

increased within endothelial cells by fluorescent immunohistochemistry (see Fig. 13E), it was speculated that endothelial cells could change from glucose metabolism to utilizing KB. Proteome analysis identified over 2200 different proteins in both dietary groups. Obviously, volcano plot of proteins of endothelial cells indicate that only a small portion of proteins changed in abundance upon KD feeding in mice (Fig. 24A). DAVID analysis revealed upregulated pathways related to cell cycle and proliferation, but with low

number of proteins and p-values below the significance threshold (Fig. 24B). Surprisingly endothelial cells seemed to decrease multiple pathways related to metabolism as indicated by suggested downregulated pathways. Therefore, further analysis was focused on metabolic pathways.

2.12.1 Endothelial cells do not increase KB utilization under ketosis

Endothelial cells are the first cells that have access to KB in the circulation. It is therefore conceivable that they use them to generate energy. As expected MCT1 and BSG were significantly increased in endothelial cells (Fig. 25A) confirming histological results. On the other hand, BDH1 and SCOT showed a minor but non-significant decrease.

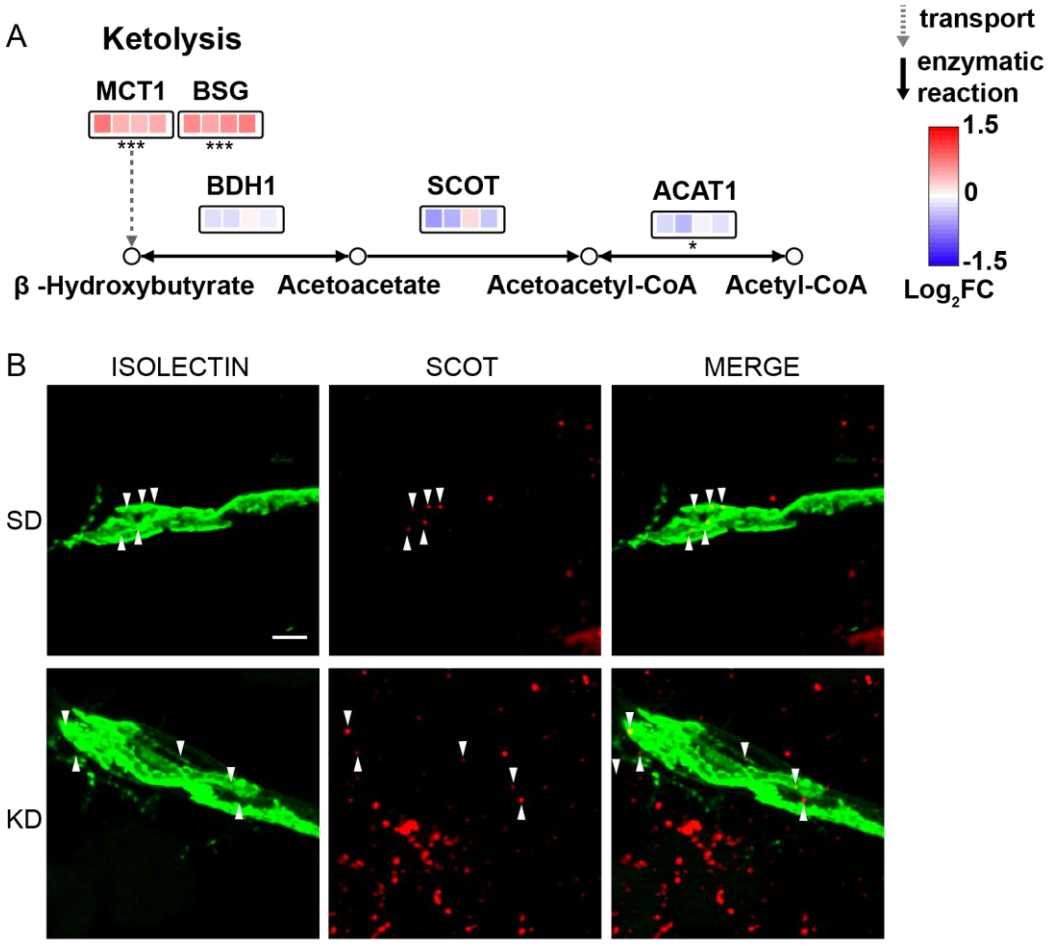

Fig. 25:Endothelial cells do not increase ketolysis

(A) Proteins identified by proteome analysis involved in transport and utilization of KB where mapped to the ketolysis pathway with corresponding Log_2 fold changes of individual sample values (n=4). Significance is indicated with *q<0.05, **q<0.005, ***q<0.001 (moderated t-statistics with multiple comparison correction; “limma” Bioconductor package). (B) Maximum intensity projection of sagittal brain sections from animals receiving KD or SD stained for isolectin (endothelial cells, green) and SCOT (red) indicated no increase in SCOT abundance. Arrowheads depict SCOT signal within endothelial cells. Scale, 2.5µm. SD= standard diet; KD= ketogenic diet.

In contrast, ACAT1 was significantly decreased in endothelial cells from cortex of KD mice. Indeed, maximum intensity projections of labeled endothelial cells within the cortex of animals co-stained with SCOT indicated no visible difference of SCOT labeling (arrowheads) (Fig. 25B). This confirms observations of the proteome analysis. These findings imply that endothelial cells do not switch under ketosis to metabolizing KB. Furthermore, they suggest that endothelial cells only facilitate the transport of KB by increased expression of MCT1. However, it raises the question which metabolic source endothelial cells use for energy production.

2.12.2 Endothelial cells may rely on glycolysis to provide energy

Endothelial cells are assumed to be highly glycolytic cells (De Bock et al., 2013; Wong et al., 2017). Indeed, *in vitro* studies indicated that nearly all glucose is metabolized to lactate while only a minimal fraction is inserted into the TCA cycle (Eelen et al., 2018; Krutzfeldt et al., 1990). Increased ketolysis was not found in endothelial cells in the current study, indicating energy production via other metabolic pathways. To address the question whether endothelial cells change glycolysis in response to reduced glucose concentration of the blood, glycolytic enzymes were analyzed. No identified glycolytic enzyme were significantly changed in endothelial cells (Fig. 26A), suggesting that these cells use glucose for energy production also in case of reduced availability. However, as already indicated by pathway analysis almost all identified TCA cycle enzymes were significantly decreased (Fig. 26B). This supports the idea that endothelial cells generate almost their entire energy from glycolysis. Endothelial cells could therefore use glucose due to the direct and continuous supply by the blood stream even under KD induced blood glucose reduction. However, these results can not explain the diminished use of the TCA cycle within endothelial cells under ketosis taken into account that TCA cycle contributes already minimal to the metabolism under normal conditions. Therefore, endothelial cell metabolism needs further investigation to address this issue.

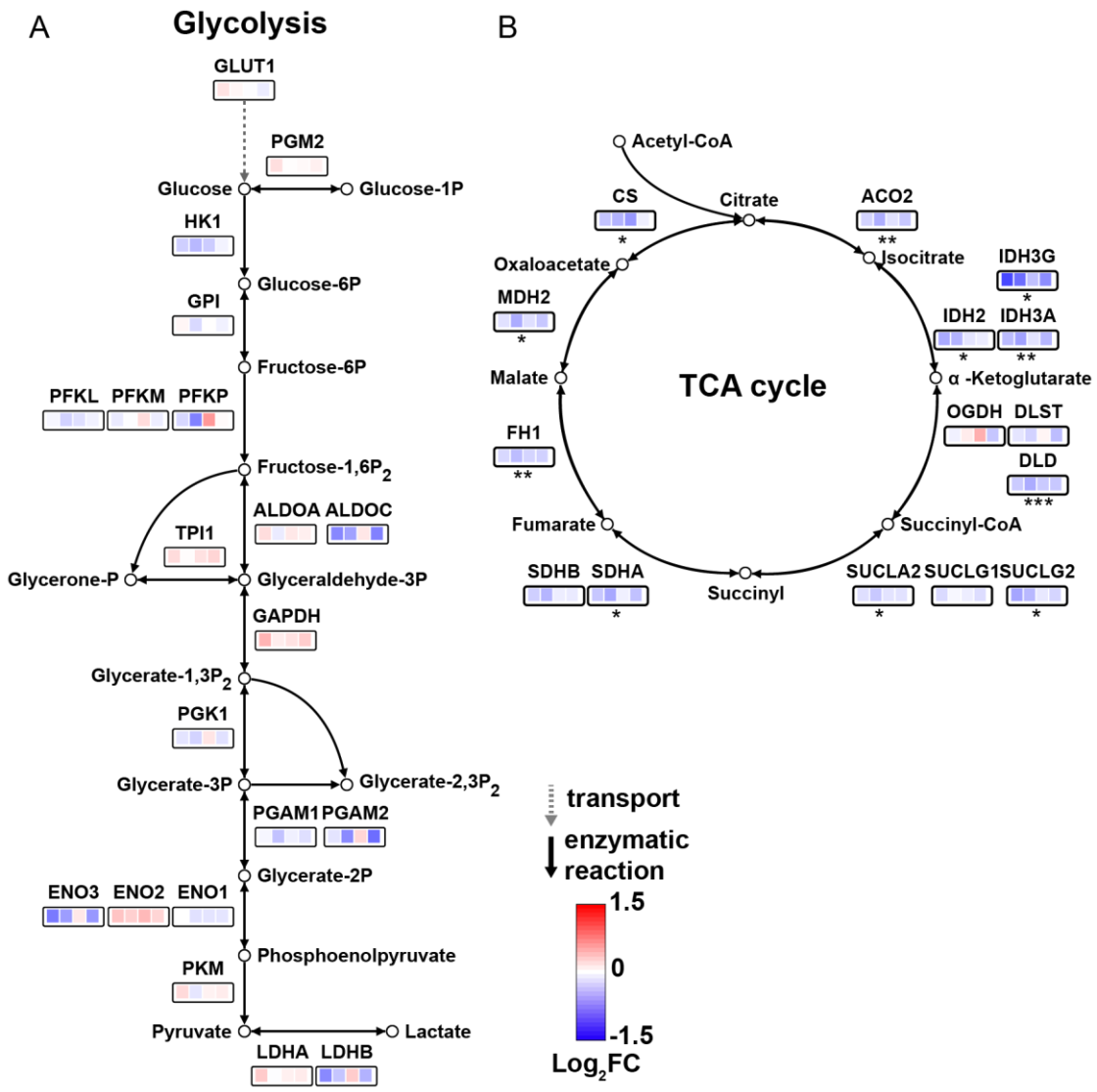

Fig. 26: Endothelial cells rely on glycolysis to produce energy

(A) Proteins identified by proteome analysis involved in glycolysis where mapped with corresponding Log_2 fold changes of individual sample values, revealing no significant changes in glycolysis in response to KD feeding. (B) Proteins identified by proteome analysis involved in TCA cycle where mapped with corresponding Log_2 fold changes of individual sample values, showing slight decreases (n=4). Significance is indicated with *q<0.05, **q<0.005, ***q<0.001 (moderated t-statistics with multiple comparison correction; “limma” Bioconductor package). See appendix for table of full protein names.

2.12.3 Fatty acid transport of endothelial cells under ketosis

In astrocytes it was found that these cell type in addition to ketolysis might use fatty acids to produce energy via ß-oxidation (see Fig. 19A). This would indicate increased amounts of fatty acids available for its breakdown within astrocytes. Since endothelial cells regulate the entry of metabolites into the brain we speculated that upon KD feeding these cell type would increase fatty acid transport proteins. To address this possibility, we focused on fatty acid transporter in our proteomic data set. Interestingly only few of the

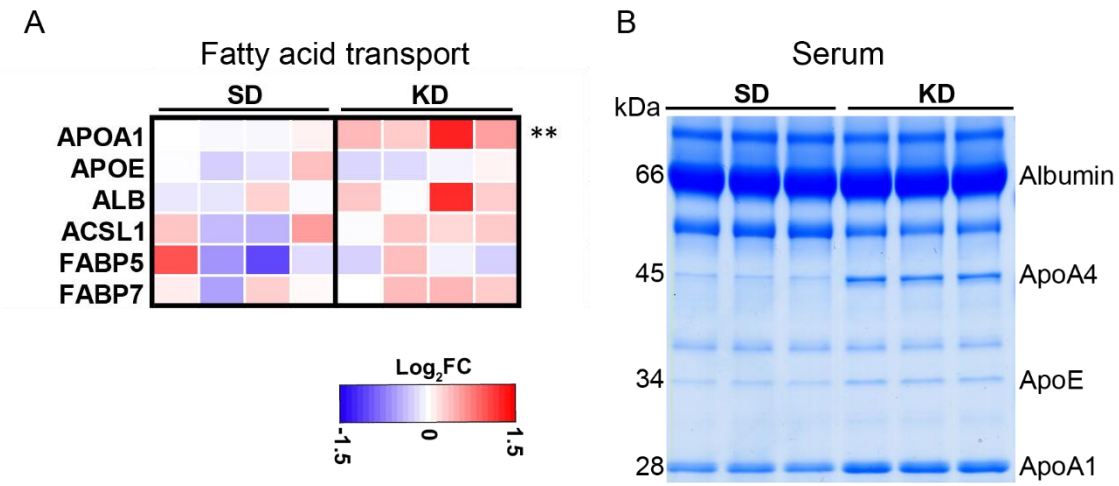

Fig. 27:Changes of fatty acid transport proteins in endothelial cells reflect serum changes induced by the ketogenic diet

(A) Heatmap of proteins involved in fatty acid transport from isolated endothelial cells reveal no drastic increase upon feeding mice a KD. Log_2 fold changes of individual samples normalized to the mean of SD condition are shown (n=4). Significance is indicated with *q<0.05, **q<0.005, ***q<0.001 (moderated t-statistics with multiple comparison correction; “limma” Bioconductor package). (B) Coomassie staining of blood serum proteins from SD and KD fed mice, reveal obvious increase in fatty acid transport proteins, identified by mass spectrometry (n=3). SD= standard diet; KD= ketogenic diet.

known transport proteins could be identified. FATP-1 and 4 the presumed major fatty acid transporter of the BBB (Hirsch et al., 1998; Mitchell et al., 2011) as well as FAT/CD36 needed for the transport of oleate (Mitchell et al., 2009) could not be detected. FABP5 the major fatty acid binding protein (Mitchell & Hatch, 2011) and FABP7 were identified but did not show changes due to KD feeding (Fig. 27A). In addition, ACSL1 also assumed to import fatty acids (Doege & Stahl, 2006) was found to be unchanged. Surprisingly different plasma lipoproteins could be detected. Together with Albumin (ALB) that did not show changes in protein abundance, different apolipoproteins could be identified, which are normally assumed as plasma located (Mahley et al., 1984). For APOA1 significant increase could be shown. Of note, APOA4 was also detected, although only in the ketogenic condition. Log_2 fold changes could therefore not be displayed for this protein. This prompted us to analyze serum for changes of lipoproteins. Indeed, Coomassie stained SDS-gels revealed changes of different protein bands, later identified by MS analysis within blood serum of KD fed animals (Fig. 27B). From the Coomassie staining, albumin did not show changes within serum of KD fed animals reflecting results of the proteome analysis within endothelial cells. In contrast, APOA1,4 and E did show obvious increased amounts within serum. It can be speculated that these lipoproteins were found within the proteome analysis of endothelial cells as residual amounts of blood serum and not to actual expression within these cells. However, these results indicate that transport of fatty acids is not actively increased in endothelial cells

in mice fed the KD. Due to increased apolipoproteins in serum indicative of elevated fatty acid concentration, transport of lipids rather might be facilitated by passive diffusion.

2.13 Proteomic analysis of cortical neurons

Neurons are believed to be the cell type with the highest energy demand within the brain (Howarth et al., 2012) metabolizing the highest amount of glucose to meet their energetic needs. It is therefore of interest in which way neurons adapt to feeding mice a ketogenic diet where glucose availability is decreased. Due to reduced glucose

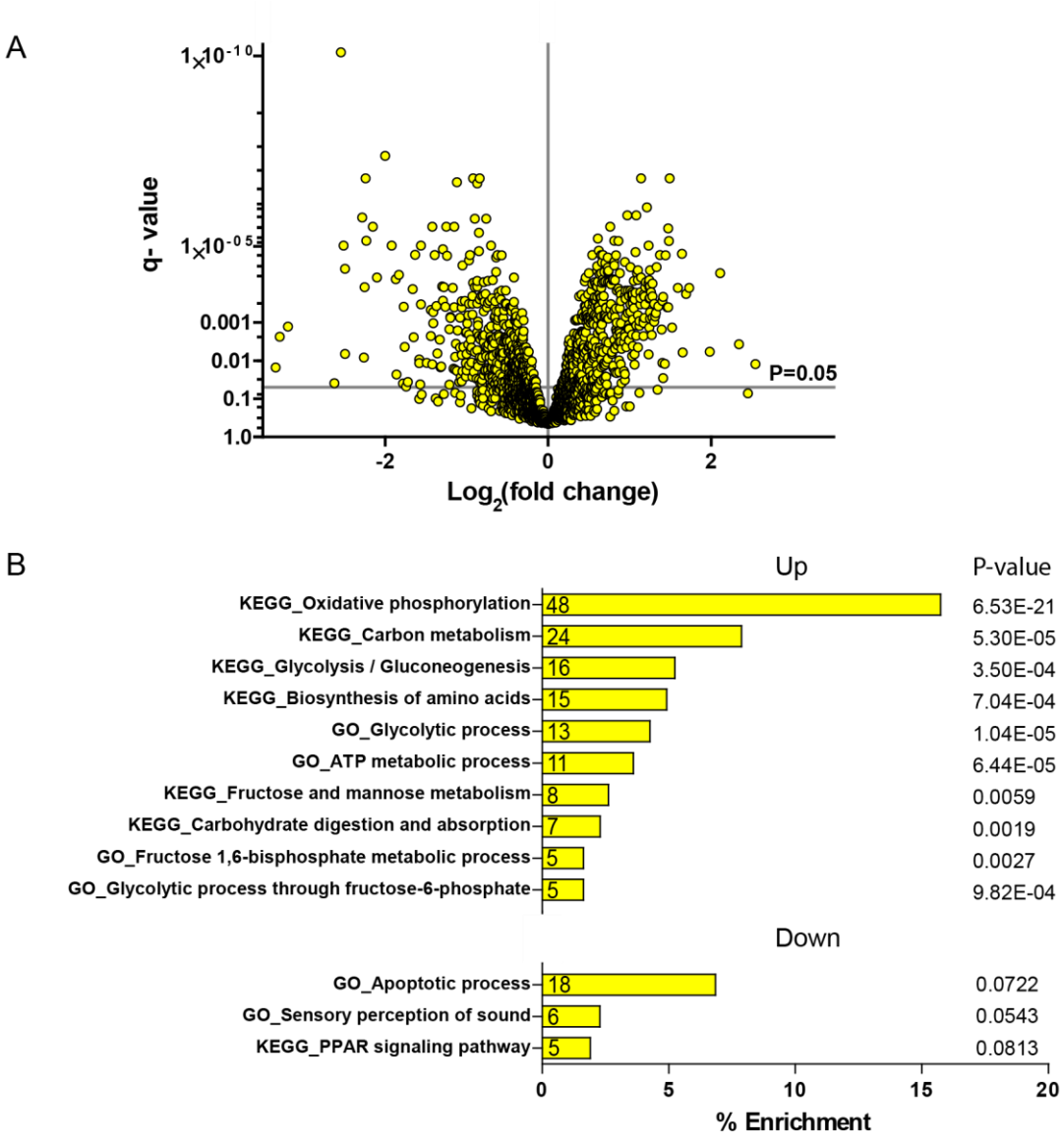

Fig. 28: Proteome analysis of cortical neurons indicate enhanced oxidative metabolism induced by KD

(A) Volcano plot of neurons isolated from cortex of mice depicting differentially regulated proteins upon feeding a KD, indicating massive changes (n=4). (B) Pathway analysis (Top10) of the most differentially regulated proteins of neurons with indicated p-values suggest strong increase in metabolic pathways. No downregulated pathway reached significance. X-axis depict percentage of enrichment of analyzed proteins. Number within Bars represent number of associated proteins.

availability and increased levels of ßOHB in cortex, we speculated that neurons will adapt similar to astrocytes by decreasing glycolysis and shift their metabolism towards KB utilization. Comparable to astrocytes, over 2100 proteins could be identified in both dietary conditions in neurons (Fig. 28A). Although three pathways were suggested to be downregulated within neurons (Fig. 28B) these did not reach statistical significance. With maximal enrichment, pathway analysis suggested enhanced oxidative phosphorylation within neurons. Surprisingly, glycolysis and carbohydrate-based pathways were detected to be increased in KEGG as well as in GO terms under ketogenic conditions. Therefore, this result was in direct contrast to the observed changes in astrocytes where glycolytic related pathways were exclusively diminished.

2.13.1 Enhanced ketolysis in isolated neurons from cortex of KD fed mice

In vitro experiments have shown that neurons are capable of ketolysis (Edmond et al., 1987). We speculated that neurons will increase ketolysis in response to KD feeding in mice due to increased ßOHB availability. Similar to all other investigated cell types, neurons increased MCT1 and BSG protein abundance suggesting enhanced uptake of KB (Fig. 29A). Significant increase of ketolytic enzymes was found with highest $\log_2$ fold changes observed for SCOT. To support this finding, in sagittal brain sections neurons were co-labeled for SCOT and NeuN. NeuN is used as mature neuron marker and stains neuronal nuclei and perinuclear cytoplasm (Gusel'nikova & Korzhevskiy, 2015) enabling identification of neuronal cells (Fig. 29B). In addition, SCOT labeling was strongly enhanced in neurons of mice fed the KD. In contrast to astrocytes, SCOT labeling was mainly located within the cell soma (compare Fig. 17B). Taken together, these results indicate that neurons adapt in response to feeding mice a KD and increase KB uptake and utilization by increasing expression of necessary transporter and enzymes. Furthermore, by comparing the magnitude of enhancement especially of SCOT, neurons might be the major consumer of KB.

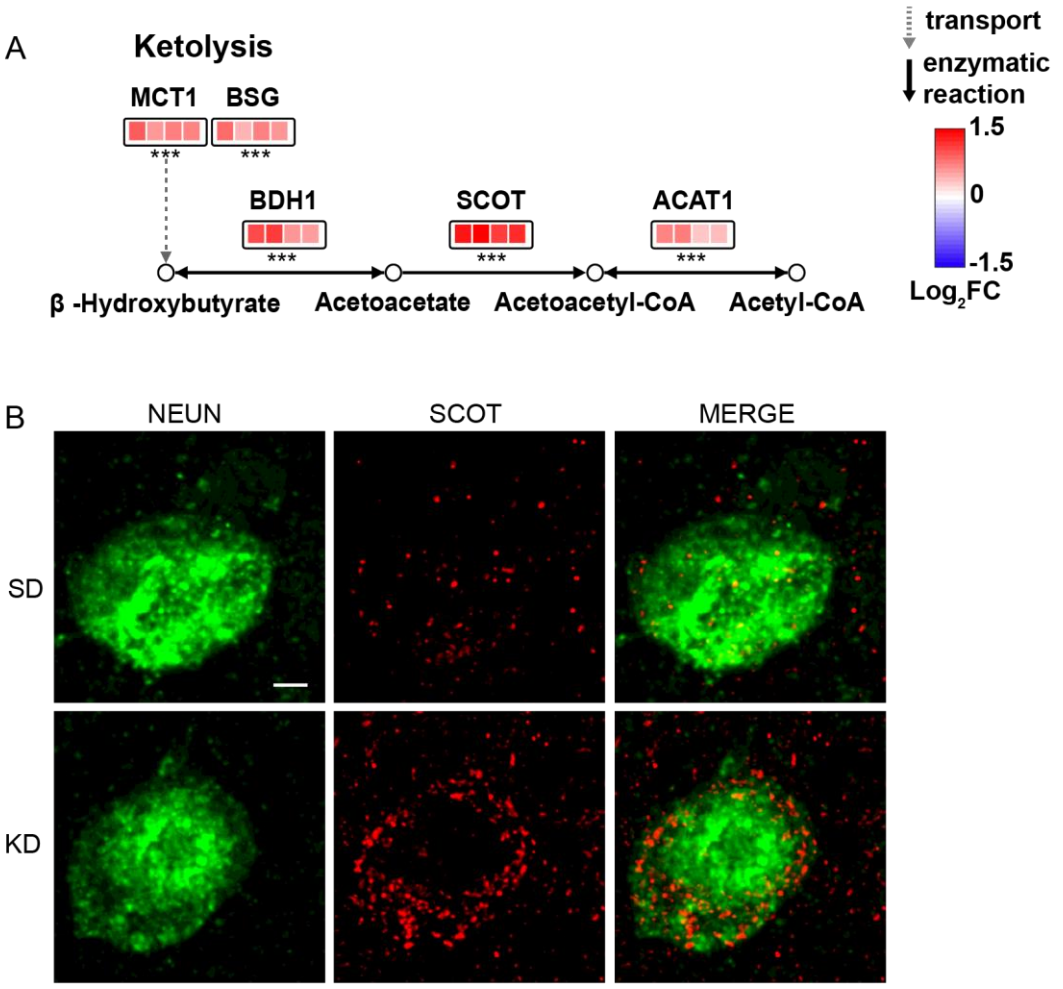

Fig. 29: Neurons react to feeding a KD by upregulation of ketolytic enzymes

(A) Proteins identified by proteome analysis from cortical neurons involved in transport and utilization of KB where mapped to the ketolytic pathway indicating strong enhancement of this pathway. Log_2 fold changes of individual sample values were depicted (n=4). Significance is indicated with *q<0.05, **q<0.005, ***q<0.001, (moderated t-statistics with multiple comparison correction; “limma” Bioconductor package). (B) Maximum intensity projection of sagittal brain sections from animals receiving KD or SD stained for SCOT (red). Neurons (NeuN) clearly accumulate SCOT signal under ketogenic conditions. Scale, 5µm. SD= standard diet; KD= ketogenic diet.

2.13.2 Neurons increase glycolysis under ketogenic conditions

Despite reduced glucose concentrations within the cortex of KD fed animals, pathway analysis within neurons suggested increased glycolytic rate. To examine this suggestion glycolytic proteins were further assessed. GLUT1 was not altered in neurons of ketogenic animals (Fig. 30). Interestingly, GLUT3 the major neuronal glucose transporter (Simpson et al., 2008) that was only detected within neurons showed marked increase indicating forced uptake of residual glucose into these cells. Except for two proteins (PGM1 and PGK2) all identified enzymes of glycolysis showed consistent increase suggesting enhanced utilization of glucose within neurons. It might be that glucose is rather

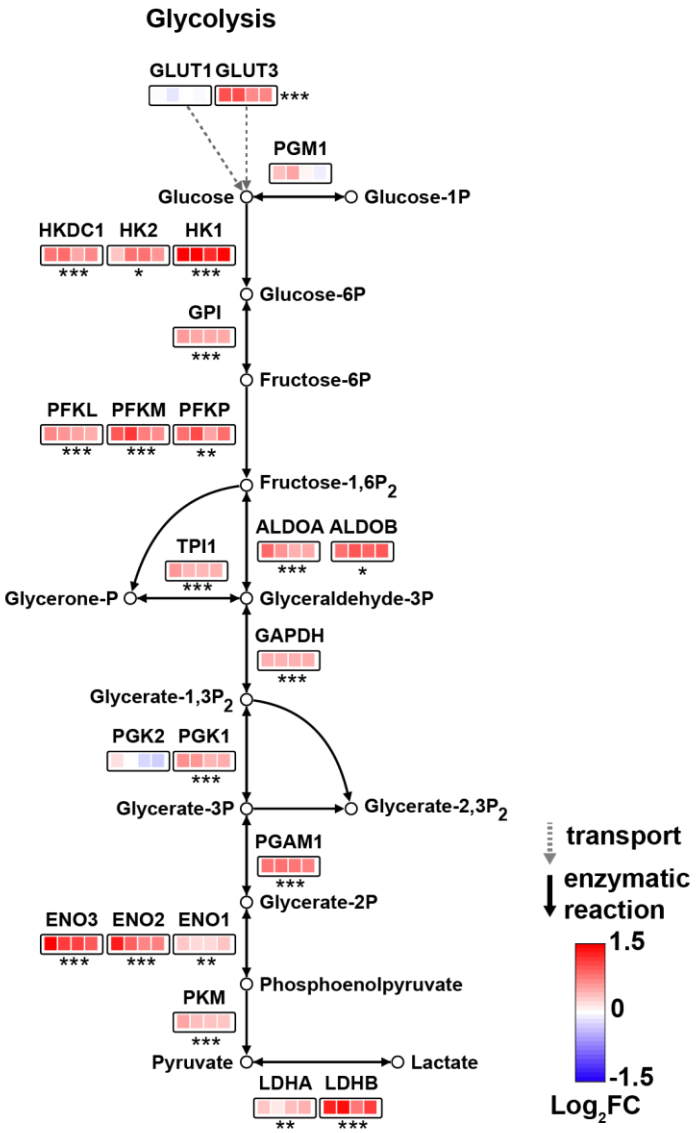

Fig. 30: Neurons enhance glycolysis when mice are fed a ketogenic diet

Proteins identified by proteome analysis from cortical neurons involved in glycolysis where mapped with corresponding Log_2 fold changes of individual sample values (n=4), revealing extensive increases upon KD feeding in mice. Significance is indicated with *q<0.05, **q<0.005, ***q<0.001, (moderated t-statistics with multiple comparison correction; “limma” Bioconductor package). See appendix for table of full protein names.

metabolized to lactate instead to pyruvate since both identified isoforms of lactate dehydrogenase LDHA and LDHB showed increased expression. However, without further experiments this remains highly speculative. Taken together, these data suggest that neurons not only rely on glycolysis to produce energy under ketosis but even increase glycolytic rate. Considering that glucose availability is diminished under ketotic conditions this appears counterintuitive and suggests further experiments in this direction.

2.13.3 Mitochondrial respiration is enhanced in neurons of mice fed KD

Ketolysis and glycolysis have been found in neurons of ketogenic animals to be increased. It therefore can be concluded that neurons may also increase mitochondrial respiration in response to this energy substrate maintaining pathways. To address this, TCA cycle proteins were analyzed to check if neurons also increase acetyl-CoA consumption. Indeed, most of the identified TCA cycle enzymes were increased in

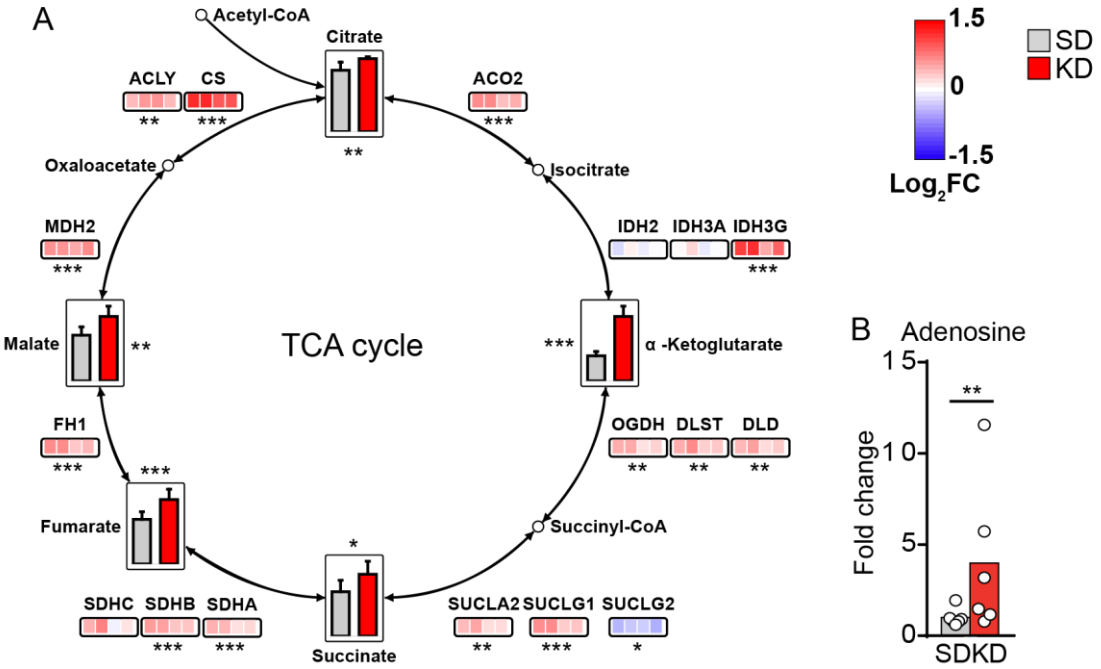

Fig. 31: Enhanced TCA cycle flux of neurons leads to increased TCA cycle intermediates in mice fed a KD

(A) Proteins identified by proteome analysis from cortical neurons involved in TCA cycle where mapped with corresponding log_2 fold changes of individual sample values (n=4), in addition to identified TCA cycle intermediates identified from total cortex of mice using GC/MS (±SEM, n=6). Increase in TCA cycle proteins correlate with enhanced TCA cycle metabolites. Values of SD condition were set to 1. (B) Enhanced levels of adenosine in cortex of KD mice might indirectly reflect enhanced neuronal TCA cycle. Significance is indicated with *q<0.05, **q<0.005, ***q<0.001, (moderated t-statistics with multiple comparison correction; "limma" Bioconductor package) for proteins and with *padj<0.05, **padj<0.005, ***padj<0.001 (Benjamini-Hochberg correction, DESeq2 R package) for metabolites. SD= standard diet; KD= ketogenic diet. See appendix for full protein names.

cortical neurons of KD fed mice (Fig. 31A). Additionally, TCA cycle metabolites identified by metabolite profiling from cortex tissue of mice were mapped to the respective position within the pathway. Values of SD fed mice were set to 1 and graphs represent fold changes of identified intermediates. All identified metabolites were increased upon feeding mice a KD and were therefore in line with enhanced TCA cycle found within neurons. This finding suggest that increased concentration of TCA cycle metabolites found within cortex of KD fed mice is attributable to increased metabolism of acetyl-CoA within neurons since TCA cycle were not detected to be increased in other cell types. It

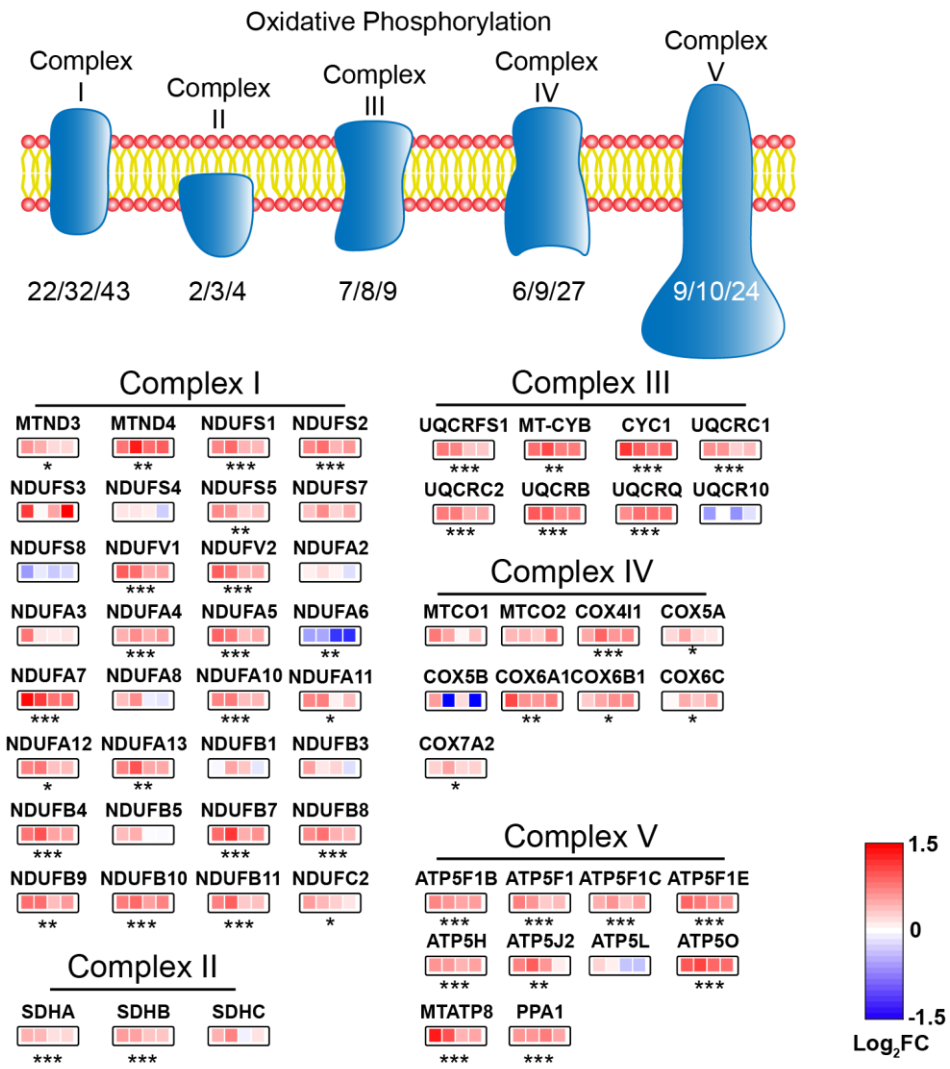

Fig. 32: Ketogenic diet enhances mitochondrial respiration in isolated neurons

Proteins identified by proteome analysis from cortical neurons associated to oxidative phosphorylation where mapped with corresponding Log_2 fold changes of individual sample values (n=4), revealing enhancing effects on mitochondrial respiration of ketogenic diet feeding in mice. Numbers below complexes denote significant/identified/overall associated proteins. Significance is indicated with *q<0.05, **q<0.005, ***q<0.001, (moderated t-statistics with multiple comparison correction; “limma” Bioconductor package). See appendix for full protein names.

has been speculated that the KD is able to increase the adenosine pool by increased production of ATP (DeVivo et al., 1978; Kim et al., 2010; Maalouf et al., 2009). The finding that adenosine was found to be increased nearly 5-fold in cortex of KD fed mice further support enhanced TCA cycle in cortical tissue of KD fed mice (Fig. 31B). As indicated from the pathway analysis, neurons are likely to enhance oxidative phosphorylation. To address this opportunity and further collect evidence that would support enhanced mitochondrial respiration in neurons under ketotic conditions, proteins involved in oxidative phosphorylation were examined. The numbers below each respiratory complex show the ratio of significantly increased to identified to overall proteins of the respective

complex (Fig. 32). Each identified protein is depicted below to assess the individual log_2 fold change. Indeed over 74% of all identified proteins involved in oxidative phosphorylation were significantly increased in neurons when mice are fed a KD. Given that the proteomic analysis covered approximately 58% of all proteins involved in oxidative phosphorylation this strongly suggest enhanced mitochondrial respiration within neurons. Taken into account that also TCA cycle enzymes in neurons and TCA cycle metabolites in cortex were increased, this finding supports the idea of enhanced energy production within neurons in ketogenic animals. However, these data do not explain to what reason neurons do enhance their metabolic rate under ketogenic conditions.

2.13.4 Synaptic transmission is enhanced in neurons of ketogenic animals

The current results indicated enhanced metabolism in cortical neurons of mice fed a KD. It has been calculated that the biggest portion (44%) of the total energy expenditure within cortical neurons is attributable to synaptic transmission (Howarth et al., 2012). It is conceivable that increased energy production in neurons would indicate enhanced synaptic transmission. To test this possibility proteins identified by proteome analysis within neurons involved in synaptic transmission were assessed to receive an impression of possible changes. 32 proteins could be identified in both dietary groups to be involved in synaptic transmission according to KEGG data sets (Fig. 33A). Among these, known representatives of synaptic vesicle loading and release like vesicular glutamate transporter 1 (VGLUT1), synaptotagmin 1 (SYT1) and vesicle-associated membrane protein 2 (VAMP2) (Park & Ryu, 2018; Schoch et al., 2001; Wojcik et al., 2004) were found. Additionally, multiple subunits of the vacuolar H^+-ATPase that are important for refilling of newly formed synaptic vesicles (Hnasko & Edwards, 2012) were identified together with additional components of the synaptic vesicle cycle. As speculated, most of the identified proteins showed marked increase in neurons of KD fed mice, suggesting enhanced neurotransmission within the cortex of ketogenic animals. However, considering that the isolated neuronal fraction is comprised of different neuronal subsets conclusions regarding the type of neurotransmission i.e. inhibitory or excitatory are not possible. Furthermore, evidence that feeding a KD does alter neurotransmission comes from metabolite profiling analysis of cortical tissue identifying the major excitatory and inhibitory neurotransmitter glutamate and GABA, respectively (Fig. 33B). Interestingly, glutamate was found to be decreased by 50%, whereas GABA concentration within the cortex was just slightly diminished. Glutamine the precursor of both neurotransmitters was unaltered. This finding might suggest that neurotransmitter balance is indeed altered upon feeding mice a KD. It just can be speculated if decreased concentration of

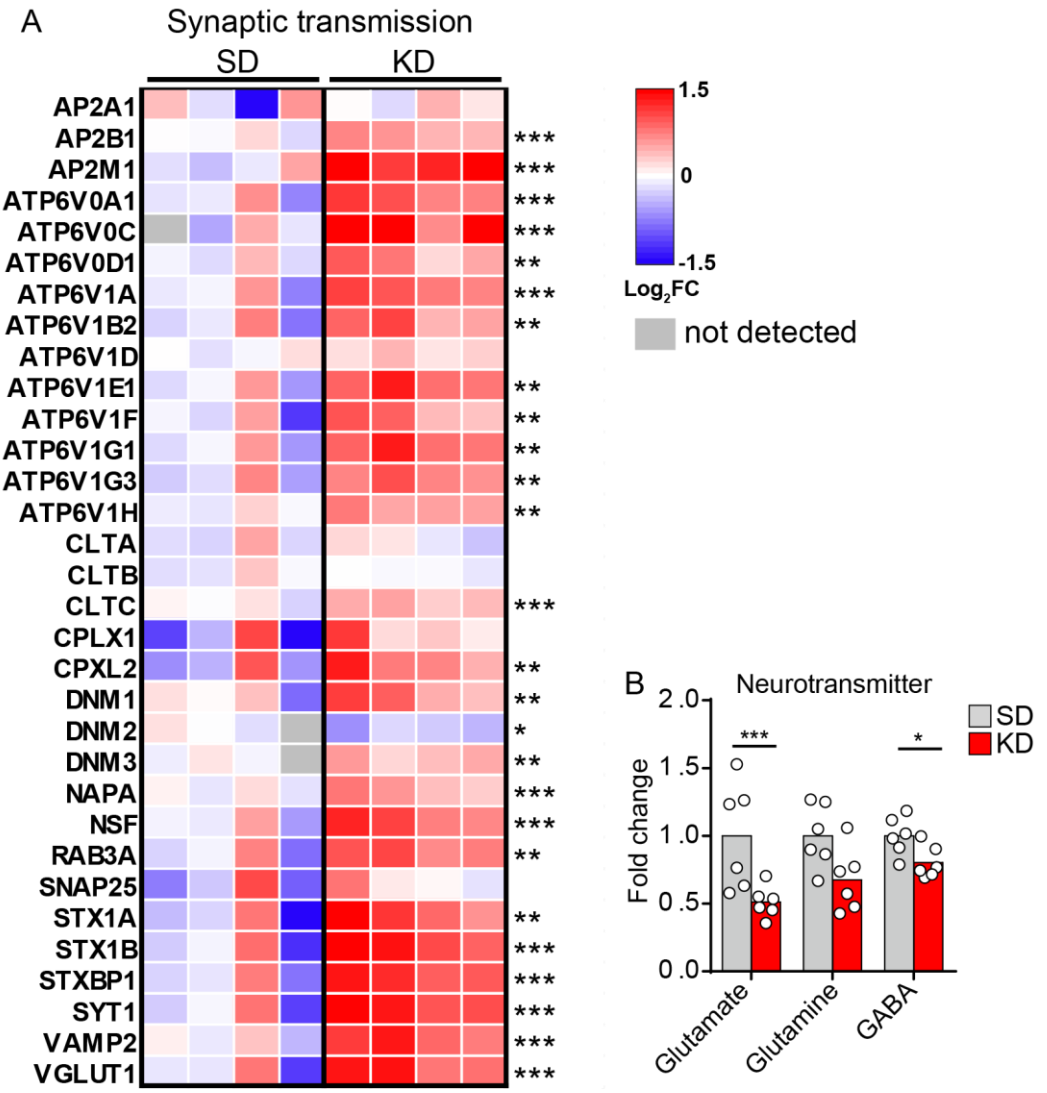

Fig. 33: KD fed mice might increase synaptic transmission in neurons inducing global changes of neurotransmitters

(A) Proteins associated with synaptic transmission are consistently upregulated, indicating enhanced neuronal activity. Depicted are log_2 fold changes of individual sample values (n=4). Significance is indicated with *q<0.05, **q<0.005, ***q<0.001, (moderated t-statistics with multiple comparison correction; “limma” Bioconductor package). (B) Neurotransmitter level measured by GC/MS in cortex of SD and KD fed mice. Bars represent mean fold change normalized to SD fed mice with individual data points (n=6). Significance is indicated with *padj<0.05, **padj<0.005, ***padj<0.001 (Benjamini-Hochberg correction, DESeq2 R package). SD= standard diet; KD= ketogenic diet. See appendix for full protein names.

glutamate is due to metabolic changes of the KD or because of enhanced synaptic transmission in neurons. Taken together, these findings strongly suggest that neurons increase synaptic transmission in response to feeding a KD in mice, which might lead to altered neurotransmitter concentrations. Precisely defined experiments need to be performed to address the question what kind of neurotransmission is enhanced in neurons and if the altered neurotransmitter concentration is a cause or consequence.

2.13.5 KD feeding in mice increases motor activity

To address the question whether altered neurotransmission could cause functional consequences an open field test was performed, that commonly measures the exploratory behavior and general activity of rodents (Gould et al., 2009). Fig. 34A shows a schematic representation of the open field and representative tracking of travel distance from SD and KD fed mice at six weeks of age. The data showed that mice fed the KD significantly increased travel distance indicative of enhanced motor activity (Fig. 34B). The open field is also a measurement of anxiety behavior as parameters like number of visits within the center or duration within the center can be assessed (Gould et al., 2009). Decreased number of visits or duration within the center would indicate increased anxiety in mice. However, visits within the center (Fig. 34C) and time spent in center (Fig. 34D) were unaltered in mice fed a KD in comparison to mice on SD. This indicates that KD does not lead to altered anxiety behavior. Taken together, these findings suggest physiological changes upon feeding mice a KD probably due to changes in neurotransmission within cortical neurons without affecting anxiety behavior.

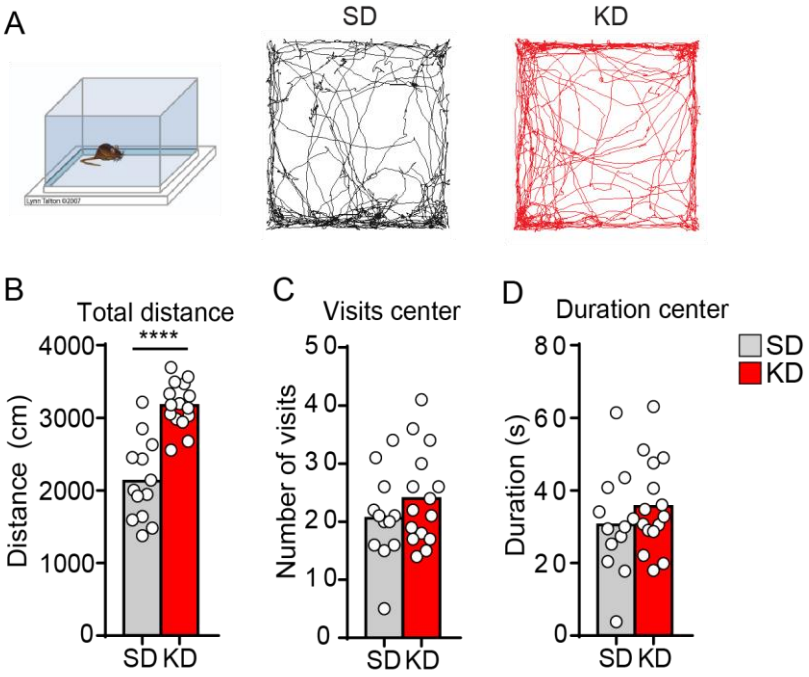

Fig. 34: Ketogenic diet enhances motor activity in mice

(A) Representative traces of travel distance from mice on SD and KD, respectively at 6 weeks of age during an Open field test to assess behavioral changes upon feeding a KD. (B) Mice on KD were significantly more active than SD fed mice, indicated by total travel distance. KD fed mice exhibited no signs for anxiety revealed by unchanged center visits (C) and duration within the center area (D). Asterisks depict significant differences with *p<0.05, **p<0.005, ***p<0.001, ****p<0.0001 (two-way ANOVA with Sidak's post test). SD= standard diet; KD= ketogenic diet.

3 Discussion

3.1 KD prevents metabolic switch upon weaning but does not influence brain development

Ketone bodies serve as important energy source for the brain during suckling but are quickly replaced by glucose after start of carbohydrate ingestion during weaning (Nehlig, 1999, 2004). In this study we asked the following questions: (1) Is it possible to increase ketolytic enzymes and KB transport by feeding a KD thereby reflecting the suckling period? (2) In which regard do brain cells change their metabolism in response to KD feeding? (3) Will they switch to ketolysis and reduce glucose utilization and (4) what are the consequence for overall brain metabolism?

Weaning mice on a KD resulted in reduced blood glucose and increased ßOHB concentration in accordance with previous results (Hernandez et al., 2018; Selfridge et al., 2015). Subsequently, KB transporter and ketolytic enzymes within the brain increased over time in KD fed animals when compared to normally fed animals. Transporter expression (e.g. MCT1) and activity of ketolytic enzymes decline after weaning in rodents fed carbohydrate rich chow (Krebs et al., 1971; Leino et al., 1999; Page et al., 1971). Hence, our results suggest that weaning mice on a KD is able to prevent the metabolic switch and maintain high expression of MCT1 and necessary enzymes such as SCOT for KB utilization. This is probably induced by increased concentration of ßOHB found in cortex tissue while glucose concentration is decreased forcing the brain to utilize KB instead of glucose. Therefore, we speculate that the metabolic switch seen upon weaning is dependent on dietary changes and not induced by a brain cell intrinsic program.

Mice fed a KD exhibited reduced body growth compared to mice on SD. Indeed, feeding a KD has been implicated with reduction in body weight in adult mice (Kennedy et al., 2007; Selfridge et al., 2015) and reduced growth in children (Vining et al., 2002). We therefore investigated whether KD feeding would lead to altered brain growth and development. Body growth during the juvenile period is assumed to be dependent on insulin and insulin like growth factor 1 (IGF1) (Bergqvist, 2012) and IGF1 was found to be decreased in children adhering to the KD for 12 month (Spulber et al., 2009) explaining the reduced growth rate. Insulin level in mice were found to be decreased when fed a KD as consequence of low carbohydrate consumption, suggesting that the slowed body growth observed in KD fed mice is attributable to altered insulin level and insulin signaling (Kennedy et al., 2007). Importantly, brain weight of mice at six weeks of

age were unaltered despite reduced body weight at that time. One explanation could be that brain volume is already stable after three weeks of age (Hammelrath et al., 2016) when body weight of KD and SD fed mice did not differ in the current study. It is also conceivable that brain growth is not dependent on insulin signaling since no alterations in Akt, GSK3ß and mTOR phosphorylation mediated by insulin could be found in mice fed the KD despite differences in peripheral insulin sensitivity (Selfridge et al., 2015).

KB are thought to be the preferred substrate for synthesis of lipids and sterols during development needed for myelination (Bergstrom et al., 1984; Edmond, 1974; Webber & Edmond, 1979). However, it appeared that myelination within the cortex was unaltered in KD fed mice at six weeks of age compared to SD fed mice indicating no influence of the KD on the speed of myelination. One could therefore assume that the developmental program of myelination in contrast to brain metabolism is controlled endogenously and not dependent on dietary supplementation. However, it has to be taken into account that only the latest time point at six weeks was investigated where effects already could have been compensated. The KD could support myelination during suckling and shortly before weaning when rate of myelination is highest (Norton & Poduslo, 1973). We did not observe differences in myelination in optic nerve at three weeks of age indicating that the KD does not influence rate of myelin formation during the peak of myelination. We speculate that the duration of KD feeding from P17 to P21 is not sufficient to induce alterations in myelin synthesis. Additionally, one has to consider that myelination in SD fed mice is already sufficient to maintain nerve conduction and insulation. It could be worth considering to test influence of KD feeding under developmental demyelination to assess possible effects of the KD under disease conditions. At two month of age nearly all axons are myelinated within the optic nerve, while myelination is still ongoing in the corpus callosum at least until four month of age (Biffiger et al., 2000; Remahl & Hildebrand, 1982; Yates & Juraska, 2007). Our investigation was based on optic nerve and cortex tissue and does not necessarily reflect the state of myelination within the corpus callosum where KD feeding could have other impacts.

Investigation of cognitive abilities by assessing memory and learning ability in KD fed mice further supported results from morphological analysis that weaning mice on a KD does not impair brain development. However, evidence from other studies report conflicting results regarding cognitive performance influenced by a KD. One study reported cognitive deficits in weanling rats fed a KD (Scichilone et al., 2016), while another study reported significant improvements of cognition in young and aged rats performing a dual task that required memory and association capability (Hernandez et

al., 2018). Therefore, conclusions drawn from our experiments regarding cognitive effects of the KD has to be considered carefully. Taken together, our data suggest that weaning mice on a KD prolongs ketosis into adulthood, thereby increasing expression of ketolytic enzymes and KB transporter. Additionally, in the current study KD did not influence brain growth, myelination or cognition in mice.

3.2 Efficient isolation of cell types from mouse cortex

The KD has been investigated extensively over the last decades *in vitro* and *in vivo*. Cell culture experiments gained insights on the KD's action but lacking the contribution of peripheral metabolism and influence of the BBB. In contrast, *in vivo* studies in the past could not resolve cell type specific changes in response to the KD although enable investigation under physiological conditions.

To overcome these obstacles, cell isolation from adult mouse brain was applied to investigate *in vivo* influence of the KD with cell type specific resolution. Therefore, we optimized the MACS technique that enabled region and cell type specific analysis from individual animals. Most studies using MACS technology were conducted using multiple whole brains to isolate sufficient number of cells (Batiuk et al., 2017; Berl et al., 2017; Sharma et al., 2015), thereby losing region specificity and differences between individual animals cannot be attributed. Here we showed that cell isolation of certain cell types is possible from as little as one single cortex enabling region specific investigation of cells in addition to analysis of biological variability. Furthermore, we were able to isolate multiple cell fractions from the same cortex enabling comparison of cell types from the same tissue, individual and brain region. Also other studies have demonstrated isolation of multiple cell fractions, however using whole brains or multiple animals (Merienne et al., 2019; Swartzlander et al., 2018). So far, only one study reported was able to isolate different cell types from single animals and comparable amounts of tissue as performed in our study (Holt & Olsen, 2016). Subsequent proteomic or transcriptomic approaches that were used in our study enabled highly specific analysis of cell types in a region-specific manner. Furthermore, comparison of different cell fractions from the same region and animal is in principal possible. In conclusion, the optimized MACS technique developed in this study coupled to –omic analyses is a powerful method to analyze cell type specific alterations in brain tissue.

3.3 Endothelial cells provide substrates for the brain under ketosis but rely on glycolysis for energy production

Brain endothelial cells controls the entry of metabolites and molecules into brain parenchyma and protect the CNS from neurotoxic substances by formation of the BBB (Abbott et al., 2010). However, little is known about endothelial cell metabolism and results obtained originate mostly from *in vitro* studies that do not fully reflect the *in vivo* situation (Eelen et al., 2018). Proteomic analysis revealed increased expression of MCT1 in endothelial cells that we also observed in histological staining's suggesting that endothelial cells react to increased concentrations of KB within the circulation induced by the KD (Fig. 35). Interestingly, endothelial cells do not seem to increase ketolysis. This indicates that KB are rather shuttled to brain cells (e.g. astrocytes) than used for energy production although KB can be utilized by brain capillaries *in vitro* (Homayoun & Bourre, 1987). Indeed, endothelial cells are highly glycolytic and produce approximately 85% of their total ATP from glycolysis (De Bock et al., 2013) and might therefore shuttle KB to other cells. That might explain the finding of unaltered glycolysis in endothelial cells under ketosis. We speculate that endothelial cells rely on glycolysis even under reduced glucose concentrations within the blood (Fig. 35). Since endothelial cells are constantly supplied with glucose by the circulatory system, reduced blood glucose might not affect glycolysis within endothelial cells.

TCA cycle enzymes were found to be decreased in endothelial cells that might implicate reduced mitochondrial respiration under ketosis. Since glucose is nearly completely metabolized to lactate by glycolysis in endothelial cells mitochondrial respiration might be fueled by other substrates like fatty acids or glutamine (Spolarics et al., 1991). Indeed, glucose deprivation *in vitro* causes increased flux of fatty acid oxidation into endothelial cells (Dagher et al., 2001). Under ketosis, increased level of fatty acids could favor ß-oxidation in endothelial cells to prevent energy depletion as consequence of reduced glucose concentrations. However, our current data do not indicate altered ß-oxidation in endothelial cells in response to KD. More recent studies indicate that fatty acid oxidation in proliferative endothelial cells is not used for energy production (Kalucka et al., 2018; Schoors et al., 2015) but supports nucleotide synthesis (Schoors et al., 2015). In contrast, quiescent endothelial cells reduce TCA cycle flux despite increased fatty acid oxidation (Kalucka et al., 2018). Therefore, the presented data suggest that endothelial cells under ketogenic conditions are likely to resemble a quiescent state due to reduction of TCA cycle enzymes.

The concentration of fatty acids in serum is increased upon ingestion of a KD (Cunnane et al., 2002; Fraser et al., 2003) (Fig. 35). The finding that astrocytes increase ß-oxidation in mice fed the KD propose enhanced availability of fatty acids within the brain. Hence, fatty acids must cross the BBB. However, increased abundance of lipid transport proteins could not be detected in endothelial cells. In addition to active transport fatty acid can cross the BBB by passive diffusion (Doege & Stahl, 2006; James A. Hamilton & Brunaldi, 2007). In line, the KD raised brain levels of docosahexaenoic and arachidonic acid (Taha et al., 2005), two fatty acids that are transported by passive diffusion (Ouellet et al., 2009). We speculate that transport of fatty acids is mainly facilitated by passive diffusion driven by increased amounts of free fatty acids within the circulation in mice on the KD.

3.4 Astrocytes spare glucose for neurons and use KB and fatty acids for energy production

Under normal glucose availability it has been proposed that astrocytes supply neurons metabolically by shuttling lactate (Pellerin & Magistretti, 1994), but it is unknown what substrates could be provided to neurons under ketosis. The present data suggest that astrocytes reduce glycolysis, in agreement with *in vitro* and *ex vivo* experiments of a previous study using fasted mice (Valdebenito et al., 2016). However, GLUT1 abundance was slightly increased suggesting that uptake or transport of glucose in astrocytes is not decreased. This predicts that residual glucose might be shuttled to other cells to increase its availability e.g. for neurons under low glucose conditions (Fig. 35).

Given that astrocytes reduce glucose metabolism under ketotic conditions they require an alternative source to meet their energy demands. Astrocytes are able to utilize KB (Edmond et al., 1987) and the KD enhanced ßOHB concentration in cortex of KD fed animals. We therefore speculated that astrocytes would switch to KB utilization to produce energy. Indeed, increased abundance of ketolytic enzymes concomitant with increased MCT1 expression in astrocytes was observed supporting our hypothesis. Surprisingly, in addition to enhanced ketolysis we observed increased ß-oxidation in astrocytes, which has not been reported so far. However, it appears likely that astrocytes also increase fatty acid oxidation taken into account that astrocytes are probably the best equipped cell type for ß-oxidation in the brain (Edmond et al., 1987; Romano et al., 2017). Furthermore, the KD increases fatty acid availability within the brain (Taha et al., 2005), enabling astrocytes to maintain the increased rate of ß-oxidation for energy production. Astrocytes might accumulate malonyl-CoA a potent inhibitor of ß-oxidation (McGarry & Brown, 1997) implicated by increased abundance of ACC and decreased FASN. Despite

this contradictory finding we speculate that astrocytes still increase ß-oxidation and prevent its inhibition by reconversion of malonyl-CoA to acetyl-CoA by MCD as indicated by increased mRNA expression of *Mcd* in cortex.
In conclusion, our data suggest that astrocytes shift their metabolism from using glucose towards ketolysis and ß-oxidation thereby utilizing KB and fatty acids. This supports the idea that glucose could be shuttled to neurons as substrate for energy production. In addition, since astrocytes seem not fully relying on ketolysis it might be that KB are partially shuttled to other cells (Fig. 35).

3.5 Oligodendrocytes do not exhibit metabolic changes but might enhance ion buffering in response to KD feeding in mice

Considering the hypothesis that astrocytes and oligodendrocytes shuttle lactate to supply neuronal metabolism (Funfschilling et al., 2012; Pellerin & Magistretti, 1994) we hypothesized that oligodendrocytes would react similar to astrocytes. Surprisingly, oligodendrocytes did not show increased usage of KB under ketogenic conditions. This was suggested by unaltered abundance of ketolytic enzymes while at the same time import by MCT1 was increased. Indeed, SCOT activity in oligodendrocytes was found to be over 50% lower compared to astrocytes (Chechik et al., 1987; Edmond et al., 1987; Poduslo, 1989), indicating that oligodendrocytes are not prepared to use KB to the same extent as astrocytes and instead rather pass it on to other cells (e.g. neurons) by MCT1 mediated transport (Fig. 35). Interestingly, although oligodendrocytes utilize glucose in comparable amounts to astrocytes they release less lactate (Amaral et al., 2016). This suggests enhanced insertion of pyruvate into TCA cycle thereby increasing efficiency of ATP production from glucose. We therefore speculate that oligodendrocytes are able to meet their metabolic needs by efficient utilization of glucose and are not dependent on additional usage of KB.

Proteomic analysis revealed increased abundance of proteins associated with ion buffering in oligodendrocytes, which was later independently supported by transcriptome analysis. It is known that oligodendrocytes are critically involved in ion homeostasis and potassium buffering through expression of connexins and K^+ channels (Kamasawa et al., 2005; Larson et al., 2018; Menichella et al., 2006). Significant changes in connexin expression in oligodendrocytes could not be detected but transcriptomic data revealed changes in expression of K^+ channel genes (e.g. *Kcnb1, Kcnma1, Kcnq2, Kcne2, Kncj13, Kcnt1*). Although the major K^+ channel Kir4.1 known to control potassium accumulation in the extracellular space (Larson et al., 2018) was not among the upregulated genes,

our data indicated enhanced need for potassium clearance in brain of ketogenic diet fed mice. Potassium buffering is especially important during neuronal activity to prevent seizures (Larson et al., 2018; Menichella et al., 2006). Considering that enhanced synaptic transmission was found in neurons leading to enhanced potassium release during signal transduction, enhanced oligodendrocytic potassium buffering becomes reasonable.

3.6 KD feeding in mice raise neuronal metabolism and increases synaptic transmission

Neurons like astrocytes are able to take up and catabolize KB for energy production (Chechik et al., 1987; Edmond et al., 1987; Maurer et al., 2011). We speculated that neurons in similarity to astrocytes change their metabolism and increase ketolysis, thereby reducing the rate of glycolysis. Indeed, ketolytic enzymes were significantly and consistently increased suggesting that neurons use KB to fuel mitochondrial respiration for energy production (Fig. 35).

Glucose concentration within the cortex was found to be reduced probably as consequence of decreased glucose blood levels. However, increased levels of glucose in cortex and plasma have been previously reported (Melo et al., 2006). The authors speculated that increased cerebral glucose concentration could reflect reduced glycolysis. At least in principle increased oxidative metabolism fueled by KB should downregulate glycolysis either by modulation of phosphofructokinase I, or by inhibition of pyruvate dehydrogenase (Ma et al., 2007; Melo et al., 2006). Indeed, in rat hippocampal slices acetyl-CoA production from glucose was significantly attenuated after adding ßOHB. This indicates that KB are capable of inhibiting glycolytic flux (Valente-Silva et al., 2015). In contrast to our expectations we found a strong and consistent increase in the abundance of glycolytic enzymes in neurons. From this we conclude that KD enhances the utilization of glucose in neurons. Our finding that neurons increased the expression of GLUT3 indicating enhanced glucose uptake further supports this observation. GLUT3 is of particular interest due to its higher affinity and transport rate compared to GLUT1 (Simpson et al., 2008). Thereby neurons may be able to take up sufficient amount of glucose even under low glucose conditions to secure glycolysis (Fig. 35). Taking into account that glucose consumption linearly correlates with HK1 mRNA expression and immunofluorescence (Lundgaard et al., 2015) and that this enzyme exhibited the highest $\log_2$ fold changes further supports our hypothesis of enhanced neuronal glucose utilization. However, from the current data the fate of glucose cannot be addressed, although increased expression of lactate dehydrogenase

isoforms indicated enhanced formation of lactate. This assumption is in agreement with the aforementioned finding that KB inhibit acetyl-CoA formation from glucose since lactate formation was not affected (Valente-Silva et al., 2015). Melo and colleagues (2006) found increased glucose concentration in cortex of KD fed rats and speculated that this would indicate reduced glycolysis. If this holds true our data would imply normal glycolytic rate in cortex of KD due to the finding that glucose concentration in cortical tissue was comparably decreased to blood. We speculate that cortical glycolytic rate is unaltered in KD fed mice due to enhanced glycolysis in neurons, thereby compensating the reduced glycolytic rate observed in astrocytes.

KB can account for 60-70% of energy production within the brain whereas the remaining 30-40% need to be generated by glucose metabolism (Cahill, 2006; Grabacka et al., 2016; Owen, 2005). In line, in neurons 38% of neuronal substrate oxidation had to be provided by glucose in fasted rats infused with ßOHB (Chowdhury et al., 2014). This is probably due to the fact that synaptic vesicle loading requires high local ATP concentrations provided by glycolytic enzymes within synapses than high overall ATP level generated in the soma (Fedorovich & Waseem, 2018). Taking into account that lactate supply from astrocytes might be diminished due to reduced glycolysis, we speculate that neurons enhance glycolysis to maintain their overall energy metabolism. In contrast to glucose, KB utilization inevitably produce acetyl-CoA thereby increasing its concentration (Yudkoff et al., 2005). As consequence, acetyl-CoA needs to be catabolized via the TCA cycle (Cotter et al., 2013; Yudkoff et al., 2005). Enhanced TCA cycle activity was found in neurons with concomitant increase in TCA cycle intermediates within the cortex. We hypothesize that acetyl-CoA derived from KB forces neurons to increase TCA cycle and subsequently oxidative phosphorylation to prevent its accumulation. As a result, ATP level could be elevated. Indeed, others have reported elevated ATP concentration under ketogenic conditions (DeVivo et al., 1978; Kim et al., 2010). Elevated adenosine levels have been assumed already earlier due to increased ATP levels in response to KD feeding (Maalouf et al., 2009). Our observation of elevated adenosine ratio in ketogenic animals now directly supports this assumption. Therefore, our findings are in agreement with previous studies indicating that KD feeding increases energy levels. We can further speculate that this occurs due to enhanced mitochondrial respiration observed in neurons.

However, these findings raise the question after the use of the additional ATP content within the brain under ketogenic conditions. Under disease conditions it has been assumed that the improved mitochondrial respiration and energy production leads to restoration of decreased energy substrates and attenuates neuronal excitability through

multiple mechanisms (Gano et al., 2014; Koppel & Swerdlow, 2018; Maalouf et al., 2009; Masino & Rho, 2018). So far, the function of increased ATP availability under physiological conditions has never been addressed. Based on the current findings, we speculate that enhanced neuronal metabolism could lead to increased synaptic transmission. The finding that KD fed mice exhibited decreased neurotransmitter levels could further indicate altered neuronal activity. However, different neuronal cell types could not be discriminated that would allow conclusions of the type of altered neuronal signaling.

In this study we based our investigation on cortical tissue including the motor cortex. Therefore, increased synaptic transmission could result in enhanced motor activity. To test this assumption, motor activity was recorded in mice fed the KD. In fact, mice fed the KD showed significantly elevated motor activity that could point to enhanced synaptic transmission. Rats fed the KD exhibited similarly enhanced motor performance (Ziegler et al., 2005) and neural activation increases in Engrailed 2 null mice when pre exposed to the KD during the juvenile period (Verpeut et al., 2016). Taken together, the current data imply that the KD is able to enhance neuronal metabolism in cortex potentially leading to increased motor activity.

3.7 Implications for overall brain metabolism

The current findings implicate that metabolic pathways within the brain are not equally used by all cell types. Rather, feeding a ketogenic diet highlights the compartmentalization of brain metabolism between different cell types. From the current findings we propose the following hypothetic model by which different cell types could interact under ketogenic conditions to contribute to overall brain metabolism (Fig. 35). Under ketogenic conditions, glycolytic endothelial cells rely on the continuous supply of glucose from the blood thereby maintaining normal glycolytic rate. To support brain metabolism in response to KD feeding they facilitate transport of metabolic substrates like KB and fatty acids as alternative to glucose that is low abundant. Astrocytes switch to utilization of KB and fatty acids transported from the circulation by endothelial cells. By relying on fatty acid and KB breakdown under ketosis astrocytes are able to provide residual glucose for neurons, which are to a certain extent dependent on sufficient glucose supply. Neurons might take up glucose via GLUT3 from the extracellular space and from astrocytes and fuel glycolysis. This explains why no alterations in glycolysis could be observed on global cortical level. While astrocytes decrease glycolysis neurons enhance it, thereby compensating the reduced glucose consumption of astrocytes. However, both cell types might contribute equally to increased abundance of SCOT observed in cortical tissue of mice fed the KD. The additional utilization of KB within

neurons might lead to increased energy production. KD feeding also increased synaptic transmission in neurons probably supported by enhanced energy levels in these cells. In contrast, oligodendrocytes do not increase ketolysis. Rather they might supply KB to axons by shuttling these substrates through MCT1 and facilitate ion homeostasis and potassium buffering under induced increased neuronal activity due to KD feeding.

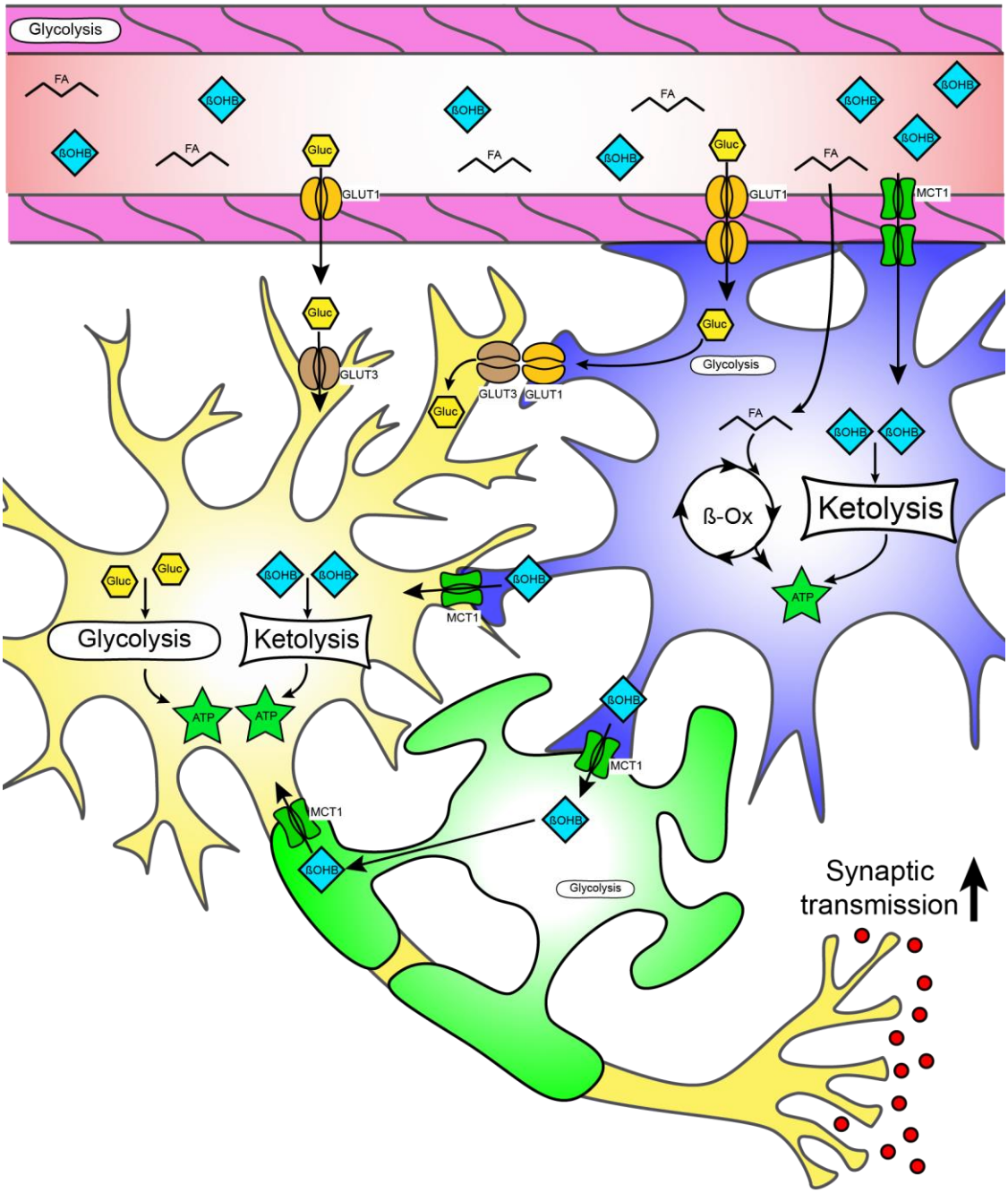

Fig. 35: Hypothetic model of metabolic changes in brain cells upon ketogenic diet feeding in mice

By feeding a ketogenic diet, the blood composition of metabolites changes to increased levels of ßOHB and fatty acids, while glucose decreases. Endothelial cells (pink) seem to decrease mitochondrial respiration and rely on glycolysis. However, astrocytes (blue) take up increased amounts of ßOHB via MCT1 and fatty acids to support ketolysis and ß-oxidation, respectively for energy production. In addition, glucose is taken up into astrocytes through GLUT1 but probably is rather shuttled to neurons than utilized within astrocytes via glycolysis. On the other hand, oligodendrocytes (green) does not change their metabolism in response to the ketogenic diet, but might take up ßOHB to pass it on to neurons. As the main consumer of the brain, neurons (yellow) take up ßOHB delivered through astrocytes and oligodendrocytes to generate energy via ketolysis and subsequent mitochondrial respiration. In addition, through increased expression of GLUT3 neurons are able to increase the uptake of glucose even under short supply conditions. This leads in turn to increased glycolysis and might end in enhanced neuronal synaptic transmission. Gluc=Glucose; FA= Fatty acids; ßOHB= ß-hydroxybutyrate; GLUT1/3= Glucose transporter 1/3; MCT1= Monocarboxylate transporter 1

4 Material and Methods

4.1 Material

If not stated otherwise, the used chemicals were provided by Sigma-Aldrich GmbH (Munich, Germany) or SERVA (Heidelberg, Germany). Laboratory materials and equipment were purchased from BD Falcon (Heidelberg, Germany), Bio-Rad (Munich, Germany), Sartorius (Göttingen, Germany), Gilson (Limburg-Offheim, Germany), Brand (Radebeul, Germany) or Eppendorf (Hamburg, Germany).

4.1.1 General laboratory equipment

4.1.1.1 Animal treatment

Freestyle Precision System	Abbot Diabetes Care
Rearing devices (shelf and box)	Custom made (In-house)

4.1.1.2 Molecular Biology

Agilent 2100 Bioanalyzer	Agilent
Light Cycler 480 II	Roche
PowerPac 300 Power Supply	Bio-Rad
SDS-PAGE gel casting/running units	Bio-Rad
Eon Microplate Spectrophotometer	BioTek
Table-top Thermomixer	Eppendorf
Table-top Centrifuge	Eppendorf
INTAS ChemoCam Imager ECL HR-16-3200	Intas
Ultra Turrax T8 homogenizer	Kinematica
Invitrogen semi-dry blotter	Invitrogen
Invitrogen wet-blot system	Invitrogen

4.1.1.3 Histology

Leica Jung Cryocut CM3000	Leica
Embedding station HMP110	Microm
Paraffin embedding center AP280	Microm
Sliding microtome HM400	Microm
Microwave inverter	Panasonic

Biowave Pro	Pelco

4.1.1.4 Tissue dissection

Razor blades	Persona
Dumont forceps	Fine Science Tools
Standard scissor	Fine Science Tools
Fine iris scissor	Fine Science Tools

4.1.1.5 Cell Isolation

Octomacs magnet	Miltenyi Biotech
Stand for Octomacs	Miltenyi Biotech
Water bath	Hecht Assistent GmbH
Sorvall wX+ Ultra Series centrifuge	Thermo Scientific
Ultra centrifuge rotor Th660	Thermo Scientific
Labofuge 400	Heraeus instruments

4.1.1.6 Electron microscopy

EM Trimm	Leica
Ultracut S	Leica
Semi 35° diamond knife	Diatome
Ultra 45° diamond knife	Diatome

4.1.1.7 Microscopes

Axio Oberserver Z1	Zeiss
Leo EM900 electron microscope	Zeiss
Leica SP8X FALCON	Leica

4.1.1.8 Behavior

Open field test	custom made (In-house)
Audiobox	TSE

4.1.1.9 Software

Adobe Illustrator CC
ImageJ/Fiji
GraphPad Prism6

Microsoft Excel 2013
Biobserve Viewer Software
Matlab
Zen 2012 Zeiss
LASX Leica
VANTED

4.1.1.10 Consumables

Syringe 1 ml	BD Bioscience
Venofix® 0.4x 10 mm	Braun
27 G cannula	BD Bioscience
Glucose test strips	Abott Diabetes Care
Ketone body test strips	Abott Diabetes Care
Cell strainer 70 µm	BD Bioscience
MS Columns	Miltenyi Biotech
HistoBond® slides	Marienfeld
Cover glass	Assistant
Tissue cassettes	Polyscience Inc.
Aqua-Poly/Mount	Polyscience Inc.
Tissue-Tek® O.C.T Compound	VWR
PVDF-Membrane Hybond-PTM	Amersham
Copper Grids	Science Services
Milk powder	Frema

4.1.1.11 Chemicals

Goat serum	Invitrogen
Horse serum	Sigma-Aldrich
Bovine serum albumin (BSA)	Biomol GmbH
Dubelco’s phosphate buffered saline (DPBS)	Gibco
RLT buffer	Qiagen

4.1.1.12 Enzymes

PhosStop phosphatase inhibitor	Roche Diagnostics GmbH
Complete Mini protease inhibitor	Roche Diagnostics GmbH

4.1.1.13 Kits

Agilent RNA 6000 Nano Kit	Agilent
DC Protein Assay (Lowry)	Bio-Rad
RNeasy Mini kit	Qiagen
SuperScript III Reverse Transcriptase	Invitrogen
Western Lightning Plus ECL	Perkin Elmer Life Sciences
Adult brain dissociation kit	Miltenyi Biotech
Neuron cell isolation kit	Miltenyi Biotech
Anti-ACSA-2 MicroBead kit	Miltenyi Biotech
Anti-O4 MicroBead kit	Miltenyi Biotech
Anti-CD31 MicroBead kit	Miltenyi Biotech

4.1.2 Solutions and buffers

4.1.2.1 1x Phosphate buffered saline (PBS)

170 mM Sodium chloride (NaCl)
3,4 mM Potassium chloride (KCL)
4 mM di-Sodium hydrogen phosphate (Na_2HPO_4 x $2H_2O$)
1,8 mM di-Potassium hydrogen phosphate (K_2HPO_4)
Adjust to pH 7.2 with 1 N NaOH.

4.1.2.2 Avertin

2% [w/v] 2,2,2-Tribrome ethanol 99%
2% [v/v] Amyl alcohol
Mixed for 30 min at 40°C, filtered before stored at -20°C

4.1.2.3 16% Paraformaldehyde (PFA, stock solution)

16% [w/v] Paraformaldehyde
Cooked at 65°C for 15 min while stirring, 5N NaOH was added until solution turned clear.
Filtered and stored at -20C°.

4.1.2.4 0.2 M Phosphate buffer

0.36% [w/v] Sodiumdihydrogenphosphate (NaH_2PO_4)
3.1% [w/v] di-Sodiumhydrogenphosphate (Na_2HPO_4)
1% [w/v] Sodium chloride

4.1.2.5 4% Paraformaldehyde

25% [v/v] PFA (16% stock solution)
50% [v/v] 0.2 M phosphate buffer
0,8% [w/v] Sodium chloride (NaCl)

4.1.2.6 Karlsson-Schultz (K+S) fixative for electron microscopy

25% [v/v] PFA (16% stock solution)
2.5% [v/v] Glutaraldehyde
50% [v/v] 0.2 M phosphate buffer
0,8% [w/v] Sodium chloride (NaCl)

4.1.3 Buffer for immunohistochemistry

4.1.3.1 Citrate buffer (0.01 M, pH 6.0)

1.8 mM Citric acid ($C_6H_8O_7.H_2O$)
8.2 mM Sodium citrate ($C_6H_5O_7Na_3.2H_2O$)
Always prepared freshly.

4.1.3.2 Tris buffer (pH 7.6)

50 mM Tris/HCl, pH 7.6
0.9% [w/v] Sodium chloride (NaCl)
Always prepared freshly.

4.1.3.3 Tris buffered milk

50 mM Tris/HCL pH 7.6
2% [w/v] milk powder
0.9% [w/v] Sodium chloride (NaCl)
Stirred for 20 min and filtered before use.

4.1.3.4 TE buffer

10 mM Tris/HCL pH 9.0
1 mM ethylenediaminetetraacetic acid (EDTA, $C_{10}H_{16}N_2O_8$)

4.1.3.5 30% Sucrose

30% [w/v] Sucrose
70% [v/v] 1x PBS pH 7.2

4.1.3.6 BSA/PBS

0.04 M Sodium di-hydrogen phosphate (NaH_2PO_4)
0.16 M di-Sodium hydrogen phosphate (Na_2HPO_4)
1.8% [w/v] Sodium chloride (NaCl)
1.0% [w/v] Bovines serum albumin (BSA)

4.1.4 Molecular biochemistry

4.1.4.1 Sucrose buffer

320 mM Sucrose
10 mM Tris-HCl pH 7.4
1 mM Sodium hydrogen carbonate ($NaHCO_3$)
1 mM Magnesium chloride ($MgCl_2$)
1 tablet of proteinase and phosphatase inhibitors were added to 10 ml of sucrose buffer.

4.1.4.2 Running buffer

25 mM TrisBase
192 mM Glycine
1% [w/v] Sodium deoxycholate (SDS)

4.1.4.3 Transfer buffer

48 mM TrisBase
39 mM Glycine
10 % [v/v] Methanol

4.1.4.4 Tris buffered saline with Tween20 (TBST)

50 mM Tris-HCl (pH 7.4)
150 mM Sodium chloride (NaCl)
0.05 % [v/v] Tween20

4.1.4.5 4x loading dye

40 % [w/v] Glycine
240 mM Tris-HCl pH 6.8
8 % [w/v] Sodium deoxycholate (SDS)
0.04% [w/v] Bromphenole blue

4.1.4.6 SDS separation gel

10-16% [v/v] Acrylamide / Bisacrylamide 29:1
0.4 M Tris-HCl pH 8.8
0.1% [w/v] Sodium deoxycholate (SDS)
0.03% [v/v] Ammonium persulfate
0.08% [v/v] TEMED

4.1.4.7 SDS stacking gel

4% [v/v] Acrylamide / Bisacrylamide 29:1
125 mM Tris-HCl pH 6.8
0.1% [w/v] Sodium deoxycholate (SDS)
0.05% [w/v] Ammonium persulfate
0.1% [w/v] TEMED

4.1.4.8 Lysis Buffer for proteomics

7 M urea
2 M thiourea
10 mM DTT
2% CHAPS
0.1 M Tris pH 8.5

4.1.4.9 Wash Buffer for proteomics

8 M urea
10 mM DTT,
0.1 M Tris pH 8.5

4.1.5 Solutions for electron microscopy

4.1.5.1 Epon (Epoxy resin)

171.3 g Glycidether 100
115 g DDSA (Dodecenyl succinic anhydride)
89 g MNA (Methyl nadic anhydride)
Mixed for 10 min before 6.5 ml DMP-30 was added.
Mixed again for 20 min

4.1.5.2 Formvar solution

1.25% [w/v] Formvar
50 ml Chloroform
Mixed for 30 min and stored protected from light at RT.

4.1.5.3 Reynolds lead citrate solutions

1.33 g Lead nitrate (N_2O_6Pb)
1.76 g Sodium citrate ($Na_3C_6H_5O_7$)
Solved in 30 ml ddH_2O while shaking. After 30 min 8 ml of 1 M NaOH was added to adjust the pH to 12. ddH_2O was added to 50 ml. Solution was sterile filtered before use.

4.1.5.4 Uranyl acetate

4% [w/v] Uranyl acetate
Filtered before use.

4.1.6 qRT-PCR Primers

Primer for qRT-PCR were synthetized by the AGCT-laboratory of the Max-Planck Institute of Experimental Medicine

Acaca (Acc1)	for:	5'-GGATGTGGATGATGGTCTGA-3'
	rev:	5'-GGCCTTGATCATCACTGGAT-3'
Acacb (Acc2)	for:	5'-CACGAGATTGCTTTCCTAGGTC-3'
	rev:	5'-GGTGGAGGCGATCTTGTC-3'
Bdnf	for:	5'-GCATCTGTTGGGGAGACAAG-3'
	rev:	5‘-TGGTCATCACTCTTCTCACCTG-3‘
Fasn	for:	5'-GTCCACCCCAAGCAGGCACA-3'

	rev:	5'-ACTCACACCCACCCAGACGC-3'
Hk1	for:	5'-GTGGACGGGACGCTCTAC-3'
	rev:	5'-TTCACTGTTTGGTGCATGATT-3'
Mbp	for:	5'-CCTCAGAGGACAGTGATGTGTTT-3'
	rev:	5'-AGCCGAGGTCCCATTGTT-3'
Mog	for:	5'-GTTGACCCAATAGAAGGGATCTT-3'
	rev:	5'-CTTCTTCAGAGACCACTCTTACCA-3'
Mlycd (Mcd)	for:	5'-TGGTCAAGGAGCTGCAGAA-3'
	rev:	5'-TAGGCGACAGGCTTGAAAAG-3'
Rplp0	for:	5'-GATGCCCAGGGAAGACAG-3'
	rev:	5'-ACAATGAAGCATTTTGGATAATCA-3'
Rps13	for:	5'-CGAAAGCACCTTGAGAGGAA-3'
	rev:	5'-TTCCAATTAGGTGGGAGCAC-3'
Slc2a1 (Glut1)	for:	5'-GACCCTGCACCTCATTGG-3'
	rev:	5'-GACCCTGCACCTCATTGG-3'
Slc16a1 (Mct1)	for:	5'-ATGCTGCCCTGTCCTCCT-3'
	rev:	5'-CCACAAGCCCAGTACGTGTAT-3'
Slc16a3 (Mct4)	for:	5'-TTGTGGGTGGCCTCTTTG-3'
	rev:	5'-TGAGAGCCAGACCCAAGC-3'
Slc16a7 (Mct2)	for:	5'-TCGTGGAGTGTTGTCCAGTT-3'
	rev:	5'-TCCAGTTATATCAAGCAATTTACCA-3'

4.1.7 Antibodies

Primary antibodies

Antigen	**Host**	**Application**	**Vendor**
ACAT1	Polyclonal rabbit	WB 1:5000	Proteintech
Actin	Monoclonal Mouse	WB 1:2500	Millipore
CNP	Monoclonal Mouse	Cryo IHC: 1:5000	Atlas Antibodies
BDH1	Polyclonal rabbit	WB 1:500	Proteintech
GLUT1	Polyclonal rabbit	WB 1:5000	Custom made
Isolectin IB4		Cryo IHC 1:50	Vector Lab
MBP	Polyclonal rabbit	Paraffin IHC 1:200	Custom made
MCT1	Polyclonal rabbit	WB 1:1000 Paraffin IHC 1:100	Custom made
NeuN	Monoclonal Mouse	Cryo IHC 1:100	Chemicon
S100ß	Polyclonal rabbit	Paraffin IHC 1:200	Abcam

SCOT	Polyclonal rabbit	WB 1: 1000; Cryo IHC 1:200	Proteintech

Secondary antibodies

Antigen	**Host**	**Application**	**Vendor**
α-rabbit-HRP	Goat	WB 1:5000	Dianova
α-mouse-HRP	Goat	WB 1:5000	Dianova
α-mouse-Alexa 488, 555	Donkey	IHC 1:1000	Invitrogen
α-rabbit-Alexa 488, 555	Donkey	IHC 1:1000	Invitrogen

4.2 Methods

4.2.1 Animals

All experiments were performed in accordance with the animal policies of the Max Planck Institute of Experimental Medicine (MPI-EM) and approved by the German Federal State of Lower Saxony. Mice used in this study were bred and kept at the animal facility of the MPI-EM at a 12/12 light-dark cycle. 5 male C57/N mice were housed together with *ad libitum* access to food and water. Maternal production of milk can be impaired by feeding ketogenic diets (Sussman et al., 2013). To achieve normal lactogenesis of damns while rearing mice solely on ketogenic diet, food separation for damns and pups was implemented. At the age of P10 of pups, a second shelf was installed into the cage with liquefied standard chow (65% ssniff V1124 and 35% ssniff E15712-10) for damns. At P14, ketogenic (KD, ssniff E15249-30) or normal chow (SD, ssniff V1124) for control animals was administrated in boxes with small holes making it only accessible for pups. Mice were weaned at P17 and kept on the respective diet. Measurement of blood glucose, ketone bodies and bodyweight were performed between 10-12 a.m. Blood were taken from tail tip and measured using the Freestyle Precision System with respective strips for glucose or ß-hydroxybutyrate (Abbott Diabetes Care, Wiesbaden, Germany). Mice were sacrificed by cervical dislocation or perfusion after anesthesia with Avertin.

4.2.2 Protein biochemistry

4.2.2.1 Tissue extraction for protein and RNA isolation

Tissue was snap frozen on dry ice and stored at -80°C until further processing. Frozen cortices were homogenized in 600 µl sucrose buffer using the Ultraturrax (T8, Ika, Staufen, Germany) at maximum speed for 30 sec. For RNA isolation 100 µl lysate were mixed with 600 µl RLT and stored at -20°C. For protein biochemical analysis detergents were added to a final concentration of 2% lithium dodecylsulfate (LDS), 1% TritonX-100 and 1% sodium deoxycholate. Samples were stored at -80°C for until further processing.

4.2.2.2 Determination of protein concentration

Protein concentration was determined using the Bio-Rad DC™ Protein Assay kit (Bio-Rad Laboratories GmbH, Munich, Germany) according to manufacturer's instructions. The principle is based on the well-established Lowry assay. Optical density for each sample was measured in triplicates at 650 nm using an Eon microplate spectrophotometer (BioTek Instruments GmbH, Bad Friedrichshall, Germany). A BSA

standard curve with known protein concentration (0-3µg/µl) was used to calculate sample concentration accordingly. Protein samples were adjusted to equal amounts in 1x SDS loading buffer containing 5% ß-mercaptoethanol and stored at -20°C.

4.2.2.3 Separation of Proteins by SDS-PAGE

Homogenates were denaturated for 10 min at 40°C on a shaker. Freshly prepared SDS-polyacrylamide gels (10-16%) were loaded with 1-10µg of total protein lysate corresponding to respective protein size and antibody conditions. 5 µl PageRuler^{TM} Plus Prestained Protein ladder (ThermoFischer) was used as marker. Protein separation was achieved according the protocol established by Laemmli (Laemmli, 1970) using the Bio-Rad system and power supply. Proteins were separated according to their size for 1h at 200V. Gels were stored in 1x transfer buffer until further processing.

4.2.2.4 Immunoblot

Proteins were transferred to methanol activated polyvinylidene difluoride (PVDF) membranes (Hybond P, biosciences) according to Towbin and colleagues (1979) using the Invitrogen semi-dry chamber (Karlsruhe, Germany). Membranes were activated for 1 min in 100% methanol, washed with ddH_2O and stored in 1x transfer buffer. Four Whatman papers incubated in transfer buffer were put onto the anode plate. The activated PVDF membrane was layered on top, followed by the gel and four additional Whatmann papers. Proteins were transferred for 40 min at 20 V.

For transfer of hydrophobic proteins (MCT1, GLUT1) wet-chamber immunoblotting (Invitrogen) was used. Therefore, three sponges soaked in 1x transfer buffer were put into the wet-chamber followed by two Whatman papers, the activated PVDF membrane and the gel. On top, two Whatman papers and three sponges were layered. The wet-chamber was closed and filled with 1x transfer buffer. Gels were blotted for 1 h at 38 V. Subsequently, membranes were blocked in TBS-T with 5% milk powder. Primary antibody incubation was carried out over night at 4°C while rotating. To avoid staining of unbound primary antibody, membranes were washed three times for 5 min in TBS-T. HRP-conjugated secondary antibody incubation was carried out at RT for 45 min. Membranes were washed again three times in TBS-T for 5 min before signal detection. For protein detection, the Western Lightning Plus-ECL-Kit (Perkin Elmer Life Sciences) was used. 1 ml of the reagent was applied to the membranes for 1 min for chemiluminescence detection with the Intas ChemoCam Imager for 1-15 min. Membranes were controlled for equal protein loading by detection of actin as loading control. Signals were analyzed with ImageJ Software and normalized to the loading

control. Values were displayed as histograms and p-values were calculated using the Student's t-test.

4.2.3 RNA isolation and analysis

4.2.3.1 RNA isolation

To isolate RNA from cortex the RNeasy Mini Prep kit (Quiagen, Hilden, Germany) was used following manaufacturer's instructions. Homogenized tissue was added with one volume (700 µl) 70% ethanol and vortexed vigorously. One volume was pipetted onto RNeasy Mini Spin columns and centrifuged for 1 min at 13.000 rpm. Flow through was discarded and the second volume was processed as described above. 700 µl RW1 buffer was added onto the column and centrifuged for 1 min at 13.000 rpm. After discarding the flow through and collection tube 500 µl RPE buffer was added and centrifuged for 1 min at 13.000 rpm. This step was repeated before drying the columns by centrifugation for 2 min at 13.000 rpm. To elute the RNA 30 µl of RNA grade H_2O was pipetted directly onto the column membrane and centrifuged for 1 min at 13.000 rpm. This step was repeated afterwards and eluted RNA was stored at -80°C.

4.2.3.2 RNA concentration measurement and quality control

To determine the quality and concentration of samples, RNA was measured using the Agilent RNA 6000 Nano Kit together with the Agilent 2100 Bioanalyzer (Agilent, Santa Clara, United States) following manufacturer's instructions. Samples with a RNA integrity number of 8.5 or higher were used for further synthesis of cDNA.

4.2.3.3 cDNA synthesis

For analysis of RNA expression profiles, isolated RNA from cortex samples was converted to a single strand of complementary DNA (cDNA). Based on a reverse transcription reaction, cDNA was synthesized by RNA dependent DNA polymerase SuperScript III (Invitrogen, Karlsruhe, Germany). In a first step a RNA-primer mix was prepared using:

4 µl RNA (500-1000 ng)
1 µl dT Primer mix (0.6 pmol/µl)
1µl N9 (random nonamers 120 pmol/µl)
This mix was incubated for 2 min at 70°C to denaturate RNA and primers and stored on ice while preparing the second premix containing:

2 µl 5x first strand buffer
0.5 µl dNTP (10 mM)
1 µl DTT (100 mM)
1 µl SuperScript III reverse transcriptase (200 U/µl)

The final reaction mixture of 10.5 µl was centrifuged and incubated in a thermocycler with the following protocol:

25°C 10 min
50°C 45 min
55°C 45 min

Synthesized cDNA was diluted with ddH_2O to a final concentration of 5 ng/µl.

4.2.3.4 Quantitative real time polymerase chain reaction (qRT-PCR)

qRT-PCR was carried out using the SybrGreen Mix (Promega, Mannheim, Germany) on the Light Cycler 480 II (Roche, Mannheim, Germany). Primer were selected using the Universal Probe Library (https://liefescience.roche.com) and checked against unspecific off- targets by using the NCBI Primer-blast tool (https://www.ncbi.nlm.nih.gov/tools/primer-blast/). For the PCR reaction the following reaction mix was prepared (in three technical replicates):

2 µl cDNA
5 µl SybrGreen
0.4 µl forward primer (10 pM)
0.4 µl reverse primer (10 pM)
2.2 µl ddH_2O

The PCR reaction was performed using the following temperature conditions:

50°C 2 min
95°C 10 min
45x cycle: 95°C 15 sec
60°C 1 min

Raw data were analyzed using the Light Cycler® software 1.5.0SP4 and cycle thresholds (CT) values were calculated from the technical replicates. To account for differences in

cDNA input, CT values were normalized to the geometric mean of the housekeeping genes Rplp0 (60s acidic ribosomal protein P) and Rps13 (Ribosomal protein s13) and analyzed by the ΔΔCT method (Pfaffl, 2004). Results were displayed as histograms normalized to levels of SD fed animals that were set to 1 using GraphPad Prism6. P-value quantification was performed using the Student's t-test.

4.2.4 Immunohistochemistry

4.2.4.1 Perfusion and tissue fixation

Mice were deeply anesthetized by intraperitoneal injection of avertin (0.2 ml/10 g of body weight). Successful anesthesia was confirmed by paw pinch test. To expose the heart, the abdomen was opened and the diaphragm was removed. A butterfly cannula (27G, Venofix) of a peristaltic pump was injected intracardial and the right atrium was opened. The blood was flushed out with PBS until the liver was decolorized. For cryo-sectioning the brain was postfixed over night in 4% PFA. To fixate the tissue for paraffin embedding 4% PFA was used for 10 min at a pump rate of 1.5 ml/min (K+S for ultrastructural analysis, respectively). Tissue was dissected and stored over night at 4°C in the respective fixative.

4.2.4.2 Immunohistochemistry of paraffin embedded tissue

After fixation of tissue with 4% PFA, brains were embedded in paraffin (Paraplast, Leica, Wetzlar, Germany) with an automated embedding system (HMP 110, MICROM) using the following program steps:

Procedure	Time
50% Ethanol	1 h
70% Ethanol	2x 2 h
96% Ethanol	2x 2 h
100% Ethanol	2x 2 h
Isopropanol	1 h
Xylol	2x 2 h
Paraffin	2x 2 h

Samples were arranged in metal forms and embedded with 60°C warm paraffin to cast blocks using the MICROM AP 280 Embedding station. Paraffin blocks were stored at RT and 5 µm thick sections were cut using the MICROM HM 400 microtome. Sections were

mounted on slides and dried over night at 37°C. Prior to staining, sections were deparaffinized by the following steps:

Procedure	Time
60°C	10 min
Xylol	2x 10 min
Xylol/Isopropanol (1:1)	10 min
100% Ethanol	5 min
90% Ethanol	5 min
70% Ethanol	5 min
50% Ethanol	5 min
ddH_2O	5 min

4.2.5 Immunolabeling of paraffin embedded tissue

For fluorescent labeling of paraffin embedded tissue, deparaffinized sections were incubated in citrate buffer (pH 6) for 5 min at RT followed by cooking in the same for 10 min using a microwave (650 W) for antigen retrieval. Sections were allowed to cool down to RT for about 20 min and washed with Tris buffer containing 2% milk powder for 5 min. Samples were transferred to a chamber filled with wet tissue paper to avoid a dry out. To prevent unspecific labeling of the primary antibody, sections were blocked for 30 min with 20% goat serum in PBS/BSA at RT. Primary antibodies were diluted according to their final concentration in PBS/BSA and sections were incubated over night at 4°C. After subsequent washing steps with Tris buffer containing 2% milk, samples were incubated for 60 min at RT with the corresponding fluorescently labeled secondary antibody. As a general nuclear counterstain, DAPI was added to the secondary antibody dilution. Sections were washed with Tris buffer (without milk) and then mounted with Aquapolymount.

4.2.5.1 Fluorescent labeling of cryosections.

After postfixation of tissue in 4% PFA overnight, sagittal cut hemispheres were transferred into 30% Sucrose for 3 days for cryoprotection. Tissue was embedded in Tissue-Tek® (O.C.T.™ Compound, Sakura) and frozen on dry ice. 14 µm thick sections were cut using a Cryotome (Leica CM 1950, Leica, Wetzlar, Germany), mounted on slides and stored at -80°C until further use. Prior to staining sections were dried for 30 min at 37°C and washed twice with PBS. Permeabilization was performed in 0.4% Triton (in PBS) for 30 min at RT. To avoid unspecific staining, sections were blocked for

additional 30 min in 4% horse serum, 0.2% Triton in PBS. Primary antibodies were diluted according to their final concentration in 1% horse serum, 0.05% Triton in PBS. Sections were incubated with primary antibodies over two days. After primary antibody incubation, slides were washed twice with PBS. Secondary antibodies were diluted according to their final concentration in 1.5% horse serum in PBS containing DAPI (1:20000) and slides were incubated for 2 hours at RT. Prior to mounting slides with Aqua-poly-mount, slides were washed twice with PBS.

4.2.5.2 Confocal microscopy of fluorescently labeled cryosections

Confocal laser scanning microscopy was performed using a Leica SP8X FALCON equipped with a 63x/1.3 HC PL APO glycerol objective controlled by using the LASX software (Leica Microsystems). Pictures were taken randomly from layer V-VI of the cortex above the rostral corpus callosum with a 5.45x magnification. Signal detection was performed sequentially to avoid cross bleeding of different filter sets. Noise detection was reduced by 2x line averaging. Pictures were taken as z-stack with spatial z-resolution of 190 nm. Deconvolution was achieved during picture processing using the LIGHTNING package of the LASX software. Pictures were displayed as maximum-intensity projection and equally adapted for brightness and contrast using FIJI.

4.2.6 Electron microscopy

4.2.6.1 Tissue embedding

K+S fixed tissue was placed into small plastic chambers filled with 0.1 M phosphate buffer, before embedding for subsequent EM imaging. An automated system (EMTP, Leica, Wetzlar, Germany) was used. Chambers were placed into the machine and samples were processed using the following protocol:

Procedure	Time
Phosphate buffer	3x 10 min
2% OsO_4	4 h
ddH_2O	3x 10 min
30% Ethanol	20 min
50% Ethanol	20 min
70% Ethanol	20 min
90% Ethanol	20 min
100% Ethanol	4x 10 min
Propylenoxid	3x 10 min

Propylenoxid/Epon 2:1	2 h
Propylenoxid/Epon 1:1	2 h
Propylenoxid/Epon 1:2	4 h
Epon	4 h

Afterwards samples were then placed into Epon filled molds and incubated over night at 60°C for polymerization.

4.2.6.2 Sectioning of Epon embedded tissue

For electron microscopic analysis of cortex myelination, epon embedded cortex samples were trimmed 450 µm (step size 1 µm) on a microtome (Ultracut S, Leica, Wetzlar, Germany) using a diamond knife (Diatome Ultra 45°) starting from the pia mater to achieve the same sample region of interest. Ultra-thin sections (50 nm) were cut with a Diatome Ultra 35° and collected on formvar polyvinyl-coated copper grids. Sections were contrasted with 2% uranylacetate for 30 min followed by 1% lead citrate solution for 12 min. After several washing steps with ddH_2O, grids were dried with a filter paper.

4.2.6.3 Electron microscopic analysis

Ultra-thin sections were analyzed with a Zeiss EM900 electron microscope (Zeiss, Oberkochen, Germany) equipped with a wide-angle dual speed 2K-CCD-Camera (TRS, Moorenweis, Germany). Per sample 10 pictures at a magnification of 7500x were taken. G-ratio measurements and quantification of axon caliber distribution were performed using the grid tool (2x2 µm) from ImageJ according to the hit-to-point method. Student's t-test was performed using GraphPad Prism6 and results were displayed with Adobe Ilustrator CS6.

4.2.7 Metabolite Profiling

Due to its rapid dynamics the metabolome is very difficult to measure (Jove et al., 2014) and postmortem degradation of metabolites frequently occurs (Sugiura et al., 2014). To overcome these difficulties, tissue extraction needed to be timed exactly and microwave irradiation was used to keep postmortem degradation to a minimum. Therefore, mice were sacrificed by cervical dislocation and decapitated. After exactly 12 s the head was transferred into a microwave (Biowave Pro, Pelco, Garching Germany) and exposed to microwave irradiation at 750 W for 16 s. The brain was extracted and transferred on ice. The cortex was dissected using a sagittal brain matrix. Tissue was snap frozen on dry ice exactly after 10 min and stored at –80°C until further processing.

Metabolomic analysis was performed in collaboration with Dr. Till Ischebeck from the department of Plant Biochemstry at the University of Göttingen. Both the metabolites and sterols were measured from the same samples by gas-chromatographic-mass spectrometry GC/MS after extraction and derivatization as described by (Rotsch et al., 2017). In brief, prior to extraction, tissue was lyophilized and dry weight was measured. .Cortices were ground to a fine powder using a beatmill (Retsch, Haan, Germany) and glass beads (5 mm, Carl Roth, Karlsruhe Germany) and extracted with 500 µl methanol:chloroform:water 129:50:25 [v/v/v]. Phase separation was induced by addition of the internal standard (250 µl 5 µg/ml *allo*-inositol in water). For the analysis of small metabolites, 100-200 µl of the upper aqueous phase was evaporated and metabolites were transformed into their methoxyimino (MEOX)- and trimethylsilyl (TMS)- derivatives by incubating overnight after addition of 15 µl methoxyamine hydrochloride and for 2-10 h after addition of 30 µl N-metyl-N-(trimethylsilyl) trifluoroacetamide (MSTFA). 1 µl of sample were injected per run. Each sample was analyzed with a longer a split of 1:10 to 1:50 on an Agilent 5977N mass selective detector connected to an Agilent 7890B gas chromatograph equipped with a capillary HP5-MS column (30 m x 0.25 mm, 0.25 µm coating thickness, Agilent Technologies). The inlet temperature was set to 280°C and a temperature gradient was applied (50°C for 2 min, 50 – 330°C at 5 K/min, 330°C for 2 min). A transfer line of 330°C was used. Spectra recording was performed in the range of *m/z* = 71-600. GC/MS data were analyzed using the Agilent MSD ChemStation data analysis software (Agilent Technologies). In case that derivatization of metabolites led to several ion peaks of interest, abundance of the total ion count (TIC) of the individual analytes was added. The abundance of identified metabolites was normalized to the internal standard and to the dry weight of the sample.

Sterols were extracted from the organic phase by adding 800 µl of MTBE:MeOH (v/v) and 200 µl of 0.9 % NaCl and 40 µl 17:0 fatty acid (0.25 mg/ml in chloroform). Each sample was measured twice. One time, 10 µl of the organic phase was used and run later with a 1:50 split to measure cholesterol. The second time, 50 µl of the organic phase was used and run later with a 1:10 split to measure other sterols. All samples were dried by N_2 stream and re-dissolved in 15 µl pyridine. 30 µl of MSTFA was added followed by an incubation time of 2-10 h. Sterols were measured by GC/MS using the same set-up as described for small metabolites except for the temperature gradient, which was run at 180°C for 1 min, 180 – 320°C at 5 K/min, 320°C for 5 min. The abundance of sterols was compared based on their TIC. Statistical evaluation was performed in R with the DESeq2 package (Love et al., 2014) to account for multiple testing (performed by Ting Sun, MPI for experimental Medicine, Göttingen)

4.2.8 Open field test

The open field test was performed as previously described (Babaev et al., 2016). Briefly, exploratory activity in a novel environment was tested in a gray arena (50x50 cm, surrounded by a wall of 50 cm height) at 20 lux light intensity. Individual animals were placed into one corner of periphery of the open field and allowed to explore it for 10 min. The exploratory behavior of the mouse was recorded using an overhead camera system and scored automatically using the Viewer software (Biobserve, St. Augustin, Germany). The overall traveled distance was analyzed as a parameter of general activity. Time, distance and visits in the center area was analyzed to measure anxiety behavior. Results were displayed as histograms and two-way ANOVA with Sidak's post test was used for statistical significance using GraphPad Prims6

4.2.9 Audiobox

Audiobox experiments were done in collaboration with Dr. Livia de Hoz from the neurogenetics department of the MPI-EM.

To assess learning ability of ketogenic fed mice, sound frequency discrimination was carried out in an Audiobox (TSE, Germany), based on an established protocol(Cruces-Solis et al., 2018). Briefly, a sterile transponder (ISO compliant 11784 transponder, 12 mm long, TSE, Germany) was implanted subcutaneously in the back of the isoflurane anaesthetized mice. The injection wound was closed using topical skin adhesive (Histoacryl, Braun, USA). This enables individual identification of mice and the behavior (nose-poking, licking) of each mouse can be detected. The Audiobox consists of the living area, where food can be accessed *ad libitum* and the Audiobox itself were water is supplied and frequency discrimination is performed. Both parts were connected through a corridor. Entrance into the Audiobox (visit) was detected by an antenna that reads the implanted transponder and a temperature sensor. The mouse can access water by nose-poking into one of the two ports, which can be opened or closed according to the demand of the experiment. For the presentation of different sounds, a loudspeaker was positioned behind the Audiobox. Sounds were generated using Matlab (Mathworks). During the whole experiment one frequency (6.67kHz) was considered "safe": if this frequency was presented during a visit, mice could drink without negative result. The "conditioned frequency" (13.34 kHz) was associated with an air-puff if a mouse nose-poked to get access to water. Therefore, mice had to learn to avoid nose-poking during a "conditioned visit". During the habituation phase only the safe sound was presented. On day 1-2 ports were open and mice were drinking freely. The ports were closed on day 3-5 and only opened after the mouse nose-poked into the port. At day 6-9 (conditioning phase) the

conditioned sound was presented in a small percentage of visits: 5% (day 6-7) or 10% (day 8-9). Nose-poking during a visit with the conditioned frequency resulted in the delivery of an air-puff and no opening of the water ports.

4.2.10 Serum protein identification

Identification of serum proteins was performed in collaboration with Dr. Olaf Jahn from the proteome facility of the MPI-EM according to (Ott et al., 2015). Briefly, gel electrophoresis for MS protein identification was performed on precast TG PRiME Tris/glycine 10% gels (Serva) according to manufacturer's instructions (Invitrogen). Proteins were visualized using colloidal Coomassie staining. Gel bands of interest were excised manually and subjected to automated in-gel digestion with trypsin. Nanoscale reversed-phase UPLC separation of tryptic peptides was performed with a nanoAcquity UPLC system equipped with a Symmetry C18 trap column (5 µm, 180 µm x 20 mm) and a BEH C18 analytical column (1.7 µm, 75µm x 100mm) (Waters Corporation). Peptides were separated at a flow rate of of 300 nl/min with a linear gradient of 1% to 45% mobile phase B (acetonitrile containing 0.1% formic acid) while mobile phase A was water containing 0.1% formic acid for 45 min. Mass spectrometric analysis of tryptic peptides was performed as described below.

4.2.11 Cell isolation from adult mouse brain

Cells were isolated according to the Adult Brain Dissociation protocol (Miltenyi Biotec GmbH, Bergisch Gladbach, Germany) with minor modifications. In brief, brains were dissected and meninges removed with Whatman paper. For isolation of oligodendrocytes, astrocytes or endothelial cells, one single cortex per sample was isolated using a brain matrix, sliced in small pieces and stored in a round bottom tube with appropriate amount of enzyme mix 1 on ice. For isolation of neurons two cortices per sample were used. As not stated otherwise every step was performed on ice and centrifugation steps were performed at 300xg for 10 min at 4°C. After adding enzyme mix 2, tubes were incubated in a 37°C water bath for 30 min. Tissue were homogenized by gentle titruation during incubation. For subsequent steps DPBS without Mg^{2+} and Ca^{2+} were used as washing buffer. Cell suspension was passed through a 70 µm strainer, washed with 10 ml DPBS and centrifuged. Supernatant was discarded and the cell pellet was resuspended in 2 ml DPBS + 600 µl Debri Removal Solution. 1.4 ml DPBS were layered on top of the cell suspension prior to centrifugation at 3000xg for 10 min at 4°C with full acceleration/brake. The two top phases were discarded and the 15 ml Falcon tube were filled up with DPBS to 11 ml containing the remaining cell solution followed by

centrifugation at 1200xg for 10 min. Supernatant was discarded and cell pellet incubated in 1x Red blood cell removal solution. After 10 min 5 ml DPBS were added and the cell solution centrifuged. For magnetic cell labeling supernatant was discarded and cells resuspended in appropriate amount of DPBS according to the respective antibody Microbead kit protocol. Oligodendrocytes were labeled with 2.5 µl anti-O4 Microbeads for 15 min in 97.5 µl DPBS. Astrocytes were labeled with 10 µl anti-ACSAII Microbeads for 15 min after resuspending in 80 µl DPBS and incubation with 10 µl FcR-Blocking Reagent for 10 min. Endothelial cells were resuspended in 90 µl DPBS and labeled with 10 µl anti-CD11b Microbeads for 15 min. To remove residual Microbeads 1 ml DPBS was added followed by centrifugation. Supernatant was discarded and labeled cells resuspended in 0.5 ml DPBS. MS Columns were attached to the Octomacs magnet and equilibrated with 0.5 ml DPBS. Labeled cells were pipetted onto the MS Columns and washed 3x with DPBS. Flow through was collected for further isolation of cell types. After washing, MS Columns were detached and cells eluted in 0.5 ml of respective Buffer or pelleted and stored at -80°C.

Negative selection using the Neuron isolation kit was performed to isolate neuronal cells. Cells were resuspended in 200 µl DPBS and incubated with 20 µl Non-Neuronal Cell-Biotin-Antibody Cocktail for 5 min. Cells were washed with 1 ml DPBS and centrifuged for 10 min at 300xg. After aspiration of supernatant, cells were resuspended in 200 µl DPBS and incubated with 20 µl Anti-Biotin Microbeads with additional 5 µl anti-O4 Microbeads for 10 min. DPBS was added to 1 ml, cell solution was splitted and pipetted on two equilibrated MS Columns. Columns were washed three times with 0.5 ml DPBS. Flow through was collected and again pipetted on two MS Columns with repeated washing steps. Flow through was centrifuged for 2 min at 13000 rpm at 4°C to pellet isolated neurons. After aspiration of supernatant neurons were stored at -80°C.

4.2.11.1 Proteome analysis of isolated cells

Proteome analysis was performed in collaboration with Dr. Olaf Jahn and Lars Piepkorn from the proteome facility of the MPI-EM.

4.2.11.1.1 Proteolytic digestion

Isolated cell fractions from adult mouse cortex were dissolved in lysis buffer and processed according to a filter-aided sample preparation (FASP) protocol previously described (Ambrozkiewicz et al., 2018; Distler et al., 2014; Distler et al., 2016). If not mentioned otherwise, all steps were automated on a liquid-handling workstation equipped with a vacuum manifold (Freedom EVO 150, Tecan) using an in-house

constructed adaptor device. In brief, samples were lysed and reduced by shaking for 30 min at 37°C and loaded on centrifugal filter units (30 kDa MWCO, Millipore). Detergents were removed by washing twice with wash buffer. Using 50 mM iodoacetamide in 8 M urea/0.1 M Tris pH 8.5 for 20 min at RT, proteins were alkylated. Excess reagent was removed by washing twice in wash buffer. Exchange of buffer was achieved by three times washing with 50 mM ammonium bicarbonate (ABC) containing 10% acetonitrile. Quantitative removal of liquids was ensured by centrifugation during three additional washing steps with 50 mM ABC/10% acetonitrile. Proteins were digested overnight at 37°C with 500 ng trypsin in 40 µl of the same buffer. Recovering of tryptic peptides was performed by centrifugation followed by two additional extraction steps with 40 µl of 50 mM ABC and 40 µl of 1% trifluoroacetic acid (TFA), respectively. For quantification purposes, aliquots of the combined flow-throughs were spiked with 10 fmol/µl Hi3 EColi standard (Waters Corporation) (Silva et al., 2006). Aliquots were analyzed by liquid chromatography coupled to electrospray mass spectrometry (LC-MS).

4.2.11.1.2 LC-MS analysis

Nanoscale reverse-phase UPLC separation of tryptic peptides was performed according to (Ambrozkiewicz et al., 2018) using an nanoAcquity UPLC system equipped with a Symmetry C18 5 µm, 180 µm × 20 mm trap column and a HSS T3 C18 1.8 µm, 75 µm × 250 mm analytical column maintained at 45 °C (Waters Corporation). Peptides were injected and trapped for 4 min at a flow rate of 8 µl/min 0.1 % TFA. Separation was performed at a flow rate of 300 nl/min for 180 min using a gradient comprised of two linear steps. Water containing 0.1% formic acid was increased in 165 min from 3-35% and acetonitrile containing 0.1% formic acid from 35-60% in the remaining 15 min.

MS analysis of tryptic peptides was performed using a Synapt G2-S quadrupole time-of-flight mass spectrometer equipped with ion mobility option (Waters Corporation) enabling acquisition of positive ions in a mass range of m/z 50 to 2000 at a minimum resolution of 20000 FWHM (full width at half maximum). Analysis was performed as described by Distler et al. (2014; 2016). Continuum LC-MS data processing was achieved using Waters ProteinLynx Global Server (PLGS) version 3.0.2 (Li et al., 2009). Protein identification was performed using the UniProtKB/Swiss-Prot mouse proteome to which the sequence information for E. coli. Chaperone protein ClpB and porcine trypsin was added. Appending the reversed entry sequence enabled determination of false discovery rate (FDR). Precursor and fragment ion mass tolerances were automatically determined by PLGS 3.0.2. Carbamidomethylation of cysteine was set to fixed whereas oxidation of methionine was assumed as variable modification. One missed trypsin cleavage was allowed and minimal ion matching requirements was: two fragments/peptide, five

fragments/protein, one peptide/protein. Threshold of FDR protein identification was set to 1%.

4.2.11.1.3 Experimental design and data analysis

Experimental design and data analysis: Cell fractions from four cortices of standard and ketogenic diet fed mice at six weeks of age were used (two cortices/cell fraction for neuron isolation). Samples were processed with replicate digestion and injection, which resulted in two technical replicates per biological replicate (16 LC-MS runs in total per cell fraction). ISOQuant (http://www.isoquant.net) that is a freely available software was used for post-identification analysis based on the TOP3 quantification approach (Distler et al., 2014; Distler et al., 2016; Kuharev et al., 2015). Peptides had to have at least seven amino acids with a score above or equal to 5.5 to be considered. FDR threshold for peptides and proteins was set to 1% and only proteins with at least two peptides were quantified. The parts per million (ppm) abundance values were log2-transformed and normalized by subtraction of the median from all data points for the respective protein. Moderated t-statistics with an empirical Bayes approach including a FDR-based correction for multiple comparisons were used to detect significant changes in protein abundance (Kammers et al., 2015). Therefore, the Bioconductor packages “limma” (Ritchie et al., 2015) and “q-value” (Storey & Tibshirani, 2003) were used in RStudio.

4.2.11.2 Transcriptomics

Transcriptome analysis of isolated cells was performed in collaboration with Prof. Dr. Moritz Rossner and Nirmal Kannaiyan from the department of Psychiatry at the LMU Munich.

4.2.11.2.1 Library Preparation

Sequencing was performed with 4-5 biological replicates for each condition. RNA was extracted with the Qiagen Micro-Rneasy Kit (Qiagen, Cat. No. 74004) according to the manufacturer’s protocol. As external control, 1 µl of ERCC RNA Spike-In Mix (ThermoFisher, Cat No. 4456740) diluted at 1:5000 was added to the isolated RNA. cDNA was synthesised with the Ovation RNA-Seq system v2 (NuGEN, Cat. No.7102). As input, 100 ng of cDNA was used for library preparation using the IonXpress plus gDNA and Amplicon library preparation kit (Thermofischer,cat no: 4471269). To achieve size selection of the library, a 2% E-Gel was used and the samples were barcoded and subsequently amplified. Further quantification for each sample library was performed

using the Kapa Library Quantification Kit (Kapa, Cat. No. KK4827). Of each sample, equal amounts were sequenced on an Ion Torrent Sequencer.

4.2.11.2.2 Transcriptome Data analysis

Based on the barcodes, the raw reads (Fastq) were split into sample specific reads and subsequently checked for sequence quality and sequence repeats. Low quality bases and short reads were trimmed or excluded from further analysis. The reads were mapped to *Mus musculus* genome (mm10) using TMAP Aligner and quantified using Ensembl annotation 86 using Partek Flow software. Genes had to have at least 5 reads in at least 80% of the samples to be considered for further analysis. Differentially expressed genes (DEGs) were determined in R with the DESeq2 package (Love et al., 2014). Genes with at least 0.5 fold change and adjusted pValue of less than or equal to 0.05 were considered as differentially expressed.

4.2.11.2.3 Pathway analysis

For analysis of relevant pathway enrichment in proteomic datasets the functional annotation tool DAVID was used (https://david.ncifcrf.gov/home.jsp) (Huang da et al., 2009a, 2009b). All identified proteins of each cell fraction were uploaded as background to achieve more reliable p-value results. For each cell fraction significantly up or downregulated proteins were analysed differently. The threshold for target proteins were set manually for each cell fraction (Astrocytes: ≤ -1.0 log2FC; ≥ 0.5 log2FC, q-value ≤ 0.0005; Oligodendrocytes: ≤ -0.25 log2FC; ≥ 0.25 log2FC, q-value ≤ 0.05; Endothelial cells: ≤ -0.25 log2FC; ≥ 0.25 log2FC, q-value ≤ 0.05; Neurons: ≤ -0.5 log2FC; ≥ 0.5 log2FC, q-value ≤ 0.05). Analysis was performed based on KEGG and GO_BP direct terms. Only distinct pathways with a minimum count of 5 proteins and a p-value ≤ 0.05 were considered for further analysis. For transcriptomic data the pre-defined affymetrix background from DAVID was used and the threshold for genes were set to ≤ -0.5log2FC; ≥ 0.5 log2FC, padj-value ≤ 0.05. The remaining procedure was unaltered.
Pathways were displayed either as heatmap depicting log_2 fold changes of individual sample values of involved proteins or were visualized using VANTED version 2.6.5 (Rohn et al., 2012) with log_2 fold changes of individual sample values.

References

Abbott, N. J., Patabendige, A. A., Dolman, D. E., Yusof, S. R., & Begley, D. J. (2010). Structure and function of the blood-brain barrier. *Neurobiol Dis, 37*(1), 13-25. doi:10.1016/j.nbd.2009.07.030

Abdelwahab, M. G., Fenton, K. E., Preul, M. C., Rho, J. M., Lynch, A., Stafford, P., & Scheck, A. C. (2012). The ketogenic diet is an effective adjuvant to radiation therapy for the treatment of malignant glioma. *PLoS One, 7*(5), e36197. doi:10.1371/journal.pone.0036197

Amaral, A. I., Hadera, M. G., Tavares, J. M., Kotter, M. R., & Sonnewald, U. (2016). Characterization of glucose-related metabolic pathways in differentiated rat oligodendrocyte lineage cells. *Glia, 64*(1), 21-34. doi:10.1002/glia.22900

Ambrozkiewicz, M. C., Schwark, M., Kishimoto-Suga, M., Borisova, E., Hori, K., Salazar-Lazaro, A., Rusanova, A., Altas, B., Piepkorn, L., Bessa, P., Schaub, T., Zhang, X., Rabe, T., Ripamonti, S., Rosario, M., Akiyama, H., Jahn, O., Kobayashi, T., Hoshino, M., Tarabykin, V., & Kawabe, H. (2018). Polarity Acquisition in Cortical Neurons Is Driven by Synergistic Action of Sox9-Regulated Wwp1 and Wwp2 E3 Ubiquitin Ligases and Intronic miR-140. *Neuron, 100*(5), 1097-1115 e1015. doi:10.1016/j.neuron.2018.10.008

Araque, A., Parpura, V., Sanzgiri, R. P., & Haydon, P. G. (1998). Glutamate-dependent astrocyte modulation of synaptic transmission between cultured hippocampal neurons. *Eur J Neurosci, 10*(6), 2129-2142.

Awan, M. M., & Saggerson, E. D. (1993). Malonyl-CoA metabolism in cardiac myocytes and its relevance to the control of fatty acid oxidation. *Biochem J, 295 (Pt 1)*, 61-66.

Babaev, O., Botta, P., Meyer, E., Muller, C., Ehrenreich, H., Brose, N., Luthi, A., & Krueger-Burg, D. (2016). Neuroligin 2 deletion alters inhibitory synapse function and anxiety-associated neuronal activation in the amygdala. *Neuropharmacology, 100*, 56-65. doi:10.1016/j.neuropharm.2015.06.016

Bailey, Pfeifer, H. H., & Thiele, E. A. (2005). The use of diet in the treatment of epilepsy. *Epilepsy Behav, 6*(1), 4-8. doi:10.1016/j.yebeh.2004.10.006

Bailey, E., & Lockwood, E. A. (1971). Formation and utilization of ketone bodies during development of the male rat. *Biochem J, 124*(2), 7P-8P.

Barnham, K. J., Masters, C. L., & Bush, A. I. (2004). Neurodegenerative diseases and oxidative stress. *Nat Rev Drug Discov, 3*(3), 205-214. doi:10.1038/nrd1330

Batiuk, M. Y., de Vin, F., Duque, S. I., Li, C., Saito, T., Saido, T., Fiers, M., Belgard, T. G., & Holt, M. G. (2017). An immunoaffinity-based method for isolating ultrapure adult astrocytes based on ATP1B2 targeting by the ACSA-2 antibody. *J Biol Chem, 292*(21), 8874-8891. doi:10.1074/jbc.M116.765313

Baumann, N., & Pham-Dinh, D. (2001). Biology of oligodendrocyte and myelin in the mammalian central nervous system. *Physiol Rev, 81*(2), 871-927. doi:10.1152/physrev.2001.81.2.871

Bergersen, L., Wærhaug, O., Helm, J., Thomas, M., Laake, P., Davies, A. J., Wilson, M. C., Halestrap, A. P., & Ottersen, O. P. (2001). A novel postsynaptic density protein: the monocarboxylate transporter MCT2 is co-localized with δ-glutamate receptors in postsynaptic densities of parallel fiber-Purkinje cell synapses. *Experimental Brain Research, 136*(4), 523-534. doi:10.1007/s002210000600

Bergqvist, A. G. (2012). Long-term monitoring of the ketogenic diet: Do's and Don'ts. *Epilepsy Res, 100*(3), 261-266. doi:10.1016/j.eplepsyres.2011.05.020

Bergstrom, J. D., Wong, G. A., Edwards, P. A., & Edmond, J. (1984). The regulation of acetoacetyl-CoA synthetase activity by modulators of cholesterol synthesis in vivo and the utilization of acetoacetate for cholesterogenesis. *J Biol Chem, 259*(23), 14548-14553.

References

Berl, S., Karram, K., Scheller, A., Jungblut, M., Kirchhoff, F., & Waisman, A. (2017). Enrichment and isolation of neurons from adult mouse brain for ex vivo analysis. *J Neurosci Methods, 283*, 15-22. doi:10.1016/j.jneumeth.2017.03.015

Bernatchez, P. N., Sharma, A., Kodaman, P., & Sessa, W. C. (2009). Myoferlin is critical for endocytosis in endothelial cells. *Am J Physiol Cell Physiol, 297*(3), C484-492. doi:10.1152/ajpcell.00498.2008

Biffiger, K., Bartsch, S., Montag, D., Aguzzi, A., Schachner, M., & Bartsch, U. (2000). Severe hypomyelination of the murine CNS in the absence of myelin-associated glycoprotein and fyn tyrosine kinase. *J Neurosci, 20*(19), 7430-7437.

Blanc, L., & Vidal, M. (2018). New insights into the function of Rab GTPases in the context of exosomal secretion. *Small GTPases, 9*(1-2), 95-106. doi:10.1080/21541248.2016.1264352

Booth, R. F., Patel, T. B., & Clark, J. B. (1980). The development of enzymes of energy metabolism in the brain of a precocial (guinea pig) and non-precocial (rat) species. *J Neurochem, 34*(1), 17-25.

Brown, A. M., & Ransom, B. R. (2007). Astrocyte glycogen and brain energy metabolism. *Glia, 55*(12), 1263-1271. doi:10.1002/glia.20557

Cahill, G. F., Jr. (2006). Fuel metabolism in starvation. *Annu Rev Nutr, 26*, 1-22. doi:10.1146/annurev.nutr.26.061505.111258

Cahoy, J. D., Emery, B., Kaushal, A., Foo, L. C., Zamanian, J. L., Christopherson, K. S., Xing, Y., Lubischer, J. L., Krieg, P. A., Krupenko, S. A., Thompson, W. J., & Barres, B. A. (2008). A transcriptome database for astrocytes, neurons, and oligodendrocytes: a new resource for understanding brain development and function. *J Neurosci, 28*(1), 264-278. doi:10.1523/JNEUROSCI.4178-07.2008

Cancilla, P. A., Baker, R. N., Pollock, P. S., & Frommes, S. P. (1972). The reaction of pericytes of the central nervous system to exogenous protein. *Lab Invest, 26*(4), 376-383.

Cataldo, A. M., & Broadwell, R. D. (1986). Cytochemical identification of cerebral glycogen and glucose-6-phosphatase activity under normal and experimental conditions. II. Choroid plexus and ependymal epithelia, endothelia and pericytes. *J Neurocytol, 15*(4), 511-524.

Chechik, T., Roeder, L. M., Tildon, J. T., & Poduslo, S. E. (1987). Ketone body enzyme activities in purified neurons, astrocytes and oligodendroglia. *Neurochem Int, 10*(1), 95-99.

Chowdhury, G. M., Jiang, L., Rothman, D. L., & Behar, K. L. (2014). The contribution of ketone bodies to basal and activity-dependent neuronal oxidation in vivo. *J Cereb Blood Flow Metab, 34*(7), 1233-1242. doi:10.1038/jcbfm.2014.77

Clanton, R. M., Wu, G., Akabani, G., & Aramayo, R. (2017). Control of seizures by ketogenic diet-induced modulation of metabolic pathways. *Amino Acids, 49*(1), 1-20. doi:10.1007/s00726-016-2336-7

Colello, R. J., Devey, L. R., Imperato, E., & Pott, U. (1995). The chronology of oligodendrocyte differentiation in the rat optic nerve: evidence for a signaling step initiating myelination in the CNS. *J Neurosci, 15*(11), 7665-7672.

Cotter, D. G., d'Avignon, D. A., Wentz, A. E., Weber, M. L., & Crawford, P. A. (2011). Obligate role for ketone body oxidation in neonatal metabolic homeostasis. *J Biol Chem, 286*(9), 6902-6910. doi:10.1074/jbc.M110.192369

Cotter, D. G., Schugar, R. C., Wentz, A. E., d'Avignon, D. A., & Crawford, P. A. (2013). Successful adaptation to ketosis by mice with tissue-specific deficiency of ketone body oxidation. *Am J Physiol Endocrinol Metab, 304*(4), E363-374. doi:10.1152/ajpendo.00547.2012

Cremer, J. E. (1982). Substrate utilization and brain development. *J Cereb Blood Flow Metab, 2*(4), 394-407. doi:10.1038/jcbfm.1982.45

Cruces-Solis, H., Jing, Z., Babaev, O., Rubin, J., Gur, B., Krueger-Burg, D., Strenzke, N., & de Hoz, L. (2018). Auditory midbrain coding of statistical learning that results from discontinuous sensory stimulation. *PLoS Biol, 16*(7), e2005114. doi:10.1371/journal.pbio.2005114

Cunnane, S. C., Musa, K., Ryan, M. A., Whiting, S., & Fraser, D. D. (2002). Potential role of polyunsaturates in seizure protection achieved with the ketogenic diet. *Prostaglandins Leukot Essent Fatty Acids, 67*(2-3), 131-135.

Czajka, D. M., A Dymsza, H. A., & A Miller, S. A. (1964). Influence of Artificial Diet on Weight Gain and Body Composition of the Neonatal Rat. *The Journal of Nutrition, 84*(2), 100-106.

Dagher, Z., Ruderman, N., Tornheim, K., & Ido, Y. (2001). Acute regulation of fatty acid oxidation and amp-activated protein kinase in human umbilical vein endothelial cells. *Circ Res, 88*(12), 1276-1282.

Dahlin, M., Martin, D. A., Hedlund, Z., Jonsson, M., von Dobeln, U., & Wedell, A. (2015). The ketogenic diet compensates for AGC1 deficiency and improves myelination. *Epilepsia, 56*(11), e176-181. doi:10.1111/epi.13193

Dangata, Y. Y., Findlater, G. S., & Kaufman, M. H. (1996). Postnatal development of the optic nerve in (C57BL x CBA)F1 hybrid mice: general changes in morphometric parameters. *J Anat, 189 (Pt 1)*, 117-125.

Daniel, P. M., Love, E. R., Moorhouse, S. R., & Pratt, O. E. (1977). The transport of ketone bodies into the brain of the rat (in vivo). *J Neurol Sci, 34*(1), 1-13.

De Bock, K., Georgiadou, M., Schoors, S., Kuchnio, A., Wong, B. W., Cantelmo, A. R., Quaegebeur, A., Ghesquiere, B., Cauwenberghs, S., Eelen, G., Phng, L. K., Betz, I., Tembuyser, B., Brepoels, K., Welti, J., Geudens, I., Segura, I., Cruys, B., Bifari, F., Decimo, I., Blanco, R., Wyns, S., Vangindertael, J., Rocha, S., Collins, R. T., Munck, S., Daelemans, D., Imamura, H., Devlieger, R., Rider, M., Van Veldhoven, P. P., Schuit, F., Bartrons, R., Hofkens, J., Fraisl, P., Telang, S., Deberardinis, R. J., Schoonjans, L., Vinckier, S., Chesney, J., Gerhardt, H., Dewerchin, M., & Carmeliet, P. (2013). Role of PFKFB3-driven glycolysis in vessel sprouting. *Cell, 154*(3), 651-663. doi:10.1016/j.cell.2013.06.037

de Hoz, L., Gierej, D., Lioudyno, V., Jaworski, J., Blazejczyk, M., Cruces-Solis, H., Beroun, A., Lebitko, T., Nikolaev, T., Knapska, E., Nelken, I., & Kaczmarek, L. (2018). Blocking c-Fos Expression Reveals the Role of Auditory Cortex Plasticity in Sound Frequency Discrimination Learning. *Cereb Cortex, 28*(5), 1645-1655. doi:10.1093/cercor/bhx060

de Hoz, L., & Nelken, I. (2014). Frequency tuning in the behaving mouse: different bandwidths for discrimination and generalization. *PLoS One, 9*(3), e91676. doi:10.1371/journal.pone.0091676

DeVivo, D. C., Fujimoto, K., Leckie, M. P., & Agrawal, H. C. (1976). Subcellular distribution of ketone body metabolizing enzymes in the rat brain. *J Neurochem, 26*(3), 635-637.

DeVivo, D. C., Leckie, M. P., Ferrendelli, J. S., & McDougal, D. B., Jr. (1978). Chronic ketosis and cerebral metabolism. *Ann Neurol, 3*(4), 331-337. doi:10.1002/ana.410030410

Dhopeshwarkar, G. A., & Mead, J. F. (1969). Fatty acid uptake by the brain. II. Incorporation of [I-14C] palmitic acid into the adult rat brain. *Biochim Biophys Acta, 187*(4), 461-467.

Dienel, G. A. (2012). Fueling and imaging brain activation. *ASN Neuro, 4*(5). doi:10.1042/AN20120021

Distler, U., Kuharev, J., Navarro, P., Levin, Y., Schild, H., & Tenzer, S. (2014). Drift time-specific collision energies enable deep-coverage data-independent acquisition proteomics. *Nat Methods, 11*(2), 167-170. doi:10.1038/nmeth.2767

Distler, U., Kuharev, J., Navarro, P., & Tenzer, S. (2016). Label-free quantification in ion mobility-enhanced data-independent acquisition proteomics. *Nat Protoc, 11*(4), 795-812. doi:10.1038/nprot.2016.042

Doege, H., & Stahl, A. (2006). Protein-mediated fatty acid uptake: novel insights from in vivo models. *Physiology (Bethesda), 21*, 259-268. doi:10.1152/physiol.00014.2006

Dyck, J. R., Barr, A. J., Barr, R. L., Kolattukudy, P. E., & Lopaschuk, G. D. (1998). Characterization of cardiac malonyl-CoA decarboxylase and its putative role in

regulating fatty acid oxidation. *Am J Physiol, 275*(6), H2122-2129. doi:10.1152/ajpheart.1998.275.6.H2122

Ebert, D., Haller, R. G., & Walton, M. E. (2003). Energy contribution of octanoate to intact rat brain metabolism measured by 13C nuclear magnetic resonance spectroscopy. *J Neurosci, 23*(13), 5928-5935.

Edmond, J. (1974). Ketone bodies as precursors of sterols and fatty acids in the developing rat. *J Biol Chem, 249*(1), 72-80.

Edmond, J., Higa, T. A., Korsak, R. A., Bergner, E. A., & Lee, W. N. (1998). Fatty acid transport and utilization for the developing brain. *J Neurochem, 70*(3), 1227-1234.

Edmond, J., Robbins, R. A., Bergstrom, J. D., Cole, R. A., & de Vellis, J. (1987). Capacity for substrate utilization in oxidative metabolism by neurons, astrocytes, and oligodendrocytes from developing brain in primary culture. *J Neurosci Res, 18*(4), 551-561. doi:10.1002/jnr.490180407

Eelen, G., de Zeeuw, P., Treps, L., Harjes, U., Wong, B. W., & Carmeliet, P. (2018). Endothelial Cell Metabolism. *Physiol Rev, 98*(1), 3-58. doi:10.1152/physrev.00001.2017

Erbslöh, F., Bernsmeier, A., & Hillesheim, H. (1958). Der Glucoseverbrauch des Gehirns und seine Abhängigkeit von der Leber. *Archiv für Psychiatrie und Nervenkrankheiten, 196*(6), 611-626.

Fachinger, G., Deutsch, U., & Risau, W. (1999). Functional interaction of vascular endothelial-protein-tyrosine phosphatase with the angiopoietin receptor Tie-2. *Oncogene, 18*(43), 5948-5953. doi:10.1038/sj.onc.1202992

Falk, M. J., Li, D., Gai, X., McCormick, E., Place, E., Lasorsa, F. M., Otieno, F. G., Hou, C., Kim, C. E., Abdel-Magid, N., Vazquez, L., Mentch, F. D., Chiavacci, R., Liang, J., Liu, X., Jiang, H., Giannuzzi, G., Marsh, E. D., Yiran, G., Tian, L., Palmieri, F., & Hakonarson, H. (2014). AGC1 Deficiency Causes Infantile Epilepsy, Abnormal Myelination, and Reduced N-Acetylaspartate. *JIMD Rep, 14*, 77-85. doi:10.1007/8904_2013_287

Farina, M., van de Bospoort, R., He, E., Persoon, C. M., van Weering, J. R., Broeke, J. H., Verhage, M., & Toonen, R. F. (2015). CAPS-1 promotes fusion competence of stationary dense-core vesicles in presynaptic terminals of mammalian neurons. *Elife, 4*. doi:10.7554/eLife.05438

Fedorovich, S. V., & Waseem, T. V. (2018). Metabolic regulation of synaptic activity. *Rev Neurosci, 29*(8), 825-835. doi:10.1515/revneuro-2017-0090

Forero-Quintero, L. S., Deitmer, J. W., & Becker, H. M. (2017). Reduction of epileptiform activity in ketogenic mice: The role of monocarboxylate transporters. *Sci Rep, 7*(1), 4900. doi:10.1038/s41598-017-05054-0

Fraser, D. D., Whiting, S., Andrew, R. D., Macdonald, E. A., Musa-Veloso, K., & Cunnane, S. C. (2003). Elevated polyunsaturated fatty acids in blood serum obtained from children on the ketogenic diet. *Neurology, 60*(6), 1026-1029.

Freeman, J. M., & Vining, E. P. (1999). Seizures decrease rapidly after fasting: preliminary studies of the ketogenic diet. *Arch Pediatr Adolesc Med, 153*(9), 946-949.

Funfschilling, U., Supplie, L. M., Mahad, D., Boretius, S., Saab, A. S., Edgar, J., Brinkmann, B. G., Kassmann, C. M., Tzvetanova, I. D., Mobius, W., Diaz, F., Meijer, D., Suter, U., Hamprecht, B., Sereda, M. W., Moraes, C. T., Frahm, J., Goebbels, S., & Nave, K. A. (2012). Glycolytic oligodendrocytes maintain myelin and long-term axonal integrity. *Nature, 485*(7399), 517-521. doi:10.1038/nature11007

Gaitonde, M. K., & Richter, D. (1966). Changes with age in the utilization of glucose carbon in liver and brain. *J Neurochem, 13*(12), 1309-1316.

Gano, L. B., Patel, M., & Rho, J. M. (2014). Ketogenic diets, mitochondria, and neurological diseases. *J Lipid Res, 55*(11), 2211-2228. doi:10.1194/jlr.R048975

Gerhart, D. Z., Enerson, B. E., Zhdankina, O. Y., Leino, R. L., & Drewes, L. R. (1997). Expression of monocarboxylate transporter MCT1 by brain endothelium and glia

in adult and suckling rats. *Am J Physiol, 273*(1 Pt 1), E207-213. doi:10.1152/ajpendo.1997.273.1.E207

Glatz, J. F., & van der Vusse, G. J. (1996). Cellular fatty acid-binding proteins: their function and physiological significance. *Prog Lipid Res, 35*(3), 243-282.

Gould, T. D., Dao, D., & Kovacsics, C. (2009). *Mood and anxiety related phenotypes in mice: characterization using behavioral tests* (Vol. 2): Springer.

Grabacka, M., Pierzchalska, M., Dean, M., & Reiss, K. (2016). Regulation of Ketone Body Metabolism and the Role of PPARalpha. *Int J Mol Sci, 17*(12). doi:10.3390/ijms17122093

Gusel'nikova, V. V., & Korzhevskiy, D. E. (2015). NeuN As a Neuronal Nuclear Antigen and Neuron Differentiation Marker. *Acta Naturae, 7*(2), 42-47.

Haces, M. L., Hernandez-Fonseca, K., Medina-Campos, O. N., Montiel, T., Pedraza-Chaverri, J., & Massieu, L. (2008). Antioxidant capacity contributes to protection of ketone bodies against oxidative damage induced during hypoglycemic conditions. *Exp Neurol, 211*(1), 85-96. doi:10.1016/j.expneurol.2007.12.029

Hamilton, J. A. (2007). New insights into the roles of proteins and lipids in membrane transport of fatty acids. *Prostaglandins Leukot Essent Fatty Acids, 77*(5-6), 355-361. doi:10.1016/j.plefa.2007.10.020

Hamilton, J. A., & Brunaldi, K. (2007). A Model for Fatty Acid Transport into the Brain. *Journal of Molecular Neuroscience, 33*(1), 12-17. doi:10.1007/s12031-007-0050-3

Hammelrath, L., Skokic, S., Khmelinskii, A., Hess, A., van der Knaap, N., Staring, M., Lelieveldt, B. P. F., Wiedermann, D., & Hoehn, M. (2016). Morphological maturation of the mouse brain: An in vivo MRI and histology investigation. *Neuroimage, 125*, 144-152. doi:10.1016/j.neuroimage.2015.10.009

Hawkins, R. A., Williamson, D. H., & Krebs, H. A. (1971). Ketone-body utilization by adult and suckling rat brain in vivo. *Biochem J, 122*(1), 13-18.

Heintz, N. (2004). Gene expression nervous system atlas (GENSAT). *Nat Neurosci, 7*(5), 483. doi:10.1038/nn0504-483

Henderson, S. T. (2008). Ketone bodies as a therapeutic for Alzheimer's disease. *Neurotherapeutics, 5*(3), 470-480. doi:10.1016/j.nurt.2008.05.004

Hernandez, A. R., Hernandez, C. M., Campos, K., Truckenbrod, L., Federico, Q., Moon, B., McQuail, J. A., Maurer, A. P., Bizon, J. L., & Burke, S. N. (2018). A Ketogenic Diet Improves Cognition and Has Biochemical Effects in Prefrontal Cortex That Are Dissociable From Hippocampus. *Front Aging Neurosci, 10*, 391. doi:10.3389/fnagi.2018.00391

Herrera, F., Chen, Q., Fischer, W. H., Maher, P., & Schubert, D. R. (2009). Synaptojanin-1 plays a key role in astrogliogenesis: possible relevance for Down's syndrome. *Cell Death Differ, 16*(6), 910-920. doi:10.1038/cdd.2009.24

Hindfelt, B., & Siesjo, B. K. (1970). The effect of ammonia on the energy metabolism of the rat brain. *Life Sci II, 9*(18), 1021-1028.

Hirsch, D., Stahl, A., & Lodish, H. F. (1998). A family of fatty acid transporters conserved from mycobacterium to man. *Proc Natl Acad Sci U S A, 95*(15), 8625-8629.

Hnasko, T. S., & Edwards, R. H. (2012). Neurotransmitter corelease: mechanism and physiological role. *Annu Rev Physiol, 74*, 225-243. doi:10.1146/annurev-physiol-020911-153315

Ho, P. W., Ho, J. W., Liu, H. F., So, D. H., Tse, Z. H., Chan, K. H., Ramsden, D. B., & Ho, S. L. (2012). Mitochondrial neuronal uncoupling proteins: a target for potential disease-modification in Parkinson's disease. *Transl Neurodegener, 1*(1), 3. doi:10.1186/2047-9158-1-3

Holt, L. M., & Olsen, M. L. (2016). Novel Applications of Magnetic Cell Sorting to Analyze Cell-Type Specific Gene and Protein Expression in the Central Nervous System. *PLoS One, 11*(2), e0150290. doi:10.1371/journal.pone.0150290

Homayoun, P., & Bourre, J. M. (1987). Ketone body utilization for energy production and lipid synthesis in isolated rat brain capillaries. *Biochim Biophys Acta, 922*(3), 345-350.

Howarth, C., Gleeson, P., & Attwell, D. (2012). Updated energy budgets for neural computation in the neocortex and cerebellum. *J Cereb Blood Flow Metab, 32*(7), 1222-1232. doi:10.1038/jcbfm.2012.35

Huang da, W., Sherman, B. T., & Lempicki, R. A. (2009a). Bioinformatics enrichment tools: paths toward the comprehensive functional analysis of large gene lists. *Nucleic Acids Res, 37*(1), 1-13. doi:10.1093/nar/gkn923

Huang da, W., Sherman, B. T., & Lempicki, R. A. (2009b). Systematic and integrative analysis of large gene lists using DAVID bioinformatics resources. *Nat Protoc, 4*(1), 44-57. doi:10.1038/nprot.2008.211

Hutagalung, A. H., & Novick, P. J. (2011). Role of Rab GTPases in membrane traffic and cell physiology. *Physiol Rev, 91*(1), 119-149. doi:10.1152/physrev.00059.2009

Huttenlocher, P. R. (1976). Ketonemia and seizures: metabolic and anticonvulsant effects of two ketogenic diets in childhood epilepsy. *Pediatr Res, 10*(5), 536-540. doi:10.1203/00006450-197605000-00006

Jahn, R., & Sudhof, T. C. (1994). Synaptic vesicles and exocytosis. *Annu Rev Neurosci, 17*, 219-246. doi:10.1146/annurev.ne.17.030194.001251

Jiang, L., Mason, G. F., Rothman, D. L., de Graaf, R. A., & Behar, K. L. (2011). Cortical substrate oxidation during hyperketonemia in the fasted anesthetized rat in vivo. *J Cereb Blood Flow Metab, 31*(12), 2313-2323. doi:10.1038/jcbfm.2011.91

Jove, M., Portero-Otin, M., Naudi, A., Ferrer, I., & Pamplona, R. (2014). Metabolomics of human brain aging and age-related neurodegenerative diseases. *J Neuropathol Exp Neurol, 73*(7), 640-657. doi:10.1097/NEN.0000000000000091

Juge, N., Gray, J. A., Omote, H., Miyaji, T., Inoue, T., Hara, C., Uneyama, H., Edwards, R. H., Nicoll, R. A., & Moriyama, Y. (2010). Metabolic control of vesicular glutamate transport and release. *Neuron, 68*(1), 99-112. doi:10.1016/j.neuron.2010.09.002

Kacem, K., Lacombe, P., Seylaz, J., & Bonvento, G. (1998). Structural organization of the perivascular astrocyte endfeet and their relationship with the endothelial glucose transporter: a confocal microscopy study. *Glia, 23*(1), 1-10.

Kalucka, J., Bierhansl, L., Conchinha, N. V., Missiaen, R., Elia, I., Bruning, U., Scheinok, S., Treps, L., Cantelmo, A. R., Dubois, C., de Zeeuw, P., Goveia, J., Zecchin, A., Taverna, F., Morales-Rodriguez, F., Brajic, A., Conradi, L. C., Schoors, S., Harjes, U., Vriens, K., Pilz, G. A., Chen, R., Cubbon, R., Thienpont, B., Cruys, B., Wong, B. W., Ghesquiere, B., Dewerchin, M., De Bock, K., Sagaert, X., Jessberger, S., Jones, E. A. V., Gallez, B., Lambrechts, D., Mazzone, M., Eelen, G., Li, X., Fendt, S. M., & Carmeliet, P. (2018). Quiescent Endothelial Cells Upregulate Fatty Acid beta-Oxidation for Vasculoprotection via Redox Homeostasis. *Cell Metab, 28*(6), 881-894 e813. doi:10.1016/j.cmet.2018.07.016

Kamasawa, N., Sik, A., Morita, M., Yasumura, T., Davidson, K. G., Nagy, J. I., & Rash, J. E. (2005). Connexin-47 and connexin-32 in gap junctions of oligodendrocyte somata, myelin sheaths, paranodal loops and Schmidt-Lanterman incisures: implications for ionic homeostasis and potassium siphoning. *Neuroscience, 136*(1), 65-86. doi:10.1016/j.neuroscience.2005.08.027

Kammers, K., Cole, R. N., Tiengwe, C., & Ruczinski, I. (2015). Detecting Significant Changes in Protein Abundance. *EuPA Open Proteom, 7*, 11-19. doi:10.1016/j.euprot.2015.02.002

Kennedy, A. R., Pissios, P., Otu, H., Roberson, R., Xue, B., Asakura, K., Furukawa, N., Marino, F. E., Liu, F. F., Kahn, B. B., Libermann, T. A., & Maratos-Flier, E. (2007). A high-fat, ketogenic diet induces a unique metabolic state in mice. *Am J Physiol Endocrinol Metab, 292*(6), E1724-1739. doi:10.1152/ajpendo.00717.2006

Kettenmann, H., & Ransom, B. R. (2005). The concept of neuroglia: a historical perspective *Neuroglia*: Oxford University Press.

Kim, D. Y., Vallejo, J., & Rho, J. M. (2010). Ketones prevent synaptic dysfunction induced by mitochondrial respiratory complex inhibitors. *J Neurochem, 114*(1), 130-141. doi:10.1111/j.1471-4159.2010.06728.x

Kirk, P., Wilson, M. C., Heddle, C., Brown, M. H., Barclay, A. N., & Halestrap, A. P. (2000). CD147 is tightly associated with lactate transporters MCT1 and MCT4 and facilitates their cell surface expression. *EMBO J, 19*(15), 3896-3904. doi:10.1093/emboj/19.15.3896

Klepper, J., Engelbrecht, V., Scheffer, H., van der Knaap, M. S., & Fiedler, A. (2007). GLUT1 deficiency with delayed myelination responding to ketogenic diet. *Pediatr Neurol, 37*(2), 130-133. doi:10.1016/j.pediatrneurol.2007.03.009

Koper, J. W., Lopes-Cardozo, M., & Van Golde, L. M. (1981). Preferential utilization of ketone bodies for the synthesis of myelin cholesterol in vivo. *Biochim Biophys Acta, 666*(3), 411-417.

Koppel, S. J., & Swerdlow, R. H. (2018). Neuroketotherapeutics: A modern review of a century-old therapy. *Neurochem Int, 117*, 114-125. doi:10.1016/j.neuint.2017.05.019

Kossoff, E. H., & Rho, J. M. (2009). Ketogenic diets: evidence for short- and long-term efficacy. *Neurotherapeutics, 6*(2), 406-414. doi:10.1016/j.nurt.2009.01.005

Kramer-Albers, E. M., Bretz, N., Tenzer, S., Winterstein, C., Mobius, W., Berger, H., Nave, K. A., Schild, H., & Trotter, J. (2007). Oligodendrocytes secrete exosomes containing major myelin and stress-protective proteins: Trophic support for axons? *Proteomics Clin Appl, 1*(11), 1446-1461. doi:10.1002/prca.200700522

Krebs, H., Williamson, D., Bates, M. W., Page, M. A., & Hawkins, R. (1971). The role of ketone bodies in caloric homeostasis. *Advances in Enzyme Regulation, 9*, 387-409.

Krutzfeldt, A., Spahr, R., Mertens, S., Siegmund, B., & Piper, H. M. (1990). Metabolism of exogenous substrates by coronary endothelial cells in culture. *J Mol Cell Cardiol, 22*(12), 1393-1404.

Kuharev, J., Navarro, P., Distler, U., Jahn, O., & Tenzer, S. (2015). In-depth evaluation of software tools for data-independent acquisition based label-free quantification. *Proteomics, 15*(18), 3140-3151. doi:10.1002/pmic.201400396

Laemmli, U. K. (1970). Cleavage of structural proteins during the assembly of the head of bacteriophage T4. *Nature, 227*(5259), 680-685.

Lappe-Siefke, C., Goebbels, S., Gravel, M., Nicksch, E., Lee, J., Braun, P. E., Griffiths, I. R., & Nave, K. A. (2003). Disruption of Cnp1 uncouples oligodendroglial functions in axonal support and myelination. *Nat Genet, 33*(3), 366-374. doi:10.1038/ng1095

Larson, V. A., Mironova, Y., Vanderpool, K. G., Waisman, A., Rash, J. E., Agarwal, A., & Bergles, D. E. (2018). Oligodendrocytes control potassium accumulation in white matter and seizure susceptibility. *Elife, 7*. doi:10.7554/eLife.34829

Lehninger, A. L., Sudduth, H. C., & Wise, J. B. (1960). D-beta-Hydroxybutyric dehydrogenase of muitochondria. *J Biol Chem, 235*, 2450-2455.

Leino, R. L., Gerhart, D. Z., & Drewes, L. R. (1999). Monocarboxylate transporter (MCT1) abundance in brains of suckling and adult rats: a quantitative electron microscopic immunogold study. *Brain Res Dev Brain Res, 113*(1-2), 47-54.

Leino, R. L., Gerhart, D. Z., Duelli, R., Enerson, B. E., & Drewes, L. R. (2001). Diet-induced ketosis increases monocarboxylate transporter (MCT1) levels in rat brain. *Neurochem Int, 38*(6), 519-527.

Lennox, W. G., & Cobb, S. (1928). EPILEPSY: FROM THE STANDPOINT OF PHYSIOLOGY AND TREATMENT. *Medicine, 7*(2), 105-290.

Leong, S. F., & Clark, J. B. (1984). Regional enzyme development in rat brain. Enzymes of energy metabolism. *Biochem J, 218*(1), 139-145.

Li, G. Z., Vissers, J. P., Silva, J. C., Golick, D., Gorenstein, M. V., & Geromanos, S. J. (2009). Database searching and accounting of multiplexed precursor and product ion spectra from the data independent analysis of simple and complex peptide mixtures. *Proteomics, 9*(6), 1696-1719. doi:10.1002/pmic.200800564

Lim, S., Chesser, A. S., Grima, J. C., Rappold, P. M., Blum, D., Przedborski, S., & Tieu, K. (2011). D-beta-hydroxybutyrate is protective in mouse models of Huntington's disease. *PLoS One, 6*(9), e24620. doi:10.1371/journal.pone.0024620

Lopaschuk, G. D., Ussher, J. R., Folmes, C. D., Jaswal, J. S., & Stanley, W. C. (2010). Myocardial fatty acid metabolism in health and disease. *Physiol Rev, 90*(1), 207-258. doi:10.1152/physrev.00015.2009

Lopes-Cardozo, M., & Klein, W. (1985). Contribution of acetoacetate to the synthesis of cholesterol and fatty acids in regions of developing rat brain in vivo. *Neurochem Int, 7*(4), 647-653.

Love, M. I., Huber, W., & Anders, S. (2014). Moderated estimation of fold change and dispersion for RNA-seq data with DESeq2. *Genome Biol, 15*(12), 550. doi:10.1186/s13059-014-0550-8

Lundgaard, I., Li, B., Xie, L., Kang, H., Sanggaard, S., Haswell, J. D., Sun, W., Goldman, S., Blekot, S., Nielsen, M., Takano, T., Deane, R., & Nedergaard, M. (2015). Direct neuronal glucose uptake heralds activity-dependent increases in cerebral metabolism. *Nat Commun, 6*, 6807. doi:10.1038/ncomms7807

Lutas, A., & Yellen, G. (2013). The ketogenic diet: metabolic influences on brain excitability and epilepsy. *Trends Neurosci, 36*(1), 32-40. doi:10.1016/j.tins.2012.11.005

Ma, W., Berg, J., & Yellen, G. (2007). Ketogenic diet metabolites reduce firing in central neurons by opening K(ATP) channels. *J Neurosci, 27*(14), 3618-3625. doi:10.1523/JNEUROSCI.0132-07.2007

Maalouf, M., Rho, J. M., & Mattson, M. P. (2009). The neuroprotective properties of calorie restriction, the ketogenic diet, and ketone bodies. *Brain Res Rev, 59*(2), 293-315. doi:10.1016/j.brainresrev.2008.09.002

Mahley, R. W., Innerarity, T. L., Rall, S. C., Jr., & Weisgraber, K. H. (1984). Plasma lipoproteins: apolipoprotein structure and function. *J Lipid Res, 25*(12), 1277-1294.

Maisonpierre, P. C., Belluscio, L., Friedman, B., Alderson, R. F., Wiegand, S. J., Furth, M. E., Lindsay, R. M., & Yancopoulos, G. D. (1990). NT-3, BDNF, and NGF in the developing rat nervous system: parallel as well as reciprocal patterns of expression. *Neuron, 5*(4), 501-509.

Mark, J., Godin, Y., & Mandel, P. (1968). Glucose and lactic acid content of the rat brain. *J Neurochem, 15*(2), 141-143.

Masino, S. A., Kawamura, M., Jr., Ruskin, D. N., Geiger, J. D., & Boison, D. (2012). Purines and neuronal excitability: links to the ketogenic diet. *Epilepsy Res, 100*(3), 229-238. doi:10.1016/j.eplepsyres.2011.07.014

Masino, S. A., Li, T., Theofilas, P., Sandau, U. S., Ruskin, D. N., Fredholm, B. B., Geiger, J. D., Aronica, E., & Boison, D. (2011). A ketogenic diet suppresses seizures in mice through adenosine A(1) receptors. *J Clin Invest, 121*(7), 2679-2683. doi:10.1172/JCI57813

Masino, S. A., & Rho, J. M. (2018). Metabolism and epilepsy: Ketogenic diets as a homeostatic link. *Brain Res*. doi:10.1016/j.brainres.2018.05.049

Maurer, G. D., Brucker, D. P., Bahr, O., Harter, P. N., Hattingen, E., Walenta, S., Mueller-Klieser, W., Steinbach, J. P., & Rieger, J. (2011). Differential utilization of ketone bodies by neurons and glioma cell lines: a rationale for ketogenic diet as experimental glioma therapy. *BMC Cancer, 11*, 315. doi:10.1186/1471-2407-11-315

McGarry, J. D., & Brown, N. F. (1997). The mitochondrial carnitine palmitoyltransferase system. From concept to molecular analysis. *Eur J Biochem, 244*(1), 1-14.

Melo, T. M., Nehlig, A., & Sonnewald, U. (2006). Neuronal-glial interactions in rats fed a ketogenic diet. *Neurochem Int, 48*(6-7), 498-507. doi:10.1016/j.neuint.2005.12.037

Menichella, D. M., Majdan, M., Awatramani, R., Goodenough, D. A., Sirkowski, E., Scherer, S. S., & Paul, D. L. (2006). Genetic and physiological evidence that oligodendrocyte gap junctions contribute to spatial buffering of potassium released during neuronal activity. *J Neurosci, 26*(43), 10984-10991. doi:10.1523/JNEUROSCI.0304-06.2006

Mergenthaler, P., Lindauer, U., Dienel, G. A., & Meisel, A. (2013). Sugar for the brain: the role of glucose in physiological and pathological brain function. *Trends Neurosci, 36*(10), 587-597. doi:10.1016/j.tins.2013.07.001

Merienne, N., Meunier, C., Schneider, A., Seguin, J., Nair, S. S., Rocher, A. B., Le Gras, S., Keime, C., Faull, R., Pellerin, L., Chatton, J. Y., Neri, C., Merienne, K., & Deglon, N. (2019). Cell-Type-Specific Gene Expression Profiling in Adult Mouse Brain Reveals Normal and Disease-State Signatures. *Cell Rep, 26*(9), 2477-2493 e2479. doi:10.1016/j.celrep.2019.02.003

Miclet, E., Stoven, V., Michels, P. A., Opperdoes, F. R., Lallemand, J. Y., & Duffieux, F. (2001). NMR spectroscopic analysis of the first two steps of the pentose-phosphate pathway elucidates the role of 6-phosphogluconolactonase. *J Biol Chem, 276*(37), 34840-34846. doi:10.1074/jbc.M105174200

Mitchell, R. W., Edmundson, C. L., Miller, D. W., & Hatch, G. M. (2009). On the mechanism of oleate transport across human brain microvessel endothelial cells. *J Neurochem, 110*(3), 1049-1057. doi:10.1111/j.1471-4159.2009.06199.x

Mitchell, R. W., & Hatch, G. M. (2011). Fatty acid transport into the brain: of fatty acid fables and lipid tails. *Prostaglandins Leukot Essent Fatty Acids, 85*(5), 293-302. doi:10.1016/j.plefa.2011.04.007

Mitchell, R. W., On, N. H., Del Bigio, M. R., Miller, D. W., & Hatch, G. M. (2011). Fatty acid transport protein expression in human brain and potential role in fatty acid transport across human brain microvessel endothelial cells. *J Neurochem, 117*(4), 735-746. doi:10.1111/j.1471-4159.2011.07245.x

Moore, T. J., Lione, A. P., Regen, D. M., Tarpley, H. L., & Raines, P. L. (1971). Brain glucose metabolism in the newborn rat. *Am J Physiol, 221*(6), 1746-1753. doi:10.1152/ajplegacy.1971.221.6.1746

Morris, A. A. (2005). Cerebral ketone body metabolism. *J Inherit Metab Dis, 28*(2), 109-121. doi:10.1007/s10545-005-5518-0

Nave, K. A., & Werner, H. B. (2014). Myelination of the nervous system: mechanisms and functions. *Annu Rev Cell Dev Biol, 30*, 503-533. doi:10.1146/annurev-cellbio-100913-013101

Neal, E. G., Chaffe, H., Schwartz, R. H., Lawson, M. S., Edwards, N., Fitzsimmons, G., Whitney, A., & Cross, J. H. (2008). The ketogenic diet for the treatment of childhood epilepsy: a randomised controlled trial. *The Lancet Neurology, 7*(6), 500-506. doi:10.1016/s1474-4422(08)70092-9

Nehlig, A. (1999). Age-dependent pathways of brain energy metabolism: the suckling rat, a natural model of the ketogenic diet. *Epilepsy Res, 37*(3), 211-221.

Nehlig, A. (2004). Brain uptake and metabolism of ketone bodies in animal models. *Prostaglandins Leukot Essent Fatty Acids, 70*(3), 265-275. doi:10.1016/j.plefa.2003.07.006

Nehlig, A., & Pereira de Vasconcelos, A. (1993). Glucose and ketone body utilization by the brain of neonatal rats. *Prog Neurobiol, 40*(2), 163-221.

Newington, J. T., Harris, R. A., & Cumming, R. C. (2013). Reevaluating Metabolism in Alzheimer's Disease from the Perspective of the Astrocyte-Neuron Lactate Shuttle Model. *J Neurodegener Dis, 2013*, 234572. doi:10.1155/2013/234572

Noh, H. S., Lee, H. P., Kim, D. W., Kang, S. S., Cho, G. J., Rho, J. M., & Choi, W. S. (2004). A cDNA microarray analysis of gene expression profiles in rat hippocampus following a ketogenic diet. *Brain Res Mol Brain Res, 129*(1-2), 80-87. doi:10.1016/j.molbrainres.2004.06.020

Norton, W. T., & Poduslo, S. E. (1973). Myelination in rat brain: changes in myelin composition during brain maturation. *J Neurochem, 21*(4), 759-773.

Orii, K. E., Fukao, T., Song, X. Q., Mitchell, G. A., & Kondo, N. (2008). Liver-specific silencing of the human gene encoding succinyl-CoA: 3-ketoacid CoA transferase. *Tohoku J Exp Med, 215*(3), 227-236.

Ott, C., Martens, H., Hassouna, I., Oliveira, B., Erck, C., Zafeiriou, M. P., Peteri, U. K., Hesse, D., Gerhart, S., Altas, B., Kolbow, T., Stadler, H., Kawabe, H., Zimmermann, W. H., Nave, K. A., Schulz-Schaeffer, W., Jahn, O., & Ehrenreich,

H. (2015). Widespread Expression of Erythropoietin Receptor in Brain and Its Induction by Injury. *Mol Med, 21*(1), 803-815. doi:10.2119/molmed.2015.00192

Ouellet, M., Emond, V., Chen, C. T., Julien, C., Bourasset, F., Oddo, S., LaFerla, F., Bazinet, R. P., & Calon, F. (2009). Diffusion of docosahexaenoic and eicosapentaenoic acids through the blood-brain barrier: An in situ cerebral perfusion study. *Neurochem Int, 55*(7), 476-482. doi:10.1016/j.neuint.2009.04.018

Owen, O. E. (2005). Ketone bodies as a fuel for the brain during starvation. *Biochemistry and Molecular Biology Education, 33*(4), 246-251. doi:10.1002/bmb.2005.49403304246

Page, M. A., Krebs, H. A., & Williamson, D. H. (1971). Activities of enzymes of ketone-body utilization in brain and other tissues of suckling rats. *Biochem J, 121*(1), 49-53.

Park, Y., & Ryu, J. K. (2018). Models of synaptotagmin-1 to trigger Ca(2+) -dependent vesicle fusion. *FEBS Lett, 592*(21), 3480-3492. doi:10.1002/1873-3468.13193

Pellerin, L., & Magistretti, P. J. (1994). Glutamate uptake into astrocytes stimulates aerobic glycolysis: a mechanism coupling neuronal activity to glucose utilization. *Proc Natl Acad Sci U S A, 91*(22), 10625-10629.

Pellerin, L., Pellegri, G., Martin, J. L., & Magistretti, P. J. (1998). Expression of monocarboxylate transporter mRNAs in mouse brain: support for a distinct role of lactate as an energy substrate for the neonatal vs. adult brain. *Proc Natl Acad Sci U S A, 95*(7), 3990-3995.

Pfaffl, M. W. (2004). Quantification strategies in real-time PCR. *AZ of quantitative PCR, 1*, 89-113.

Phillips, C. M., Goumidi, L., Bertrais, S., Field, M. R., Cupples, L. A., Ordovas, J. M., McMonagle, J., Defoort, C., Lovegrove, J. A., Drevon, C. A., Blaak, E. E., Kiec-Wilk, B., Riserus, U., Lopez-Miranda, J., McManus, R., Hercberg, S., Lairon, D., Planells, R., & Roche, H. M. (2010). ACC2 gene polymorphisms, metabolic syndrome, and gene-nutrient interactions with dietary fat. *J Lipid Res, 51*(12), 3500-3507. doi:10.1194/jlr.M008474

Poduslo, S. E. (1989). Induction of ketone body enzymes in glial cells. *Arch Biochem Biophys, 272*(2), 318-322.

Puchalska, P., & Crawford, P. A. (2017). Multi-dimensional Roles of Ketone Bodies in Fuel Metabolism, Signaling, and Therapeutics. *Cell Metab, 25*(2), 262-284. doi:10.1016/j.cmet.2016.12.022

Purves, D., Augustine, G. J., Fitzpatrick, D., Hall, W., LaMantia, A., McNamara, J., & White, L. (2004). Neuroscience Sinauer Associates. *Inc., USA*.

Ransohoff, R. M., & Cardona, A. E. (2010). The myeloid cells of the central nervous system parenchyma. *Nature, 468*(7321), 253-262. doi:10.1038/nature09615

Remahl, S., & Hildebrand, C. (1982). Changing relation between onset of myelination and axon diameter range in developing feline white matter. *Journal of the neurological sciences, 54*(1), 33-45.

Renkonen, R., Paavonen, T., Nortamo, P., & Gahmberg, C. G. (1992). Expression of endothelial adhesion molecules in vivo. Increased endothelial ICAM-2 expression in lymphoid malignancies. *Am J Pathol, 140*(4), 763-767.

Ritchie, M. E., Phipson, B., Wu, D., Hu, Y., Law, C. W., Shi, W., & Smyth, G. K. (2015). limma powers differential expression analyses for RNA-sequencing and microarray studies. *Nucleic Acids Res, 43*(7), e47. doi:10.1093/nar/gkv007

Rogawski, M. A., Loscher, W., & Rho, J. M. (2016). Mechanisms of Action of Antiseizure Drugs and the Ketogenic Diet. *Cold Spring Harb Perspect Med, 6*(5). doi:10.1101/cshperspect.a022780

Rohn, H., Junker, A., Hartmann, A., Grafahrend-Belau, E., Treutler, H., Klapperstuck, M., Czauderna, T., Klukas, C., & Schreiber, F. (2012). VANTED v2: a framework for systems biology applications. *BMC Syst Biol, 6*, 139. doi:10.1186/1752-0509-6-139

Romano, A., Koczwara, J. B., Gallelli, C. A., Vergara, D., Micioni Di Bonaventura, M. V., Gaetani, S., & Giudetti, A. M. (2017). Fats for thoughts: An update on brain fatty acid metabolism. *Int J Biochem Cell Biol, 84*, 40-45. doi:10.1016/j.biocel.2016.12.015

Rotsch, A. H., Kopka, J., Feussner, I., & Ischebeck, T. (2017). Central metabolite and sterol profiling divides tobacco male gametophyte development and pollen tube growth into eight metabolic phases. *Plant J, 92*(1), 129-146. doi:10.1111/tpj.13633

Rouach, N., Koulakoff, A., Abudara, V., Willecke, K., & Giaume, C. (2008). Astroglial metabolic networks sustain hippocampal synaptic transmission. *Science, 322*(5907), 1551-1555. doi:10.1126/science.1164022

Roy, M., Beauvieux, M. C., Naulin, J., El Hamrani, D., Gallis, J. L., Cunnane, S. C., & Bouzier-Sore, A. K. (2015). Rapid adaptation of rat brain and liver metabolism to a ketogenic diet: an integrated study using (1)H- and (13)C-NMR spectroscopy. *J Cereb Blood Flow Metab, 35*(7), 1154-1162. doi:10.1038/jcbfm.2015.29

Saher, G., Rudolphi, F., Corthals, K., Ruhwedel, T., Schmidt, K. F., Lowel, S., Dibaj, P., Barrette, B., Mobius, W., & Nave, K. A. (2012). Therapy of Pelizaeus-Merzbacher disease in mice by feeding a cholesterol-enriched diet. *Nat Med, 18*(7), 1130-1135. doi:10.1038/nm.2833

Schaffer, J. E. (2002). Fatty acid transport: the roads taken. *Am J Physiol Endocrinol Metab, 282*(2), E239-246. doi:10.1152/ajpendo.00462.2001

Schaffer, J. E., & Lodish, H. F. (1994). Expression cloning and characterization of a novel adipocyte long chain fatty acid transport protein. *Cell, 79*(3), 427-436.

Schnyder, S., Svensson, K., Cardel, B., & Handschin, C. (2017). Muscle PGC-1alpha is required for long-term systemic and local adaptations to a ketogenic diet in mice. *Am J Physiol Endocrinol Metab, 312*(5), E437-E446. doi:10.1152/ajpendo.00361.2016

Schoch, S., Deak, F., Konigstorfer, A., Mozhayeva, M., Sara, Y., Sudhof, T. C., & Kavalali, E. T. (2001). SNARE function analyzed in synaptobrevin/VAMP knockout mice. *Science, 294*(5544), 1117-1122. doi:10.1126/science.1064335

Schoors, S., Bruning, U., Missiaen, R., Queiroz, K. C., Borgers, G., Elia, I., Zecchin, A., Cantelmo, A. R., Christen, S., Goveia, J., Heggermont, W., Godde, L., Vinckier, S., Van Veldhoven, P. P., Eelen, G., Schoonjans, L., Gerhardt, H., Dewerchin, M., Baes, M., De Bock, K., Ghesquiere, B., Lunt, S. Y., Fendt, S. M., & Carmeliet, P. (2015). Fatty acid carbon is essential for dNTP synthesis in endothelial cells. *Nature, 520*(7546), 192-197. doi:10.1038/nature14362

Schroeder, H., Bomont, L., & Nehlig, A. (1991). Influence of early chronic phenobarbital treatment on cerebral arteriovenous differences of glucose and ketone bodies in the developing rat. *Int J Dev Neurosci, 9*(5), 453-461.

Schulz, H. (2002). Oxidation of fatty acids in eukaryotes *New comprehensive biochemistry* (Vol. 36, pp. 127-150): Elsevier.

Schwenk, R. W., Holloway, G. P., Luiken, J. J., Bonen, A., & Glatz, J. F. (2010). Fatty acid transport across the cell membrane: regulation by fatty acid transporters. *Prostaglandins Leukot Essent Fatty Acids, 82*(4-6), 149-154. doi:10.1016/j.plefa.2010.02.029

Scichilone, J. M., Yarraguntla, K., Charalambides, A., Harney, J. P., & Butler, D. (2016). Environmental Enrichment Mitigates Detrimental Cognitive Effects of Ketogenic Diet in Weanling Rats. *J Mol Neurosci, 60*(1), 1-9. doi:10.1007/s12031-016-0753-4

Scolding, N. J., Frith, S., Linington, C., Morgan, B. P., Campbell, A. K., & Compston, D. A. (1989). Myelin-oligodendrocyte glycoprotein (MOG) is a surface marker of oligodendrocyte maturation. *J Neuroimmunol, 22*(3), 169-176.

Selfridge, J. E., Wilkins, H. M., E, L., Carl, S. M., Koppel, S., Funk, E., Fields, T., Lu, J., Tang, E. P., Slawson, C., Wang, W., Zhu, H., & Swerdlow, R. H. (2015). Effect of one month duration ketogenic and non-ketogenic high fat diets on mouse brain

bioenergetic infrastructure. *J Bioenerg Biomembr, 47*(1-2), 1-11. doi:10.1007/s10863-014-9570-z

Sepehrband, F., Alexander, D. C., Clark, K. A., Kurniawan, N. D., Yang, Z., & Reutens, D. C. (2016). Parametric Probability Distribution Functions for Axon Diameters of Corpus Callosum. *Front Neuroanat, 10*, 59. doi:10.3389/fnana.2016.00059

Sharma, K., Schmitt, S., Bergner, C. G., Tyanova, S., Kannaiyan, N., Manrique-Hoyos, N., Kongi, K., Cantuti, L., Hanisch, U. K., Philips, M. A., Rossner, M. J., Mann, M., & Simons, M. (2015). Cell type- and brain region-resolved mouse brain proteome. *Nat Neurosci, 18*(12), 1819-1831. doi:10.1038/nn.4160

Shibata, T., Yamada, K., Watanabe, M., Ikenaka, K., Wada, K., Tanaka, K., & Inoue, Y. (1997). Glutamate transporter GLAST is expressed in the radial glia-astrocyte lineage of developing mouse spinal cord. *J Neurosci, 17*(23), 9212-9219.

Shimazu, T., Hirschey, M. D., Newman, J., He, W., Shirakawa, K., Le Moan, N., Grueter, C. A., Lim, H., Saunders, L. R., Stevens, R. D., Newgard, C. B., Farese, R. V., Jr., de Cabo, R., Ulrich, S., Akassoglou, K., & Verdin, E. (2013). Suppression of oxidative stress by beta-hydroxybutyrate, an endogenous histone deacetylase inhibitor. *Science, 339*(6116), 211-214. doi:10.1126/science.1227166

Silva, J. C., Gorenstein, M. V., Li, G. Z., Vissers, J. P., & Geromanos, S. J. (2006). Absolute quantification of proteins by LCMSE: a virtue of parallel MS acquisition. *Mol Cell Proteomics, 5*(1), 144-156. doi:10.1074/mcp.M500230-MCP200

Simpson, I. A., Carruthers, A., & Vannucci, S. J. (2007). Supply and demand in cerebral energy metabolism: the role of nutrient transporters. *J Cereb Blood Flow Metab, 27*(11), 1766-1791. doi:10.1038/sj.jcbfm.9600521

Simpson, I. A., Dwyer, D., Malide, D., Moley, K. H., Travis, A., & Vannucci, S. J. (2008). The facilitative glucose transporter GLUT3: 20 years of distinction. *Am J Physiol Endocrinol Metab, 295*(2), E242-253. doi:10.1152/ajpendo.90388.2008

Sivitz, W., DeSautel, S., Walker, P. S., & Pessin, J. E. (1989). Regulation of the glucose transporter in developing rat brain. *Endocrinology, 124*(4), 1875-1880. doi:10.1210/endo-124-4-1875

Sokoloff, L., Reivich, M., Kennedy, C., Des Rosiers, M. H., Patlak, C. S., Pettigrew, K. D., Sakurada, O., & Shinohara, M. (1977). The [14C]deoxyglucose method for the measurement of local cerebral glucose utilization: theory, procedure, and normal values in the conscious and anesthetized albino rat. *J Neurochem, 28*(5), 897-916.

Song, B. J., Elbert, A., Rahman, T., Orr, S. K., Chen, C. T., Febbraio, M., & Bazinet, R. P. (2010). Genetic ablation of CD36 does not alter mouse brain polyunsaturated fatty acid concentrations. *Lipids, 45*(4), 291-299. doi:10.1007/s11745-010-3398-z

Spolarics, Z., Lang, C. H., Bagby, G. J., & Spitzer, J. J. (1991). Glutamine and fatty acid oxidation are the main sources of energy for Kupffer and endothelial cells. *Am J Physiol, 261*(2 Pt 1), G185-190. doi:10.1152/ajpgi.1991.261.2.G185

Spulber, G., Spulber, S., Hagenas, L., Amark, P., & Dahlin, M. (2009). Growth dependence on insulin-like growth factor-1 during the ketogenic diet. *Epilepsia, 50*(2), 297-303. doi:10.1111/j.1528-1167.2008.01769.x

Stenmark, H., & Olkkonen, V. M. (2001). The Rab GTPase family. *Genome Biol, 2*(5), REVIEWS3007.

Stincone, A., Prigione, A., Cramer, T., Wamelink, M. M., Campbell, K., Cheung, E., Olin-Sandoval, V., Gruning, N. M., Kruger, A., Tauqeer Alam, M., Keller, M. A., Breitenbach, M., Brindle, K. M., Rabinowitz, J. D., & Ralser, M. (2015). The return of metabolism: biochemistry and physiology of the pentose phosphate pathway. *Biol Rev Camb Philos Soc, 90*(3), 927-963. doi:10.1111/brv.12140

Storch, J., & Corsico, B. (2008). The emerging functions and mechanisms of mammalian fatty acid-binding proteins. *Annu Rev Nutr, 28*, 73-95. doi:10.1146/annurev.nutr.27.061406.093710

Storey, J. D., & Tibshirani, R. (2003). Statistical significance for genomewide studies. *Proc Natl Acad Sci U S A, 100*(16), 9440-9445. doi:10.1073/pnas.1530509100

Stremmel, W., Lotz, G., Strohmeyer, G., & Berk, P. D. (1985). Identification, isolation, and partial characterization of a fatty acid binding protein from rat jejunal microvillous membranes. *J Clin Invest, 75*(3), 1068-1076. doi:10.1172/JCI111769

Stumpf, S. K., Berghoff, S. A., Trevisiol, A., Spieth, L., Duking, T., Schneider, L. V., Schlaphoff, L., Dreha-Kulaczewski, S., Bley, A., Burfeind, D., Kusch, K., Mitkovski, M., Ruhwedel, T., Guder, P., Rohse, H., Denecke, J., Gartner, J., Mobius, W., Nave, K. A., & Saher, G. (2019). Ketogenic diet ameliorates axonal defects and promotes myelination in Pelizaeus-Merzbacher disease. *Acta Neuropathol*. doi:10.1007/s00401-019-01985-2

Su, L., Li, X., Lin, R., Sheng, H., Feng, Z., & Liu, L. (2017). Clinical and molecular analysis of 6 Chinese patients with isoleucine metabolism defects: identification of 3 novel mutations in the HSD17B10 and ACAT1 gene. *Metab Brain Dis, 32*(6), 2063-2071. doi:10.1007/s11011-017-0097-y

Sugiura, Y., Honda, K., Kajimura, M., & Suematsu, M. (2014). Visualization and quantification of cerebral metabolic fluxes of glucose in awake mice. *Proteomics, 14*(7-8), 829-838. doi:10.1002/pmic.201300047

Supplie, L. M., Duking, T., Campbell, G., Diaz, F., Moraes, C. T., Gotz, M., Hamprecht, B., Boretius, S., Mahad, D., & Nave, K. A. (2017). Respiration-Deficient Astrocytes Survive As Glycolytic Cells In Vivo. *J Neurosci, 37*(16), 4231-4242. doi:10.1523/JNEUROSCI.0756-16.2017

Sussman, D., Ellegood, J., & Henkelman, M. (2013). A gestational ketogenic diet alters maternal metabolic status as well as offspring physiological growth and brain structure in the neonatal mouse. *BMC Pregnancy Childbirth, 13*, 198. doi:10.1186/1471-2393-13-198

Swartzlander, D. B., Propson, N. E., Roy, E. R., Saito, T., Saido, T., Wang, B., & Zheng, H. (2018). Concurrent cell type-specific isolation and profiling of mouse brains in inflammation and Alzheimer's disease. *JCI Insight, 3*(13). doi:10.1172/jci.insight.121109

Taha, A. Y., Ryan, M. A., & Cunnane, S. C. (2005). Despite transient ketosis, the classic high-fat ketogenic diet induces marked changes in fatty acid metabolism in rats. *Metabolism, 54*(9), 1127-1132. doi:10.1016/j.metabol.2005.03.018

Thio, L. L., Erbayat-Altay, E., Rensing, N., & Yamada, K. A. (2006). Leptin contributes to slower weight gain in juvenile rodents on a ketogenic diet. *Pediatr Res, 60*(4), 413-417. doi:10.1203/01.pdr.0000238244.54610.27

Tieu, K., Perier, C., Caspersen, C., Teismann, P., Wu, D.-C., Yan, S.-D., Naini, A., Vila, M., Jackson-Lewis, V., Ramasamy, R., & Przedborski, S. (2003). D-β-Hydroxybutyrate rescues mitochondrial respiration and mitigates features of Parkinson disease. *Journal of Clinical Investigation, 112*(6), 892-901. doi:10.1172/jci200318797

Towbin, H., Staehelin, T., & Gordon, J. (1979). Electrophoretic transfer of proteins from polyacrylamide gels to nitrocellulose sheets: procedure and some applications. *Proc Natl Acad Sci U S A, 76*(9), 4350-4354.

Valdebenito, R., Ruminot, I., Garrido-Gerter, P., Fernandez-Moncada, I., Forero-Quintero, L., Alegria, K., Becker, H. M., Deitmer, J. W., & Barros, L. F. (2016). Targeting of astrocytic glucose metabolism by beta-hydroxybutyrate. *J Cereb Blood Flow Metab, 36*(10), 1813-1822. doi:10.1177/0271678X15613955

Valente-Silva, P., Lemos, C., Kofalvi, A., Cunha, R. A., & Jones, J. G. (2015). Ketone bodies effectively compete with glucose for neuronal acetyl-CoA generation in rat hippocampal slices. *NMR Biomed, 28*(9), 1111-1116. doi:10.1002/nbm.3355

van Deijk, A. F., Camargo, N., Timmerman, J., Heistek, T., Brouwers, J. F., Mogavero, F., Mansvelder, H. D., Smit, A. B., & Verheijen, M. H. (2017). Astrocyte lipid metabolism is critical for synapse development and function in vivo. *Glia, 65*(4), 670-682. doi:10.1002/glia.23120

Vanitallie, T. B., Nonas, C., Di Rocco, A., Boyar, K., Hyams, K., & Heymsfield, S. B. (2005). Treatment of Parkinson disease with diet-induced hyperketonemia: a

feasibility study. *Neurology, 64*(4), 728-730. doi:10.1212/01.WNL.0000152046.11390.45

Vannucci, S. J. (1994). Developmental expression of GLUT1 and GLUT3 glucose transporters in rat brain. *J Neurochem, 62*(1), 240-246.

Verity, A. N., & Campagnoni, A. T. (1988). Regional expression of myelin protein genes in the developing mouse brain: in situ hybridization studies. *J Neurosci Res, 21*(2-4), 238-248. doi:10.1002/jnr.490210216

Verpeut, J. L., DiCicco-Bloom, E., & Bello, N. T. (2016). Ketogenic diet exposure during the juvenile period increases social behaviors and forebrain neural activation in adult Engrailed 2 null mice. *Physiol Behav, 161*, 90-98. doi:10.1016/j.physbeh.2016.04.001

Vining, E. P., Pyzik, P., McGrogan, J., Hladky, H., Anand, A., Kriegler, S., & Freeman, J. M. (2002). Growth of children on the ketogenic diet. *Dev Med Child Neurol, 44*(12), 796-802.

Virchow, R. (1854). Ueber das ausgebreitete Vorkommen einer dem Nervenmark analogen Substanz in den thierischen Geweben. *Archiv für pathologische Anatomie und Physiologie und für klinische Medicin, 6*(4), 562-572. doi:10.1007/bf02116709

Waxman, S. G. (1980). Determinants of conduction velocity in myelinated nerve fibers. *Muscle Nerve, 3*(2), 141-150. doi:10.1002/mus.880030207

Webber, R. J., & Edmond, J. (1979). The in vivo utilization of acetoacetate, D-(-)-3-hydroxybutyrate, and glucose for lipid synthesis in brain in the 18-day-old rat. Evidence for an acetyl-CoA bypass for sterol synthesis. *J Biol Chem, 254*(10), 3912-3920.

Wheless, J. W. (2008). History of the ketogenic diet. *Epilepsia, 49 Suppl 8*, 3-5. doi:10.1111/j.1528-1167.2008.01821.x

Winters, J. J., Ferguson, C. J., Lenk, G. M., Giger-Mateeva, V. I., Shrager, P., Meisler, M. H., & Giger, R. J. (2011). Congenital CNS hypomyelination in the Fig4 null mouse is rescued by neuronal expression of the PI(3,5)P(2) phosphatase Fig4. *J Neurosci, 31*(48), 17736-17751. doi:10.1523/JNEUROSCI.1482-11.2011

Witkowski, A., Rangan, V. S., Randhawa, Z. I., Amy, C. M., & Smith, S. (1991). Structural organization of the multifunctional animal fatty-acid synthase. *Eur J Biochem, 198*(3), 571-579.

Wojcik, S. M., Rhee, J. S., Herzog, E., Sigler, A., Jahn, R., Takamori, S., Brose, N., & Rosenmund, C. (2004). An essential role for vesicular glutamate transporter 1 (VGLUT1) in postnatal development and control of quantal size. *Proc Natl Acad Sci U S A, 101*(18), 7158-7163. doi:10.1073/pnas.0401764101

Wong, B. W., Wang, X., Zecchin, A., Thienpont, B., Cornelissen, I., Kalucka, J., Garcia-Caballero, M., Missiaen, R., Huang, H., Bruning, U., Blacher, S., Vinckier, S., Goveia, J., Knobloch, M., Zhao, H., Dierkes, C., Shi, C., Hagerling, R., Moral-Darde, V., Wyns, S., Lippens, M., Jessberger, S., Fendt, S. M., Luttun, A., Noel, A., Kiefer, F., Ghesquiere, B., Moons, L., Schoonjans, L., Dewerchin, M., Eelen, G., Lambrechts, D., & Carmeliet, P. (2017). The role of fatty acid beta-oxidation in lymphangiogenesis. *Nature, 542*(7639), 49-54. doi:10.1038/nature21028

Yates, M. A., & Juraska, J. M. (2007). Increases in size and myelination of the rat corpus callosum during adulthood are maintained into old age. *Brain Res, 1142*, 13-18. doi:10.1016/j.brainres.2007.01.043

Yeh, Y. Y., Streuli, V. L., & Zee, P. (1977). Ketone bodies serve as important precursors of brain lipids in the developing rat. *Lipids, 12*(11), 957-964.

Yudkoff, M., Daikhin, Y., Nissim, I., Horyn, O., Lazarow, A., Luhovyy, B., Wehrli, S., & Nissim, I. (2005). Response of brain amino acid metabolism to ketosis. *Neurochem Int, 47*(1-2), 119-128. doi:10.1016/j.neuint.2005.04.014

Zhang, Y., Kuang, Y., Xu, K., Harris, D., Lee, Z., LaManna, J., & Puchowicz, M. A. (2013). Ketosis proportionately spares glucose utilization in brain. *J Cereb Blood Flow Metab, 33*(8), 1307-1311. doi:10.1038/jcbfm.2013.87

Zhao, Z., Lange, D. J., Voustianiouk, A., MacGrogan, D., Ho, L., Suh, J., Humala, N., Thiyagarajan, M., Wang, J., & Pasinetti, G. M. (2006). A ketogenic diet as a potential novel therapeutic intervention in amyotrophic lateral sclerosis. *BMC Neurosci, 7*, 29. doi:10.1186/1471-2202-7-29

Zhou, W., Mukherjee, P., Kiebish, M. A., Markis, W. T., Mantis, J. G., & Seyfried, T. N. (2007). The calorically restricted ketogenic diet, an effective alternative therapy for malignant brain cancer. *Nutr Metab (Lond), 4*, 5. doi:10.1186/1743-7075-4-5

Ziegler, D. R., Gamaro, G. D., Araujo, E., Bassani, M. G., Perry, M. L., Dalmaz, C., & Goncalves, C. A. (2005). Nociception and locomotor activity are increased in ketogenic diet fed rats. *Physiol Behav, 84*(3), 421-427. doi:10.1016/j.physbeh.2005.01.003

Appendix

List of full protein and gene names

Protein	
ACAA1A	3-ketoacyl-CoA thiolase A
ACAA1B	3-ketoacyl-CoA thiolase B
ACAA2	3-ketoacyl-CoA thiolase
ACADL	Long-chain specific acyl-CoA dehydrogenase
ACADM	Medium-chain specific acyl-CoA dehydrogenase
ACADSB	Short/branched chain specific acyl-CoA dehydrogenase
ACADVL	Very long-chain specific acyl-CoA dehydrogenase
ACAT1	Acetyl-CoA acetyltransferase
ACC1	Acetyl-CoA carboxylase 1
ACC2	Acetyl-CoA carboxylase 2
ACLS1	Long-chain-fatty-acid-CoA ligase 1
ACLS3	Long-chain-fatty-acid-CoA ligase 3
ACLY	ATP-citrate synthase
ACO2	Aconitate hydratase
ACOX1	Peroxisomal acyl-coenzyme A oxidase 1
ACSBG1	Long-chain-fatty-acid-CoA ligase ACSBG1
ACSL6	Long-chain-fatty-acid-CoA ligase 6
ALB	Albumin
ALDH1L1	Cytosolic 10-formyltetrahydrofolate dehydrogenase
ALDOA	Fructose-bisphosphate aldolase A
ALDOB	Fructose-bisphosphate aldolase B
ALDOC	Fructose-bisphosphate aldolase C
AP1B1	AP-1 complex subunit beta-1
AP2A1	AP-2 complex subunit alpha-1
AP2A2	AP-2 complex subunit alpha-2
AP2B1	AP-2 complex subunit bet
AP2M1	AP-2 complex subunit mu
APOA1	Apolipoprotein A-I
APOE	Apolipoprotein E
ARF5	ADP-ribosylation factor 5
ATP2A2	Sarcoplasmic/endoplasmic reticulum calcium ATPase 2
ATP2B4	Plasma membrane calcium-transporting ATPase 4
ATP5F1	ATP synthase F(0) complex subunit B1
ATP5F1B	ATP synthase subunit beta
ATP5F1C	ATP synthase subunit gamma
ATP5F1E	ATP synthase subunit epsilon
ATP5H	ATP synthase subunit d
ATP5J2	ATP synthase subunit f
ATP5L	ATP synthase subunit g
ATP5O	ATP synthase subunit O
ATP6V0A1	V-type proton ATPase 116 kDa subunit a isoform 1
ATP6V0C	V-type proton ATPase 16 kDa proteolipid subunit
ATP6V0D1	V-type proton ATPase subunit d 1
ATP6V1A	V-type proton ATPase catalytic subunit A

ATP6V1B2	V-type proton ATPase subunit B_ brain isoform
ATP6V1D	V-type proton ATPase subunit D
ATP6V1E1	V-type proton ATPase subunit E 1
ATP6V1F	V-type proton ATPase subunit F
ATP6V1G1	V-type proton ATPase subunit G 1
ATP6V1G3	V-type proton ATPase subunit G 3
ATP6V1H	V-type proton ATPase subunit H
BDH1	D-beta-hydroxybutyrate dehydrogenase
BSG	Basigin
CAPS1	Calcium-dependent secretion activator 1
CLTA	Clathrin light chain A
CLTB	Clathrin light chain B
CLTC	Clathrin light chain C
CNP	2'_3'-cyclic-nucleotide 3'-phosphodiesterase
COX4I1	Cytochrome c oxidase subunit 4 isoform 1
COX5A	Cytochrome c oxidase subunit 5A
COX5B	Cytochrome c oxidase subunit 5B
COX6A1	Cytochrome c oxidase subunit 6A1
COX6B1	Cytochrome c oxidase subunit 6B1
COX6C	Cytochrome c oxidase subunit 6C
COX7A2	Cytochrome c oxidase subunit 7A2
CPLX1	Complexin-1
CPT1A	Carnitine O-palmitoyltransferase 1_ liver isoform
CPT2	Carnitine O-palmitoyltransferase 2
CPLX2	Complexin-2
CS	Citrate synthase
CYC1	Cytochrome c1_ heme protein
DLD	Dihydrolipoyl dehydrogenase
DLST	Dihydrolipoyllysine-residue succinyltransferase component of 2-oxoglutarate dehydrogenase complex
DNM1	Dynamin-1
DNM2	Dynamin-2
DNM3	Dynamin-3
ECHS1	Enoyl-CoA hydratase
ECI1	Enoyl-CoA delta isomerase 1
ECI2	Enoyl-CoA delta isomerase 2
EIF5A2	Eukaryotic translation initiation factor 5A-2
ENO1	Alpha-enolase
ENO2	Gamma-enolase
ENO3	Beta-enolase
FABP5	Fatty acid-binding protein_ epidermal
FABP7	Fatty acid-binding protein_ brain
FASN	Fatty acid synthase
FH1	Fumarate hydratase
G6PD2	Glucose-6-phosphate 1-dehydrogenase 2
G6PDX	Glucose-6-phosphate 1-dehydrogenase X
GAPDH	Glyceraldehyde-3-phosphate dehydrogenase

GLAST	Glutamate aspartate transporter
GLUT1	Glucose transporter 1
GLUT3	Glucose transporter 3
GPI	Glucose-6-phosphate isomerase
GYS1	Glycogen synthase
HADH	Hydroxyacyl-coenzyme A dehydrogenase
HADHA	Trifunctional enzyme subunit alpha
HADHB	Trifunctional enzyme subunit beta
HK1	Hexokinase-1
HK2	Hexokinase-2
HKDC1	Putative hexokinase HKDC1
ICAM2	Intercellular adhesion molecule 2
IDH2	Isocitrate dehydrogenase [NADP]
IDH3A	Isocitrate dehydrogenase [NAD] subunit alpha
IDH3G	Isocitrate dehydrogenase [NAD] subunit gamma 1
LDHA	L-lactate dehydrogenase A chain
LDHB	L-lactate dehydrogenase B chain
MBP	Myelin basic protein
MCT1	Monocarboxylate transporter 1
MDH2	Malate dehydrogenase
MTATP8	ATP synthase protein 8
MTCO1	Cytochrome c oxidase subunit 1
MTCO2	Cytochrome c oxidase subunit 2
MT-CYB	Cytochrome b
MTND3	NADH-ubiquinone oxidoreductase chain 3
MTND4	NADH-ubiquinone oxidoreductase chain 4
MYOF	Myoferlin
NAPA	Alpha-soluble NSF attachment protein
NDUFA10	NADH dehydrogenase [ubiquinone] 1 alpha subcomplex subunit 10
NDUFA11	NADH dehydrogenase [ubiquinone] 1 alpha subcomplex subunit 11
NDUFA12	NADH dehydrogenase [ubiquinone] 1 alpha subcomplex subunit 12
NDUFA13	NADH dehydrogenase [ubiquinone] 1 alpha subcomplex subunit 13
NDUFA2	NADH dehydrogenase [ubiquinone] 1 alpha subcomplex subunit 2
NDUFA3	NADH dehydrogenase [ubiquinone] 1 alpha subcomplex subunit 3
NDUFA4	NADH dehydrogenase [ubiquinone] 1 alpha subcomplex subunit 4
NDUFA5	NADH dehydrogenase [ubiquinone] 1 alpha subcomplex subunit 5
NDUFA6	NADH dehydrogenase [ubiquinone] 1 alpha subcomplex subunit 6
NDUFA7	NADH dehydrogenase [ubiquinone] 1 alpha subcomplex subunit 7
NDUFA8	NADH dehydrogenase [ubiquinone] 1 alpha subcomplex subunit 8
NDUFB1	NADH dehydrogenase [ubiquinone] 1 beta subcomplex subunit 1
NDUFB10	NADH dehydrogenase [ubiquinone] 1 beta subcomplex subunit 10
NDUFB11	NADH dehydrogenase [ubiquinone] 1 beta subcomplex subunit 11
NDUFB3	NADH dehydrogenase [ubiquinone] 1 beta subcomplex subunit 3
NDUFB4	NADH dehydrogenase [ubiquinone] 1 beta subcomplex subunit 4
NDUFB5	NADH dehydrogenase [ubiquinone] 1 beta subcomplex subunit 5
NDUFB7	NADH dehydrogenase [ubiquinone] 1 beta subcomplex subunit 7
NDUFB8	NADH dehydrogenase [ubiquinone] 1 beta subcomplex subunit 8

NDUFB9	NADH dehydrogenase [ubiquinone] 1 beta subcomplex subunit 9
NDUFC2	NADH dehydrogenase [ubiquinone] 1 subunit C2
NDUFS1	NADH-ubiquinone oxidoreductase 75 kDa subunit
NDUFS2	NADH dehydrogenase [ubiquinone] iron-sulfur protein 2
NDUFS3	NADH dehydrogenase [ubiquinone] iron-sulfur protein 3
NDUFS4	NADH dehydrogenase [ubiquinone] iron-sulfur protein 4
NDUFS5	NADH dehydrogenase [ubiquinone] iron-sulfur protein 5
NDUFS7	NADH dehydrogenase [ubiquinone] iron-sulfur protein 7
NDUFS8	NADH dehydrogenase [ubiquinone] iron-sulfur protein 8
NDUFV1	NADH dehydrogenase [ubiquinone] flavoprotein 1
NDUFV2	NADH dehydrogenase [ubiquinone] flavoprotein 2
NSF	Vesicle-fusing ATPase
OGDH	2-oxoglutarate dehydrogenase
PFKL	ATP-dependent 6-phosphofructokinase_ liver type
PFKM	ATP-dependent 6-phosphofructokinase_ muscle type
PFKP	ATP-dependent 6-phosphofructokinase_ platelet type
PGAM1	Phosphoglycerate mutase 1
PGAM2	Phosphoglycerate mutase 2
PGK1	Phosphoglycerate kinase 1
PGK2	Phosphoglycerate kinase 2
PGLS	6-phosphogluconolactonase
PGM1	Phosphoglucomutase-1
PKM	Pyruvate kinase
PLP1	Myelin proteolipid protein
PPA1	Inorganic pyrophosphatase
PRPS2	Ribose-phosphate pyrophosphokinase 2
PTPRB	Receptor-type tyrosine-protein phosphatase beta
RAB11B	Ras-related protein Rab-11B
RAB18	Ras-related protein Rab-18
RAB21	Ras-related protein Rab-21
RAB2A	Ras-related protein Rab-2A
RAB3A	Ras-related protein Rab-3A
RAB3B	Ras-related protein Rab-3B
RAB6B	Ras-related protein Rab-6B
RAB5C	Ras-related protein Rab-5C
SCOT	Succinyl-CoA:3-ketoacid coenzyme A transferase 1
SDHA	Succinate dehydrogenase [ubiquinone] flavoprotein subunit
SDHB	Succinate dehydrogenase [ubiquinone] iron-sulfur subunit
SDHC	Succinate dehydrogenase cytochrome b560 subunit
SLC12A2	Solute carrier family 12 member 2
SLC4A4	Electrogenic sodium bicarbonate cotransporter 1
SNAP25	Synaptosomal-associated protein 25
STX1A	Syntaxin-1A
STX1B	Syntaxin-1B
STXBP1	Syntaxin-binding protein 1
SUCLA2	Succinate--CoA ligase [ADP-forming] subunit beta
SUCLG1	Succinate--CoA ligase [ADP/GDP-forming] subunit alpha

SUCLG2	Succinate--CoA ligase [GDP-forming] subunit beta
SYNJ1	Synaptojanin-1
SYNPR	Synaptoporin
SYT1	Synaptotagmin-1
TALDO1	Transaldolase
TKT	Transketolase
TPI1	Triosephosphate isomerase
UQCR10	Cytochrome b-c1 complex subunit 9
UQCRB	Cytochrome b-c1 complex subunit 7
UQCRC1	Cytochrome b-c1 complex subunit 1
UQCRC2	Cytochrome b-c1 complex subunit 2
UQCRFS1	Cytochrome b-c1 complex subunit Rieske
UQCRQ	Cytochrome b-c1 complex subunit 8
VAMP2	Vesicle-associated membrane protein 2
VGLUT1	Vesicular glutamate transporter 1

Gene	
Abca4	*ATP binding cassette subfamily A member 4*
Atp1b1	*ATPase Na+/K+ transporting subunitbBeta 1*
Atp2b2	*ATPase plasma membrane Ca2+ transporting 2*
Cacng2	*Calcium voltage-gated channel auxiliary subunit gamma 2*
Clic6	*Chloride intracellular channel 6*
Folr1	*Folate receptor 1*
Gabrr2	*Gamma-aminobutyric acid type A receptor rho2 subunit*
Gria3	*Glutamate ionotropic receptor AMPA type subunit 3*
Itpr1	*Inositol 1,4,5-trisphosphate receptor type 1*
Kcnb1	*Potassium voltage-gated channel subfamily B member 1*
Kcne2	*Potassium voltage-gated channel subfamily E regulatory subunit 2*
Kcnj13	*Potassium voltage-gated channel subfamily J member 13*
Kcnma1	*Potassium calcium-activated channel subfamily M alpha 1*
Kcnq2	*Potassium voltage-gated channel subfamily Q member 2*
Kcnt1	*Potassium sodium-activated channel subfamily T member 1*
Pitpnm2	*Phosphatidylinositol transfer protein membrane associated 2*
Sfxn2	*Sideroflexin 2*
Slc13a4	*Solute carrier family 13 member 4*
Slc24a4	*Solute carrier family 23 member 4*
Slc29a4	*Solute carrier family 29 member 4*
Slc4a5	*Solute carrier family 4 member 5*
Slc5a3	*Solute carrier family 5 member 3*
Steap2	*STEAP2 metalloreductase*
Stra6	*Stimulated by retinoic acid 6*
Ttr	*Transthyretin*